61. Top Quark

Revised September 2023 by T.M. Liss (City Coll. of New York), F. Maltoni (CP3 U. catholique de Louvain; Bologna U.) and A. Quadt (Göttingen U.).

61.1 Introduction and SM theory overview

In the Standard Model (SM), the left-handed top quark is the $Q = 2/3$, $T_3 = +1/2$ member of the weak-isospin doublet containing the bottom quark, while the right-handed top is an $SU(2)_L$ singlet (see, e.g., the review "Electroweak Model and Constraints on New Physics" here). Its phenomenology is driven by its large mass, $m_t \simeq \frac{v}{\sqrt{2}}$, where $v = 246$ GeV is the vacuum expectation value of the Higgs field, i.e., it is the only quark whose Yukawa coupling to the Higgs boson is of order unity. As it is heavier than the W boson, it is the only quark that decays semi-weakly into a real W boson and a b quark. This results in a lifetime that is shorter than the time that is needed for strong interactions to modify its properties or to bind it into a hadron. In this respect, the top is the only quark that, in its brief life, behaves as a free one. Because of its large mass and Yukawa coupling to the Higgs boson, it also gives important contributions (via loops) to Standard Model precision observables measured at lower scales.

For these reasons, the top quark provides a unique laboratory to test our understanding of matter and fundamental interactions at the ElectroWeak (EW) symmetry-breaking scale and beyond. In addition, since it is abundantly produced at the Large Hadron Collider (LHC), a precise knowledge of its properties (mass, couplings, production cross sections, decay branching ratios, *etc.*) can be achieved. This review provides a concise discussion of the experimental and theoretical issues involved in the determination of the top-quark properties.

61.1.1 *Properties*

61.1.1.1 *Mass*

The top quark mass determines to a large extent the unique phenomenology of this quark. In the SM quark masses are derived parameters from the Yukawa coupling and the vacuum expectation value. At the loop level, with the Higgs boson discovery and per mil measurement of its mass, the values of the W-boson and top quark mass are correlated, so that their precise determinations provides a strong test of the SM (see Section 10 "Electroweak Model and constraints on new physics" of this *Review*). At present there is some tension at the $1.7\,\sigma$ level, between the indirect top quark (pole) mass determination from electroweak precision data (176.12 ± 1.9 GeV) and the combination of direct measurements at the LHC that yields $172.52 \pm 0.14(stat.) \pm 0.30(syst.)$ GeV [1].

The top mass value is also critical in the issue of vacuum stability in the SM [2–4]. At high scales, the Higgs quartic coupling λ evolves to increasingly small values as m_t grows. Above $m_t = 171$ GeV, i.e., very close to the most precise measurements, λ becomes negative at the Planck scale leading to a meta-stable electroweak vacuum, while for slightly larger values, $m_t > 176$ GeV the electroweak vacuum would become unstable. Current top-quark measurements therefore point to a Higgs quartic coupling which is nearly vanishing at the Planck scale. While being quite suggestive, in absence of a clear UV picture this argument allows only to conclude that comparison between our best SM predictions and the data does not imply new physics below the Planck scale (see Section 11.2.3 of "Status of Higgs Boson Physics" in this *Review*).

Given its importance and the large samples of top quarks produced at the LHC, the top mass determination has been one of the most important goals in the precision measurement campaign of the ATLAS and CMS collaborations. The basic methodology rests on the idea of fitting m_t-dependent kinematic distributions to fully-exclusive (Monte Carlo) predictions, via the full or partial reconstruction of the system of the t and $\bar{t}$ decay products. These are called "direct measurements"

and aim at a target accuracy in the permil range. With an absolute uncertainty of order or better than $\Lambda_{\rm QCD}$, however, a clear relation between the extracted mass and a well defined quantum field theory parameter of the underlying theory has become necessary.

Several mass parameter definitions exist with a precise field-theoretical meaning, that can be organised in two broad classes, the long-distance ones, such as the "pole mass", and short-distance masses, such as $\overline{\rm MS}$ mass. A mass definition, the MSR mass [5], exists that interpolates between the two. The one measured through direct measurements is sometimes referred to as "Monte Carlo" mass. Several other observables have been put forward that could be expressed in terms of well-defined masses and then overcome the problems of the direct measurements, yet with a target accuracy not quite competitive with the direct determination.

A top mass cannot be defined solely in terms of the mass of the system of its decay products: the top quark is a colored object, therefore it cannot be an asymptotic state of the theory and no final-state hadronic system can be unambiguously associated with it. On the other hand, final state observables such as those arising from its decay, can be related to the top mass through computations, which have perturbative as well as non-perturbative components, as Monte Carlo generators.

From a purely theoretical (calculational) point of view, the top mass parameter is defined within a given renormalization scheme, since divergent perturbative corrections arise order by order in perturbation theory, and need to be subtracted. The pole mass scheme prescribes to subtract the divergent mass corrections so that the pole in the quark propagator remains fixed order by order in perturbation theory. The $\overline{\rm MS}$ scheme prescribes to employ dimensional regularization and subtract the pure $1/\epsilon$ pole in the divergent mass correction. In doing so, the corresponding mass becomes scale dependent. In this scheme the pole in the top propagator receives corrections at all orders in perturbation theory. This scheme has the advantage that it makes the relation between the mass and the Yukawa coupling straightforward in the SM and is independent from non-perturbative corrections.

The relation between the top pole mass $m_t^{\rm pole}$ and $m_t^{\overline{\rm MS}}$ up to four loops reads [6]

$$m_t^{\rm pole} = m_t^{\overline{\rm MS}}(m_t)[1 + 0.4244\,\alpha_s + 0.8345\,\alpha_s^2 + 2.375\,\alpha_s^3 + (8.49 \pm 0.25)\,\alpha_s^4], \qquad (61.1)$$

which for $\alpha_s = \alpha_s^{(6)}(m) = 0.1088$ and $m_t^{\rm pole} = 172.5$ GeV gives $m_t^{\overline{\rm MS}}(m_t) = 162.69 \pm 0.006$ GeV. The two definitions lead to perturbatively equivalent theories: a perturbative expression of the pole mass in terms of the $\overline{m}^{\rm MS}$ mass can be translated to a physical result in the pole mass scheme into the corresponding physical result in the $\overline{\rm MS}$ scheme. However, the relation above has only a perturbative meaning, as the two masses differ by non-perturbative, long-distance effects. The difference between the top pole mass and the mass extracted in direct measurements, $\Delta m_{\rm MC}$, arises due to non-perturbative effects, that are currently modelled by shower Monte Carlo programs. It is expected to be of order $Q_0 \cdot \alpha_s(Q_0)$ with $Q_0 \sim 1$ GeV and estimated of order 0.5 GeV. An overview on the on-going efforts to precisely define and to estimate the uncertainties of the top mass can be found in Refs. [7,8].

61.1.1.2 *Couplings*

The SM couplings involving top quarks are of two types: gauge couplings, which are universal, and Yukawa couplings, which instead depend on the generation. Following the notation of Sections

9 and 10 of this *Review*, after EWSB and in the mass eigenstate basis, top quark interactions read

$$
\mathcal{L}_t^{\text{SM}} = \bar{\psi}_t \left[i\slashed{\partial} - m_t \right] \psi_t - g_s \bar{\psi}_t \gamma^\mu t^C \psi_t \mathcal{A}_\mu^C - e Q_t \bar{\psi}_t \gamma^\mu \psi_t A_\mu \tag{61.2}
$$
$$
- \frac{g}{2\sqrt{2}} \bar{\Psi} \gamma^\mu (1 - \gamma^5)(T^+ W_\mu^+ + T^- W_\mu^-) \Psi - \frac{g}{2\cos\theta_W} \bar{\psi}_t \gamma^\mu \left(g_V^t - g_A^t \gamma^5 \right) \psi_t Z_\mu
$$
$$
- \frac{m_t}{v} H \bar{\psi}_t \psi_t \, ,
$$

where in the first line we include the coupling to the $SU(3)$ field $\mathcal{A}_\mu$, and $\Psi = (t, b')$ with $b' = V_{tb}\, b + V_{ts}\, s + V_{td}\, d$. There are no neutral flavor changing interactions in the SM at tree level.

Table 61.1: List of SMEFT operators at dimension six, assuming $U(2)_q \times U(2)_u \times U(2)_d$ flavor symmetry. For more details on notation and conventions, see reference in the text.

Operator	Field content	Operator	Field content
Four-quark		Two-quark-two-lepton	
$O_{qq}^{1(ijkl)}$	$(\bar{q}_i \gamma^\mu q_j)(\bar{q}_k \gamma_\mu q_l)$	$O_{lq}^{1(ijkl)}$	$(\bar{l}_i \gamma^\mu l_j)(\bar{q}_k \gamma^\mu q_l)$
$O_{qq}^{3(ijkl)}$	$(\bar{q}_i \gamma^\mu \tau^I q_j)(\bar{q}_k \gamma_\mu \tau^I q_l)$	$O_{lq}^{3(ijkl)}$	$(\bar{l}_i \gamma^\mu \tau^I l_j)(\bar{q}_k \gamma^\mu \tau^I q_l)$
$O_{qu}^{1(ijkl)}$	$(\bar{q}_i \gamma^\mu q_j)(\bar{u}_k \gamma_\mu u_l)$	$O_{lu}^{(ijkl)}$	$(\bar{l}_i \gamma^\mu l_j)(\bar{u}_k \gamma^\mu u_l)$
$O_{qu}^{8(ijkl)}$	$(\bar{q}_i \gamma^\mu T^A q_j)(\bar{u}_k \gamma_\mu T^A u_l)$	$O_{eq}^{(ijkl)}$	$(\bar{e}_i \gamma^\mu e_j)(\bar{q}_k \gamma^\mu q_l)$
$O_{qd}^{1(ijkl)}$	$(\bar{q}_i \gamma^\mu q_j)(\bar{d}_k \gamma_\mu d_l)$	$O_{eu}^{(ijkl)}$	$(\bar{e}_i \gamma^\mu e_j)(\bar{u}_k \gamma^\mu u_l)$
$O_{qd}^{8(ijkl)}$	$(\bar{q}_i \gamma^\mu T^A q_j)(\bar{d}_k \gamma_\mu T^A d_l)$	$\ddagger O_{lequ}^{1(ijkl)}$	$(\bar{l}_i e_j)\, \varepsilon \, (\bar{q}_k u_l)$
$O_{uu}^{(ijkl)}$	$(\bar{u}_i \gamma^\mu u_j)(\bar{u}_k \gamma_\mu u_l)$	$\ddagger O_{lequ}^{3(ijkl)}$	$(\bar{l}_i \sigma^{\mu\nu} e_j)\, \varepsilon \, (\bar{q}_k \sigma_{\mu\nu} u_l)$
$O_{ud}^{1(ijkl)}$	$(\bar{u}_i \gamma^\mu u_j)(\bar{d}_k \gamma_\mu d_l)$	$\ddagger O_{ledq}^{(ijkl)}$	$(\bar{l}_i e_j)(\bar{d}_k q_l)$
$O_{ud}^{8(ijkl)}$	$(\bar{u}_i \gamma^\mu T^A u_j)(\bar{d}_k \gamma_\mu T^A d_l)$		
$\ddagger O_{quqd}^{1(ijkl)}$	$(\bar{q}_i u_j)\, \varepsilon \, (\bar{q}_k d_l)$		
$\ddagger O_{quqd}^{8(ijkl)}$	$(\bar{q}_i T^A u_j)\, \varepsilon \, (\bar{q}_k T^A d_l)$		
Two-quark operators		Baryon- and lepton-number-violating	
$\ddagger O_{u\varphi}^{(ij)}$	$\bar{q}_i u_j \tilde{\varphi} \, (\varphi^\dagger \varphi)$	$\ddagger O_{qqu}^{(ijkl)}$	$(\overline{q^c}_{i\alpha} \varepsilon q_{j\beta})(\overline{u^c}_{k\gamma} e_l)\, \epsilon^{\alpha\beta\gamma}$
$O_{\varphi q}^{1(ij)}$	$(\varphi^\dagger i \overleftrightarrow{D}_\mu \varphi)(\bar{q}_i \gamma^\mu q_j)$	$\ddagger O_{qqq}^{1(ijkl)}$	$(\overline{q^c}_{i\alpha} \varepsilon q_{j\beta})(\overline{q^c}_{k\gamma} \varepsilon l_l)\, \epsilon^{\alpha\beta\gamma}$
$O_{\varphi q}^{3(ij)}$	$(\varphi^\dagger i \overleftrightarrow{D}^I_\mu \varphi)(\bar{q}_i \gamma^\mu \tau^I q_j)$	$\ddagger O_{qqq}^{3(ijkl)}$	$(\overline{q^c}_{i\alpha} \tau^I \varepsilon q_{j\beta})(\overline{q^c}_{k\gamma} \tau^I \varepsilon l_l)\, \epsilon^{\alpha\beta\gamma}$
$O_{\varphi u}^{(ij)}$	$(\varphi^\dagger i \overleftrightarrow{D}_\mu \varphi)(\bar{u}_i \gamma^\mu u_j)$	$\ddagger O_{duu}^{(ijkl)}$	$(\overline{d^c}_{i\alpha} u_{j\beta})(\overline{u^c}_{k\gamma} e_l)\, \epsilon^{\alpha\beta\gamma}$
$\ddagger O_{\varphi ud}^{(ij)}$	$(\tilde{\varphi}^\dagger i D_\mu \varphi)(\bar{u}_i \gamma^\mu d_j)$		
$\ddagger O_{uW}^{(ij)}$	$(\bar{q}_i \sigma^{\mu\nu} \tau^I u_j)\, \tilde{\varphi} W^I_{\mu\nu}$		
$\ddagger O_{dW}^{(ij)}$	$(\bar{q}_i \sigma^{\mu\nu} \tau^I d_j)\, \varphi W^I_{\mu\nu}$		
$\ddagger O_{uB}^{(ij)}$	$(\bar{q}_i \sigma^{\mu\nu} u_j) \quad \tilde{\varphi} B_{\mu\nu}$		
$\ddagger O_{uG}^{(ij)}$	$(\bar{q}_i \sigma^{\mu\nu} T^A u_j)\, \tilde{\varphi} G^A_{\mu\nu}$		

In absence of evidence for physics beyond the SM at the weak scale or below, the Standard Model Effective Field Theory (SMEFT) [9–11] provides a simple and consistent framework to systematically parameterise possible deviations from the SM predictions in the interactions among the known particles, using minimal theoretical assumptions. It amounts to extend the Lagrangian of the SM, by all higher-dimensional operators that respect the gauge symmetry

$$
\mathcal{L}^{\text{SMEFT}} = \mathcal{L}^{\text{SM}} + \sum_{D>4} \sum_i^{N_D} \frac{C_i^{(D)} O_i^{(D)}}{\Lambda^{D-4}} \, , \tag{61.3}
$$

where D is the dimension of the operator $O_i^{(D)}$ and Λ provides an upper bound for the scale of new physics. An EFT model is generally characterised by power counting rules that identify a hierarchy among operators. In the case of the SMEFT, a minimal approach is considered where the large scale Λ provides a universal suppression factor for the higher dimensional operators.

The currently adopted parametrization for SMEFT interpretations of top quark measurements relies on the Warsaw basis of gauge-invariant dimension-six operators [11] and it is presented in Tab. 61.1 as detailed in Ref. [12] (see [13,14] for early discussions of top-quark related operators). For convenience, often specific degrees of freedom are identified from combinations of Warsaw-basis operator coefficients aligned with the directions of the EFT parameter space which appear in given processes, in interferences with SM amplitudes, and in top-quark interactions with some of the gauge boson mass eigenstates. Model implementations are available for tree-level and even one-loop Monte Carlo simulations.

The definitions of the SMEFT operators can be organised in four categories: Four-quark, two-quark, two-quark-two-lepton, and baryon-lepton-number violating operators. The overwhelming number of four-fermion operators is tamed by adopting simplifying assumptions about beyond-the-standard-model flavor structures. A baseline flavor scenario in the quark sector and motivated by the minimal flavor violation (MFV) ansatz [15–17] corresponds to imposing a $U(2)_q \times U(2)_u \times U(2)_d$ symmetry among the first two generations. In this case the following numbers of degrees of freedom are produced for the operators of each category of field content:

$$
\begin{array}{rl}
\text{four heavy quarks} & 11 + 2 \text{ CPV} \\
\text{two light and two heavy quarks} & 14 \\
\text{two heavy quarks and bosons} & 9 + 6 \text{ CPV} \\
\text{two heavy quarks and two leptons} & (8 + 3 \text{ CPV}) \times 3 \text{ lepton flavors}
\end{array}
$$

where we counted separately CP-conserving and CP-violating (CPV) parameters. They are collected in Table 61.1. Other less restricted scenarios, such as that obtained by imposing $U(2)_{q+u+d}$ symmetry featuring additional $10 + 10$ CPV degrees of freedom, or more restricted ones, such as *top-philic* scenario where it is assumed that new physics couples dominantly to the left-handed doublet and right-handed up-type quark singlet of the third generation as well as to bosons, featuring only 19+6 (CPV) degrees of freedom, are often considered. It is also customary to analyse top-quark flavor-changing neutral currents (FCNCs) separately as, at the tree level, they enter only quadratically. More details can be found in Ref. [12].

61.1.2 *Decay*

As other unstable elementary particles, the lifetime of the top quark, and therefore its width, is perturbatively calculable within the SM. With a mass above the Wb threshold, and $|V_{tb}| \gg |V_{td}|$, $|V_{ts}|$, the decay width of the top quark is expected to be dominated by the two-body channel $t \to Wb$. Neglecting terms of order m_b^2/m_t^2, α_s^2, and $(\alpha_s/\pi)M_W^2/m_t^2$, the width predicted in the SM at NLO is [18]:

$$
\Gamma_t = \frac{G_F m_t^3}{8\pi\sqrt{2}} \left(1 - \frac{M_W^2}{m_t^2}\right)^2 \left(1 + 2\frac{M_W^2}{m_t^2}\right) \left[1 - \frac{2\alpha_s}{3\pi}\left(\frac{2\pi^2}{3} - \frac{5}{2}\right)\right], \tag{61.4}
$$

where m_t refers to the top-quark pole mass. The order α_s^2 QCD corrections to Γ_t as well as the EW NLO corrections are known [19,20], thereby improving the overall theoretical accuracy to better than 1%. As a result, between $m_t = 170$ GeV and 175 GeV the width changes from 1.258 GeV to 1.394 GeV, with a linear dependence ($\alpha_s(M_Z) = 0.1179$ and $m_W = 80.377$ GeV). At the reference value of $m_t = 172.5$ GeV, $\Gamma_t = 1.326$ GeV.

With its correspondingly short lifetime of about 0.5×10^{-24} s, the top quark is expected to decay before top-flavored hadrons or $t\bar{t}$-quarkonium-bound states can form [21]. In fact, since the decay time is close to the would-be-resonance binding time, a peak will be visible in e^+e^- scattering at the $t\bar{t}$ threshold [22] and it is in principle present (yet very difficult to measure) in hadron collisions too [23, 24].

As mentioned above, flavor changing neutral interactions are allowed starting at one loop. The branching ratios to charm final state are estimated to be [25, 26]:

$$\mathrm{Br}^{\mathrm{SM}}(t \to gc) = 5 \cdot 10^{-12}, \mathrm{Br}^{\mathrm{SM}}(t \to gu) = 4 \cdot 10^{-14},$$
$$\mathrm{Br}^{\mathrm{SM}}(t \to \gamma c) = 5 \cdot 10^{-14}, \mathrm{Br}^{\mathrm{SM}}(t \to \gamma u) = 4 \cdot 10^{-16},$$
$$\mathrm{Br}^{\mathrm{SM}}(t \to Zc) = 1 \cdot 10^{-14}, \mathrm{Br}^{\mathrm{SM}}(t \to Zu) = 7 \cdot 10^{-17},$$
$$\mathrm{Br}^{\mathrm{SM}}(t \to Hc) = 3 \cdot 10^{-15}, \mathrm{Br}^{\mathrm{SM}}(t \to Hu) = 2 \cdot 10^{-17}.$$

61.1.3 *Production*

61.1.3.1 *Pair production*

In hadron collisions, top quarks are produced dominantly in pairs through the processes $q\bar{q} \to t\bar{t}$ and $gg \to t\bar{t}$, at leading order in QCD. At the Tevatron ($p\bar{p}$ at 1.96 TeV) approximately 85% of the production cross section is from $q\bar{q}$ annihilation, with the remainder from gluon-gluon fusion. Conversely, at the LHC about 90% (80%) of $t\bar{t}$ production is from gluon-gluon fusion at $\sqrt{s} = 13$ TeV ($\sqrt{s} = 7$ TeV).

Predictions for the top-quark production total cross sections are available at next-to-next-to leading order (NNLO) [27, 28], also including next-to-next-to-leading-log (NNLL) soft gluon resummation. Assuming a top-quark mass of 173.3 GeV, close to the Tevatron + LHC combination [29], the resulting theoretical prediction of the top-quark pair cross-section at NNLO+NNLL accuracy at the Tevatron at $\sqrt{s} = 1.96$ TeV is $\sigma_{t\bar{t}} = 7.16^{+0.11+0.17}_{-0.20-0.12}$ pb where the first uncertainty is from scale dependence and the second from parton distribution functions. At the LHC, assuming a top-quark mass of 172.5 GeV the cross sections are: $\sigma_{t\bar{t}} = 179.6^{+4.8+6.1}_{-6.2-6.1}$ pb at $\sqrt{s} = 7$ TeV, $\sigma_{t\bar{t}} = 256.0^{+6.7+8.0}_{-8.9-8.0}$ pb at $\sqrt{s} = 8$ TeV, $\sigma_{t\bar{t}} = 833.9^{+20.5+21.0}_{-30.0-21.0}$ pb at $\sqrt{s} = 13$ TeV, $\sigma_{t\bar{t}} = 923.6^{+22.6+22.8}_{-33.4-22.8}$ pb at $\sqrt{s} = 13.6$ TeV, and $\sigma_{t\bar{t}} = 985.7^{+24.1+24.1}_{-35.7-24.1}$ pb at $\sqrt{s} = 14$ TeV [27], where the first uncertainty is from scale dependence and the second from parton distribution functions and α_s.

The identification of $t\bar{t}$ events at a collider has to take into account that top quarks decay at microscopic scales and only their decay products can be detected. The final states for the leading pair-production process can be divided into three classes:

A. $t\bar{t} \to W^+ b\, W^- \bar{b} \to q\bar{q}'\, bq''\, \bar{q}'''\, \bar{b},$ (45.7%)
B. $t\bar{t} \to W^+ b\, W^- \bar{b} \to q\bar{q}'\, b\ell^- \bar{\nu}_\ell\, \bar{b} + \ell^+ \nu_\ell\, b\, q''\bar{q}'''\, \bar{b},$ (43.8%)
C. $t\bar{t} \to W^+ b\, W^- \bar{b} \to \ell^+ \nu_\ell\, b\, \ell'^- \bar{\nu}_{\ell'}\, \bar{b}.$ (10.5%)

The quarks in the final state evolve into jets of hadrons. A, B, and C are referred to as the all-hadronic, lepton+jets (ℓ+jets), and dilepton ($\ell\ell$) channels, respectively. Their relative contributions, including hadronic corrections, are given in parentheses assuming lepton universality. While ℓ in the above processes refers to e, μ, or τ, most of the analyses distinguish the e and μ from the τ channel, which is more difficult to reconstruct. Therefore, in what follows, we will use ℓ to refer to e or μ, unless otherwise noted. Here, typically leptonic decays of τ are included. In addition to the quarks resulting from the top-quark decays, extra QCD radiation (quarks and gluons) from the colored particles in the event can lead to extra jets.

The number of jets reconstructed in the detectors depends on the decay kinematics, as well as on the algorithm for reconstructing jets used by the analysis. Information on the transverse momenta, p_T of the neutrinos is obtained from the imbalance in transverse momentum measured in each event, the missing p_T, whose magnitude is also called missing transverse energy, E_T.

61.1.3.2 *Single top production*

Electroweak single top-quark production mechanisms, namely from $q\bar{q}' \to t\bar{b}$ [30], $qb \to q't$ [31], mediated by virtual s-channel and t-channel W-bosons, and Wt-associated production, through $bg \to W^-t$, lead to somewhat smaller cross sections. For example, t-channel production, while suppressed by the weak coupling with respect to the strong pair production, is kinematically enhanced, resulting in a sizeable cross section both at Tevatron and LHC energies. At the Tevatron, the t- and s-channel cross sections for top quarks are identical to those for antitop quarks, while at the LHC they are not, due to the charge-asymmetric initial state. NNLO cross sections for t-channel single top-quark production $(t + \bar{t})$ are calculated for $m_t = 173.2$ GeV to be $2.08^{+0.04+0.08}_{-0.03-0.10}$ pb in $p\bar{p}$ collisions at $\sqrt{s} = 1.96$ TeV, where the first uncertainty is from scale dependence and the second from parton distribution functions. [32]. A calculation at NNLO accuracy for the t-channel cross section at the LHC has first appeared in [33], superseded by more recent calculations [32, 34] which predict ($m_t = 172.5$ GeV): $\sigma_{t+\bar{t}} = 30.3^{+0.4+0.6}_{-0.3-0.4}$ pb at $\sqrt{s} = 5.02$ TeV, $\sigma_{t+\bar{t}} = 63.7^{+0.9+1.1}_{-0.5-0.7}$ pb at $\sqrt{s} = 7$ TeV, $\sigma_{t+\bar{t}} = 84.3^{+1.1+1.4}_{-0.7-0.9}$ pb at $\sqrt{s} = 8$ TeV, $\sigma_{t+\bar{t}} = 214.2^{+2.4+3.3}_{-1.7-2.0}$ pb at $\sqrt{s} = 13$ TeV, $\sigma_{t+\bar{t}} = 232.2^{+2.6+3.4}_{-1.7-2.2}$ pb at $\sqrt{s} = 13.6$ TeV, and $\sigma_{t+\bar{t}} = 244.5^{+2.7+3.5}_{-2.0-2.5}$ pb at $\sqrt{s} = 14$ TeV, where the first uncertainty is from scale dependence and the second from parton distribution functions and α_s. The corresponding fraction of top quarks are 67%, 65%, 65%, 63%, 62%, and 62%. For the s-channel, NNLO approximated calculations yield $1.03^{+0.05}_{-0.05}$ pb for the Tevatron [35]. An NNLO calculation gives $(t + \bar{t})$, $3.00^{+0.03}_{-0.03}$ pb, $3.61^{+0.03}_{-0.03}$ pb, $6.84^{+0.06}_{-0.03}$ pb, and $7.25^{+0.06}_{-0.04}$ pb, for $\sqrt{s} = 7, 8, 13, 13.6$ TeV at the LHC, respectively, where the uncertainty is from scale dependence only. While negligible at the Tevatron, at LHC energies Wt-associated production becomes relevant. At $\sqrt{s} = 7, 8, 13, 13.6, 14$ TeV, an NLO+NLL calculation gives $(t + \bar{t})$, $17.1^{+0.4+0.7}_{-0.3-0.7}$ pb, $24.4^{+0.6+0.9}_{-0.5-0.9}$ pb, $79.3^{+1.9+2.2}_{-1.8-2.2}$ pb, $87.9^{+2.0+2.3}_{-1.9-2.4}$ pb, and $93.8^{+2.2+2.5}_{-2.1-2.5}$ pb, respectively, where the first uncertainty is from scale dependence and the second from parton distribution functions and α_s. In this process, an equal proportion of top and anti-top quarks is foreseen. [36].

Assuming $|V_{tb}| \gg |V_{td}|, |V_{ts}|$ (see the Section "The CKM Quark-Mixing Matrix" in this *Review* for more information), the cross sections for single top production are proportional to $|V_{tb}|^2$, and no extra hypothesis is needed on the number of quark families or on the unitarity of the CKM matrix in extracting $|V_{tb}|$. Separate measurements of the s- and t-channel processes provide sensitivity to physics beyond the Standard Model [37].

The identification of top quarks in the electroweak single top channel is much more difficult than in the QCD $t\bar{t}$ channel, due to a less distinctive signature and significantly larger backgrounds, mostly due to $t\bar{t}$ and W+jets production.

61.1.3.3 *Monte Carlo predictions*

Fully exclusive predictions via Monte Carlo generators for the $t\bar{t}$ and single top production processes at NLO accuracy in QCD, including top-quark decays and possibly off-shell effects are available [38,39] through the MC@NLO [40] and POWHEG [41] methods. Recently, the first Monte Carlo implementation of the NNLO QCD computation has become available [42].

61.1.3.4 *Associated production*

Besides fully inclusive QCD or EW top-quark production, more exclusive final states can be accessed at hadron colliders, whose cross sections are typically much smaller, yet can provide key information on the properties of the top quark. For all relevant final states (*e.g.*, $t\bar{t}V$, $t\bar{t}VV$ with

$V = \gamma, W, Z, t\bar{t}H, t\bar{t}+\text{jets}, t\bar{t}b\bar{b}, t\bar{t}t\bar{t}$) automatic or semi-automatic predictions at NLO accuracy both in QCD and EW expansions, also in the form of event generators are available (see the review "Monte Carlo event generators" for more information). Results for total cross sections at NLO+NLL in QCD and NLO EW, are available for $t\bar{t}Z, t\bar{t}W, t\bar{t}H$ [43] and for $t\bar{t}t\bar{t}$ [44]. Recently, approximate NNLO QCD predictions for and $t\bar{t}H$ and $t\bar{t}W$ have become available [45, 46].

61.2 Top-quark and precision SM tests

Since the discovery of the top quark, direct measurements of $t\bar{t}$ production have been made at seven center-of-mass energies in pp or $p\bar{p}$ and in pPb or $PbPb$ collisions, providing stringent tests of QCD and electroweak theory including parton distribution functions, the strong coupling α_s and the dependence on the top-quark mass m_{top}. The first measurements were made in Run I at the Tevatron at $\sqrt{s} = 1.8$ TeV. In Run II at the Tevatron relatively precise measurements were made at $\sqrt{s} = 1.96$ TeV. Finally, beginning in 2010, measurements have been made at the LHC at $\sqrt{s} = 7$ TeV, $\sqrt{s} = 8$ TeV, and $\sqrt{s} = 13$ TeV, later also in dedicated low energy runs at $\sqrt{s} = 5.02$ TeV in pp and at $\sqrt{s} = 5.02$ TeV in $PbPb$ collisions and at 8.16 TeV in pPb collisions and recently at $\sqrt{s} = 13.6$ TeV in pp. With the enormous number of over 120 million top quark pairs produced at the LHC, we are entering the era of high precision measurements in the top quark sector.

Production of single top quarks through electroweak interactions has now been measured with good precision at the Tevatron at $\sqrt{s} = 1.96$ TeV, and at the LHC at $\sqrt{s} = 5$ TeV, $\sqrt{s} = 7$ TeV, $\sqrt{s} = 8$ TeV, and also at $\sqrt{s} = 13$ TeV. Measurements at the Tevatron have managed to separate the s- and t-channel production cross sections, and at the LHC, the tW mechanism as well, though the t-channel is measured with best precision to date. The measurements allow an extraction of the CKM matrix element V_{tb}. Also more exclusive production modes and top-quark properties have been measured in single-top production.

With approximately 10 fb^{-1} of Tevatron data, and 255 pb^{-1} at 5 TeV, almost 5 fb^{-1} at 7 TeV, 20 fb^{-1} at 8 TeV, 139 fb^{-1} at 13 TeV and 29 fb^{-1} at 13.6 TeV at the LHC, many properties of the top quark have been measured with high precision. These include properties related to the production mechanism, such as $t\bar{t}$ spin correlations, forward-backward or charge asymmetries, and differential production cross sections, as well as properties related to the tWb decay vertex, such as the helicity of the W-bosons from the top-quark decay. Also studies of the $t\bar{t}b\bar{b}, t\bar{t}t\bar{t}, t\bar{t}\gamma, t\bar{t}Z$, $t\bar{t}h, th, tZq, t\gamma q$ or tWZ processes and the corresponding vertices as well as contact interactions have been made, most yielding observations, while first evidence for tWZ has been found and th is still far from evidence. Those processes probe genuinely new aspects of the top-quark such as electroweak couplings to neutral gauge bosons or possibly four-top-quark production via contact interactions. Recently, also first studies for the very fundamental concept of quantum entanglement in top-quark production were pursued. In addition, many searches for physics beyond the Standard Model are being performed with increasing reach in both production and decay channels.

In the following sections we review the current status of measurements of the characteristics of the top quark.

61.2.1 *Top-quark production*
61.2.1.1 *$t\bar{t}$ production*

Fig. 61.1 summarizes the $t\bar{t}$ production cross-section measurements from both, the Tevatron and LHC. Please note that some cross section measurements at the LHC have luminosity-related uncertainties which have improved in the meantime [47]. The latest measurement from DØ [48] ($p\bar{p}$ at $\sqrt{s} = 1.96$ TeV), combining the measurements from the dilepton and lepton plus jets final states in 9.7 fb^{-1}, is 7.26 ± 0.13 (stat.)$^{+0.57}_{-0.50}$ (syst.) pb (7.5%). From CDF the most precise measurement made [49] is in 8.8 fb^{-1} in the dilepton channel requiring at least one b-tag, yielding

7.09 ± 0.84 pb. Both of these measurements assume a top-quark mass of 172.5 GeV/c^2. The dependence of the cross-section measurements on the value chosen for the mass is less than that of the theory calculations because it only affects the determination of the acceptance. In some analyses also the shape of topological variables might be modified.

Combining the recent cross section measurements with older ones in other channels yields $\sigma_{t\bar{t}} = 7.63 \pm 0.50$ pb (6.6%) for CDF, $\sigma_{t\bar{t}} = 7.56 \pm 0.59$ pb (7.8%) for DØ and $\sigma_{t\bar{t}} = 7.60 \pm 0.41$ pb (5.4%) for the Tevatron combination [50]. The contributions to the uncertainty are 0.20 pb from statistical sources, 0.29 pb from systematic sources, and 0.21 pb from the uncertainty on the integrated luminosity. The combined result is in good agreement with the SM expectation of $7.35^{+0.28}_{-0.33}$ pb at NNLO+NNLL in perturbative QCD [27] for a top mass of 172.5 GeV/c^2.

CDF has measured the $t\bar{t}$ production cross section in the dilepton channel with one hadronically decaying tau in 9.0 fb^{-1}, yielding $\sigma_{t\bar{t}} = 8.1 \pm 2.1$ pb. By separately identifying the single-tau and the ditau components, they measure the branching fraction of the top quark into the tau lepton, tau neutrino, and bottom quark to be $(9.6 \pm 2.8)\%$ [51]. CDF has also performed measurements of the $t\bar{t}$ production cross section normalized to the Z production cross section in order to reduce the impact of the luminosity uncertainty [52].

DØ has performed a measurement of differential $t\bar{t}$ cross sections in 9.7 fb^{-1} of lepton+jets data as a function of the transverse momentum, and absolute value of the rapidity of the top quarks as well as of the invariant mass of the $t\bar{t}$ pair [53]. Observed differential cross sections are consistent with SM predictions.

The LHC experiments ATLAS and CMS use similar techniques to measure the $t\bar{t}$ cross section in pp collisions. The most precise measurements typically come from the dilepton channel, and in particular the $e\mu$ channel. In order to test consistency of the cross-section measurements with some systematic uncertainties cancelling out while testing pQCD and PDFs, cross-section ratios between measurements at 7 TeV and at 8 TeV are performed and quoted in several cases. In other cases, the cross-section ratio between $t\bar{t}$- and Z-production is determined as that is independent of luminosity uncertainties, but keeps its sensitivity to the ratio of gluon versus quark PDFs. These experimental results should be compared to the theoretical calculations at NNLO+NNLL that yield $7.16^{+0.20}_{-0.23}$ pb for top-quark mass of 173.3 GeV/c^2 at $\sqrt{s} = 1.96$ TeV' [27], for top-quark mass of 172.5 GeV/c^2 $\sigma_{t\bar{t}} = 68.2^{+5.2}_{-15.4}$ pb at $\sqrt{s} = 5$ TeV [54], $\sigma_{t\bar{t}} = 158^{+23}_{-24}$ pb at $\sqrt{s} = 7$ TeV [55, 56], $\sigma_{t\bar{t}} = 253^{+13}_{-15}$ pb at $\sqrt{s} = 8$ TeV [27, 54, 57–60], $\sigma_{t\bar{t}} = 832.0^{+46}_{-51}$ pb at $\sqrt{s} = 13$ TeV [27, 54, 58–60], $\sigma_{t\bar{t}} = 924^{+32}_{-40}$ pb at $\sqrt{s} = 13.6$ TeV [27, 57–61]. Unless noted otherwise, the theoretical prediction is in agreement with the measurements. Both are aiming for further improvements in precision. The exact details of the measurements such as the top-quark mass assumption at which the cross section values are quoted can be found in the original publications.

$\sqrt{s} = \textbf{5.02 TeV measurements:}$ In a special run, ATLAS recorded 257 pb^{-1}. The $t\bar{t}$ cross-section is measured in both the dilepton and single-lepton final states of the $t\bar{t}$ system and then combined. The combination of the two measurements yields $\sigma_{t\bar{t}} = 67.5 \pm 0.9(stat.) \pm 2.3(syst.) \pm 1.1(lumi.) \pm 0.2(beam)$ pb [62], giving a total uncertainty of 3.9%. The result is in agreement with theoretical QCD calculations at NLO in the strong coupling constant, including the resummation of NNLL soft-gluon terms, and constrains the parton distribution functions of the proton at large Bjorken-x. CMS has measured the $t\bar{t}$ production cross section, accumulating 27.4 pb^{-1} of data. The measurement is performed by analyzing events with at least one charged lepton. The measured cross section is $\sigma_{t\bar{t}} = 69.5 \pm 8.4$ pb [63], with a relative precision of 12%, in agreement with the expectation from the Standard Model. The impact of the presented measurement on the determination of the gluon distribution function is also investigated. In addition, they performed a measurement in opposite-sign $e\mu$-dilepton events with at least two jets using 302 pb^{-1}. They obtain a Drell-Yan scale factor under the Z-boson mass to estimate the background and extract

a cross section using a counting technique of $\sigma_{t\bar{t}} = 60.7 \pm 5.0(stat) \pm 2.8(syst) \pm 1.1(lumi)$ pb. A combination with the result in the single lepton + jets channel is performed, yielding $\sigma_{t\bar{t}} = 63.0 \pm 4.1(stat) \pm 3.0(syst + lumi)$ pb [64].

$\sqrt{s} = 7$ **TeV measurements:** At $\sqrt{s} = 7$ TeV, ATLAS uses the full dataset of 4.6 fb^{-1} of $e\mu$ events, yielding $\sigma_{t\bar{t}} = 182.9 \pm 7.1$ pb, corresponding to 3.9% precision [65]. Other measurements by ATLAS include a measurement in 0.7 fb^{-1} in the lepton+jets channel [66], in the dilepton channel [67], and in 1.02 fb^{-1} in the all-hadronic channel [68], which together yield a combined value of $\sigma_{t\bar{t}} = 177 \pm 3(stat.)^{+8}_{-7}(syst.) \pm 7(lumi.)$ pb (6.2%) [69]. Further analyses in the hadronic τ plus jets channel in 1.67 fb^{-1} [70] and the hadronic τ + lepton channel in 2.05 fb^{-1} [71], and the all-hadronic channel in 4.7 fb^{-1} [72] yield consistent albeit less precise results. Recently, ATLAS performed a cross section measurement in the lepton+jets channel using 4.6 fb^{-1} using a three-class, multidimensional event classifier based on support vector machines to differentiate $t\bar{t}$ events from $W/Z + b\bar{b}$ and other background processes, yielding $\sigma_{t\bar{t}} = 168.5 \pm 0.7(stat.)^{+6.2}_{-5.9}(syst.)^{+3.4}_{-3.2}(lumi.)$ pb [73].

CMS measures the $t\bar{t}$ cross section in the dilepton channel using 2.3 fb^{-1} to $\sigma_{t\bar{t}} = 161.9 \pm 2.5(stat.)^{+5.1}_{-5.0}(syst.) \pm 3.6(lumi.)$ pb, corresponding to a 4.2% precision [74]. The most precise measurement from CMS is also obtained in the dilepton channel using 5 fb^{-1}, where they measure $\sigma_{t\bar{t}} = 173.6 \pm 2.1(stat.)^{+4.5}_{-4.0}(syst.) \pm 3.8(lumi.)$ pb, corresponding to a 3.6% precision [75]. Other measurements use 2.3 fb^{-1} in the e/μ+jets channel [76], with 3.5 fb^{-1} in the all-hadronic channel [77], with 2.2 fb^{-1} in the lepton+τ channel [78], and with 3.9 fb^{-1} in the τ+jets channel [79]. ATLAS and CMS also provide a legacy combined cross section of $\sigma_{t\bar{t}} = 178.5 \pm 4.7$ pb using 5 fb^{-1}, yielding a precision of 2.6% [80].

$\sqrt{s} = 8$ **TeV measurements:** At $\sqrt{s} = 8$ TeV, ATLAS measures the $t\bar{t}$ cross section with 20.3 fb^{-1} using $e\mu$ dilepton events, with a simultaneous measurement of the $b-$tagging efficiency, yielding $\sigma_{t\bar{t}} = 242.9 \pm 1.7(stat.) \pm 5.5(syst.) \pm 5.1(lumi.) \pm 4.2(beam\,energy)$ pb [81] (3.6% precision). In the $\ell + jets$ channel, they measure $\sigma_{t\bar{t}} = 260 \pm 1(stat.)^{+20}_{-23}(syst.) \pm 8(lumi.) \pm 4(beam\,energy)$ pb [82] in 20.3 fb^{-1} using a likelihood discriminant fit and b-jet identification. Subsequently, ATLAS performed a new analysis in 20.2 fb^{-1} using $\ell + jets$ events. They model the W+jets background using Z+jets data and employ neural networks in three jet-multiplicity and b-jet multiplicity regions for the signal and background separation, yielding $\sigma_{t\bar{t}} = 248.3 \pm 0.7(stat.) \pm 13.4(syst.) \pm 4.7(lumi.)$ pb [83]. ATLAS also performed a cross section measurement in the hadronic τ+jets channel yielding consistent, albeit less precise results [84].

CMS performs a template fit to the M_{lb} mass distribution using 19.6 fb^{-1} in the lepton+jets channel yielding $\sigma_{t\bar{t}} = 228.5 \pm 3.8(stat.) \pm 13.7(syst.) \pm 6.0(lumi.)$ pb [85] (6.7% precision). In the $e\mu$ channel, initially using 5.3 fb^{-1} [86] the cross sections are extracted using a binned likelihood fit to multi-differential final state distributions related to identified b quark and other jets in the event, yielding $\sigma_{t\bar{t}} = 239 \pm 2(stat.) \pm 11(sys.) \pm 6(lumi.)$ pb (5.3% precision). Later, they also use the full dataset of 19.7 fb^{-1}, yielding $\sigma_{t\bar{t}} = 244.9 \pm 1.4(stat)^{+6.3}_{-5.5}(syst) \pm 6.4(lumi)$ pb (3.7% precision) [75]. This most precise CMS measurement at 8 TeV is also used to determine the top pole mass and set SUSY limits. The cross section is also measured in the hadronic τ+jets channel, yielding $\sigma_{t\bar{t}} = 257 \pm 3(stat.) \pm 24(syst.) \pm 7(lumi.)$ pb [87] and in the all-hadronic final state giving $\sigma_{t\bar{t}} = 275.6 \pm 6.1(stat.) \pm 37.8(syst.) \pm 7.2(lumi.)$ pb [88]. In combination of the most precise $e\mu$ measurements in 5.3 − 20.3 fb^{-1}, ATLAS and CMS together yield $\sigma_{t\bar{t}} = 241.5 \pm 1.4(stat.) \pm 5.7(syst.) \pm 6.2(lumi.)$ pb [89] (3.5% precision), challenging the precision of the corresponding theoretical predictions. ATLAS and CMS also provide a legacy combined cross section of $\sigma_{t\bar{t}} = 243.3^{+6.0}_{-5.9}$ pb using 20 fb^{-1} (2.5% precision) [80]. The combinations also provide the ratio between cross sections at 8 and 7 TeV, the top quark pole mass, and the strong coupling.

The LHCb collaboration presented the first observation of top-quark production in the forward region in pp-collisions in the e+jets or μ+jets channel. The results are based on data corresponding

to integrated luminosities of 1.0 and 2.0 fb^{-1} collected at center-of-mass energies of 7 and 8 TeV by LHCb. The inclusive top quark production cross sections in the fiducial region are $\sigma_{t\bar{t}} = 239 \pm 53(stat.) \pm 38(syst.)$ pb at 7 TeV, and $\sigma_{t\bar{t}} = 289 \pm 43(stat.) \pm 46(syst.)$ pb at 8 TeV [90].

$\sqrt{s}$ = **13 TeV** **measurements:** In 36.1 fb^{-1} of $e\mu$ data with one or two b-tags, ATLAS measures $\sigma_{t\bar{t}} = 826.4 \pm 3.6(stat.) \pm 11.5(syst.) \pm 15.7(lumi.) \pm 1.9(beam)$ pb (2.4% precision). This measurement is also used to determine the top quark pole mass and to derive ratios and double ratios of $t\bar{t}$ and Z cross-sections at different energies as well as absolute and normalised differential cross-sections as functions of single lepton and dilepton kinematic variables [91]. In the $\ell + jets$ channel, using 85 pb^{-1}, the cross-section is extracted by counting the number of events with exactly one e or μ and at least four jets, at least one of which is identified as originating from a b-quark, yielding $\sigma_{t\bar{t}} = 817 \pm 13(stat.) \pm 103(syst.) \pm 88(lumi.)$ pb [92]. Later, ATLAS measures the inclusive $t\bar{t}$ cross section in 139 fb^{-1} in the $\ell + jets$ through a profile-likelihood fit to be $\sigma_{t\bar{t}} = 830.4 \pm 0.4(stat.) \pm 36(syst.) \pm 14(lumi)$ pb (4.6% precision) [93].

Recently, using the complete Run-2 dataset of 140 fb^{-1} in events containing an oppositely charged $e\mu$ pair and b-tagged jets, ATLAS has presented their legacy measurement of $\sigma_{t\bar{t}} = 829 \pm 1(stat) \pm 13(syst) \pm 8(lumi) \pm 2(beam)$ pb [94], corresponding to a precision of 1.8%. They also measure differential and double-differential distributions of kinematic variables of leptons from decays of top-quark pairs. The results are compared with predictions from several Monte Carlo generators. While no prediction is found to be consistent with all distributions, a better agreement with measurements of the lepton p_T distributions is obtained by reweighting the $t\bar{t}$ sample so as to reproduce the top-quark p_T distribution from an NNLO calculation.

Using 35.9 fb^{-1} of dilepton data, they use a likelihood fit and yield $\sigma_{t\bar{t}} = 803 \pm 2(stat.) \pm 25(syst.) \pm 20(lumi.)$ pb (4.0%). This result is also used to extract the top quark mass in both the pole and the $\overline{\text{MS}}$ schemes at NNLO and the strong coupling constant [95]. Using the same dataset in the dilepton channel with a hadronically decaying τ, they measure $\sigma_{t\bar{t}} = 781 \pm 7(stat.) \pm 62(syst.) \pm 20(lumi.)$ pb (8.3%) [96]. A first measurement of the total inclusive and the normalized differential cross section in the $\ell + jets$ channel is made in 42 pb^{-1} yielding $\sigma_{t\bar{t}} = 836 \pm 27(stat.) \pm 88(syst.) \pm 100(lumi.)$ pb [97]. Using 2.2 fb^{-1} of data, $\ell + jets$ events are categorized according to the accompanying jet multiplicity. From a likelihood fit to the invariant mass distribution of the isolated lepton and a b-jet, the cross section is measured to be $\sigma_{t\bar{t}} = 888 \pm 2(stat.)^{+26}_{-28}(syst.) \pm 20(lumi)$ pb [98]. This result is also used to extract the top-quark mass. Using the full Run-2 dataset of 137 pb^{-1}, CMS measures the $t\bar{t}$ cross section in four regions determined by top p_T and b-tag score in the $\ell + jets$ channel. They employ a combined χ^2 fit considering the migration matrices. Most of the measured differential cross sections are well described by standard model predictions with the exception of some double-differential distributions. They obtain $\sigma_{t\bar{t}} = 791 \pm 1(stat.) \pm 21(syst.) \pm 14(lumi)$ pb (3.2%) [99]. In the all-hadronic channel, CMS uses 2.53 fb^{-1} of data, yielding a cross section of $\sigma_{t\bar{t}} = 834 \pm 25(stat.)^{+118}_{-104}(syst.) \pm 23(lumi.)$ pb [100]. Also differential cross sections as a function of the leading top quark transverse momentum are measured. Very recently, CMS presents a first search for the central exclusive production of $t\bar{t}$ pairs using proton-tagged events, using 29.4 fb^{-1}. The $t\bar{t}$ decay products are reconstructed using the central CMS detector, while forward protons are measured in the CMS-TOTEM precision proton spectrometer. An observed (expected) upper bound on the production cross section of 0.59 (1.14) pb [101] is set at 95% confidence level, for collisions of protons with fractional momentum losses between 2 and 20%.

Using 1.93 fb^{-1}, LHCb studies forward top quark pair production in pp collisions in the μeb final state. The cross-section is measured in a fiducial region defined by both leptons transverse momenta and pseudorapidities as well as their angular separation, the b-jet transverse momentum and its angular separation from the leptons, yielding $\sigma_{t\bar{t}} = 126 \pm 19(stat.) \pm 16(syst.) \pm 5(lumi)$ fb [102].

$\sqrt{s} = 13.6$ **TeV measurements:** Being one year into the Run-3 data taking at $\sqrt{s} = 13.6$ TeV with an expected increase in the $t\bar{t}$ cross section by approximately 10%, both experiments, ATLAS and CMS, present the first $t\bar{t}$ cross section measurements already.

ATLAS uses 29 fb^{-1} of data in events with an opposite-charge $e\mu$ pair and b-tagged jets to obtain $\sigma_{t\bar{t}} = 850 \pm 3(stat.) \pm 18(syst.) \pm 20(lumi.)$ pb. Simultaneously, the Z-boson cross section is determined for inclusive e^+e^- and $\mu^+\mu^-$ events in a fiducial phase space, taking cancellation of several systematic uncertainties into account yielding for the ratio $R_{t\bar{t}/Z} = 1.145 \pm 0.003(stat.) \pm 0.021(syst.) \pm 0.002(lumi.)$ [103].

CMS presents the first measurement at this energy using 1.21 fb^{-1} in events with one or two charged leptons (e or μ) and additional jets. A maximum likelihood fit is performed in event categories defined by the number and flavors of the leptons, the number of jets, and the number of jets identified as originating from b quarks. An inclusive $t\bar{t}$ production cross section of $881 \pm 23(stat + syst) \pm 20(lumi)$ pb is measured [104].

proton-lead pPb and lead-lead $PbPb$ heavy ion collision measurements: CMS establishes first evidence for the production of top-quark pairs in $PbPb$ collision data at a nucleon-nucleon center-of-mass energy of 5.02 TeV using evens with charged leptons (electrons or muons) and bottom quarks. They obtain $\sigma_{t\bar{t}} = 2.54^{+0.84}_{-0.74}$ μb [105]. CMS also performed a measurement of top-quark pair production in proton-lead pPb heavy ion collisions at $\sqrt{s} = 8.16$ TeV in 174 nb^{-1} of lepton+jets events. They measure a cross section of $\sigma_{t\bar{t}} = 45 \pm 8$ nb [106]. Recently, also ATLAS presents a $t\bar{t}$ cross section measurement in 165 nb^{-1} of pPb collisions at $\sqrt{s} = 8.16$ TeV in the lepton+jets and the dilepton channels, with a significance well over 5 standard deviations in both channels separately, yielding a combination of $\sigma_{t\bar{t}} = 57.9 \pm 2.0(stat.)^{+4.9}_{-4.5}(syst.)$ nb (9%) [107]. Both measurements are consistent with pQCD calculations and with the scaled pp data.

In Fig. 61.1, one sees the importance of $p\bar{p}$ at Tevatron energies where the valence antiquarks in the antiprotons contribute to the dominant $q\bar{q}$ production mechanism. At LHC energies, the dominant production mode is gluon-gluon fusion and the pp-$p\bar{p}$ difference nearly disappears. The excellent agreement of these measurements with the theory calculations is a strong validation of QCD and the soft-gluon resummation techniques employed in the calculations. The measurements reach high precision and provide stringent tests of pQCD calculations at NNLO+NNLL level including their respective PDF uncertainties.

Most of these measurements assume a $t \to Wb$ branching ratio of 100%. CDF and DØ have made direct measurements of the $t \to Wb$ branching ratio [108, 109]. Comparing the number of events with 0, 1 and 2 tagged b jets in the lepton+jets channel, and also in the dilepton channel, using the known b-tagging efficiency, the ratio $R = B(t \to Wb)/\sum_{q=d,s,b} B(t \to Wq)$ can be extracted. In 5.4 fb^{-1} of data, DØ measures $R = 0.90 \pm 0.04$, which is 2.5 standard deviations from unity. The currently most precise measurement was made by CMS in 19.7 fb^{-1} at $\sqrt{s} = 8$ TeV. They find $R = 1.014 \pm 0.003(stat.) \pm 0.032(syst.)$ and $R > 0.955$ at 95% C.L. [110]. A significant deviation of R from unity would imply either non-SM top-quark decay (for example a flavor-changing neutral-current decay), or a fourth generation of quarks. The latter is excluded by other measurements.

61.2.1.2 *Differential $t\bar{t}$ cross sections*

Thanks to the large available event samples, the Tevatron and the LHC experiments also performed single-, double- or recently even triple-differential cross-section measurements in $t\bar{t}$ production. Such measurements are crucial, as they allow even more stringent tests of perturbative QCD as description of the production mechanism, and allow along with other data the extraction of PDFs in PDF fits. In addition, they enhance the sensitivity to possible new physics contributions, especially now that NNLO predictions for the main differential observables in $t\bar{t}$ prediction have
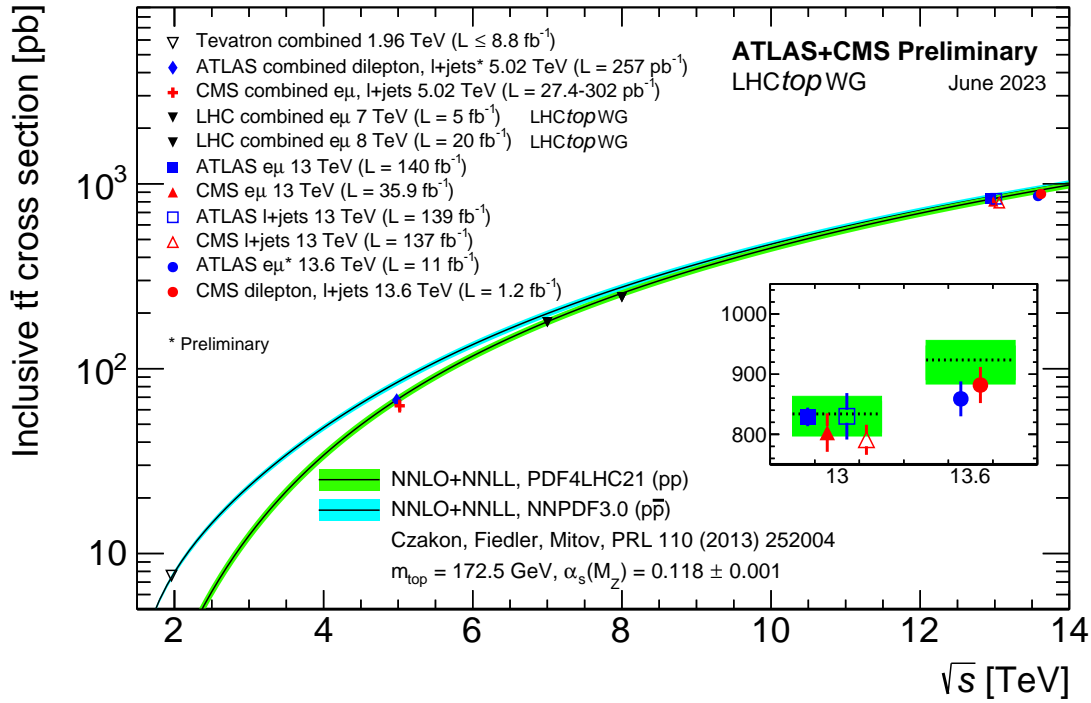
Figure 61.1: Measured and predicted $t\bar{t}$ production cross sections from Tevatron energies in $p\bar{p}$ collisions to LHC energies in *pp* collisions. The plot is kindly provided by the LHCtopWG working group, status as of June 2023, see https://twiki.cern.ch/twiki/bin/view/LHCPhysics/LHCTopWGSummaryPlots.

become available [111] and later confirmed [28]. Furthermore, such measurements reduce the uncertainty in the description of $t\bar{t}$ production as background in Higgs physics and searches for rare processes or beyond Standard Model physics.

Differential cross sections are typically measured by a selection of candidate events, their kinematic reconstruction and subsequent unfolding of the obtained event counts in bins of kinematic distributions in order to correct for detector resolution effects, acceptance and migration effects. In some cases a bin-by-bin unfolding is used, while other analyses use more sophisticated techniques. Most commonly used unfolding techniques are the iterative Bayesian unfolding (IBU) [112] as implemented in the `RooUnfold` package [113] and the profile-likelihood unfolding [114] [115], but also a singular value composition approach [116] or maximum likelihood fit methods [117] are used. As general feature across channels, it is found that the measured top quark p_T spectrum is significantly softer than the NLO+PS theory predictions considered in the corresponding publications.

$\sqrt{s} = 7$ **TeV measurements:** At $\sqrt{s} = 7$ TeV, ATLAS and CMS measure single-differential $t\bar{t}$ cross sections with respect to jet multiplicity, the top-quark transverse momentum, and of the mass, transverse momentum and rapidity of the top quark, the antitop quark as well as the $t\bar{t}$ system or kinematic properties of the final-state charged leptons and jets associated to *b*-quarks. While CMS finds in general good agreement with the pQCD calculations [118–120], ATLAS finds the data to be softer, in particular in the $t\bar{t}$ mass and the top-quark p_T than the `Alpgen+Herwig` generator. Also some disagreement in the rapidity spectrum is observed indicating a preference for the HERAPDF1.5 pdf set over CT10 [121–123].

$\sqrt{s} = $ **8 TeV measurements:** At $\sqrt{s} = 8$ TeV, ATLAS measures single-differential cross sections in the dilepton and lepton+jets channel with respect to the mass, the transverse momentum and the rapidity of the $t\bar{t}$ system and event-level kinematic observables [124] [125]. The results are consistent or in fair agreement with the predictions over a wide kinematic range. Predictions beyond NLO accuracy improve the agreement with data at high top-quark transverse momenta. Using the current settings in the Monte Carlo programs and parton distribution functions, improve the agreement with the rapidity distributions. ATLAS also performs a dedicated differential $t\bar{t}$ cross-section measurement of highly boosted top quarks in the lepton+jets channel, where the hadronically decaying top quark has a transverse momentum above 300 GeV [126]. Jet substructure techniques are employed to identify top quarks, which are reconstructed with an anti-k_t jet with a radius parameters $R = 1.0$. The predictions of NLO and LO matrix element plus parton shower Monte Carlo generators are found to generally overestimate the measured cross sections.

CMS measures normalized differential cross sections for $t\bar{t}$ production in lepton+jets events with respect to four kinematic event variables: the missing transverse energy; the scalar sum of the jet transverse momentum (p_T); the scalar sum of the p_T of all objects in the event; and the p_T of leptonically decaying W bosons from top quark decays [119]. Using 19.7 fb^{-1}, they measure the normalized differential cross section in the lepton+jets (e/μ+jets) and in the dilepton (e^+e^-, $\mu^+\mu^-$, and $e^\pm\mu^\pm$) decay channels as a function of the kinematic properties of the charged leptons, the jets associated to b quarks, the top quarks, and the $t\bar{t}$ system. The data are compared with several predictions from perturbative QCD up to approximate next-to-next-to-leading-order precision [127]. Using the same dataset, in the dilepton $e\mu$ channel, they measure normalized double-differential cross sections for $t\bar{t}$ production as a function of various pairs of observables characterizing the kinematics of the top quark and $t\bar{t}$ system [128]. This result has a significant impact on the gluon distribution when included in PDF fits. Overall agreement is observed with the predictions, which is improved when the latest parton distribution functions are used [128]. They also perform a dedicated boosted-top analysis in the e or μ+jets channel where the hadronically decaying top quark is reconstructed as a single large-radius jet and identified as a top candidate using jet substructure techniques [129].

$\sqrt{s} = $ **13 TeV measurements:** At $\sqrt{s} = 13$ TeV, ATLAS measures the differential $t\bar{t}$ cross section in the lepton+jets and the dilepton channel as a function of the transverse momentum and absolute rapidity of the top quark, and of the transverse momentum, absolute rapidity and invariant mass of the $t\bar{t}$ system [130] [131] [91]. They find in general good agreement with the theory models with the exception of the `Powheg-Box`+ `Herwig++` predictions, which differ significantly from the data in both the transverse momentum of the top quark and the mass of the $t\bar{t}$ system. ATLAS measures the single- and double-differential $t\bar{t}$ cross-section in the lepton + jets channel at particle and parton level. Two topologies, resolved and boosted, are considered [132]. In the all-hadronic channel, measurements are presented in the boosted regime [133] as well as in the resolved regime with six separately resolved jets [134].

Using the full Run-2 datset of 140 fb^{-1}, ATLAS measures differential cross sections in the $\ell + jets$ channel and fully hadronic channels in a boosted topology with at least one large-R "top-jet" from a hadronic decay with high-p_T, also as a function of variables that characterise the additional radiation in the events [135]. The measured distribution of the top-quark p_T is used to set limits on the Wilson coefficients describing physics beyond the standard model. The modelling of the additional radiation events show some mild disagreements to the data. Further differential cross-section measurements were made that are specifically useful for MC generator tuning. This includes the ATLAS measurement of the one- and two-dimensional differential cross-sections for eight substructure variables, defined using only the charged components of the jets, in a particle-level phase space by correcting for the smearing and acceptance effects induced by the

detector [136] [94]. The QCD predictions for measures of energy-flow are found to be in good agreement with the measurements while variables sensitive to the three-body structure of the top-quark jets exhibit some tensions with the measured distributions. In another example, a measurement of observables sensitive to effects of color reconnection in top-quark pair-production events is presented, in particular for the charged-particle multiplicity, the scalar sum of the transverse momenta of the charged particles, and the same scalar sum in bins of charged-particle multiplicity. These observables are unfolded to the stable-particle level. The particle-level measurements are compared with different color reconnection models in Monte Carlo generators. These measurements disfavour some of the color reconnection models and provide inputs to future optimisation of the parameters in Monte Carlo generators [137]. Furthermore, several observables sensitive to the fragmentation of b-quarks into b-hadrons are measured. Jets containing b-hadrons are used to construct observables that characterize the longitudinal and transverse momentum distributions of the b-hadron within the jet. The measurements have been corrected for detector effects and provide a test of heavy-quark-fragmentation modeling at the LHC in a system where the top-quark decay products are color-connected to the proton beam remnants. The unfolded distributions are compared with the predictions of several modern Monte Carlo parton-shower generators and generator tunes, and a wide range of agreement with the data is observed. These measurements complement similar measurements from e^+e^- collider experiments in which the b-quarks originate from a color-singlet Z/γ^* [138].

CMS measures single- and double-differential $t\bar{t}$ cross sections in the dilepton and the lepton+jets channel as a function of the kinematic properties of the leptons, jets from bottom quark hadronization, top quarks, and top quark pairs and jet multiplicity [139–144]. While in general good agreement is observed, in a dilepton analysis, significant disagreement is observed between data and all predictions for several observables. The measurements are used to constrain the top quark chromomagnetic dipole moment in an effective field theory framework at NLO in QCD and to extract $t\bar{t}$ and leptonic charge asymmetries [145]. In a later dilepton channel analysis, even a triple-differential measurement is performed as a function of the invariant mass and rapidity of the $t\bar{t}$ system and the multiplicity of additional jets at particle level. The measurement is used to extract the strong coupling constant and the top-quark pole mass and parton distribution functions [146]. In the all-hadronic and $\ell + jets$ events in a boosted topology with at least two large-R jets with a b-tag inside and $p_T > 400$ GeV or one large-R jet, respectively, CMS measures the differential cross section as a function of kinematic variables of individual top quarks or of the $t\bar{t}$ system [147]. The observed absolute cross sections are significantly lower than the predictions from theory. Using the full Run-2 dataset of 137 fb^{-1} in $\ell + jets$ data, arranged in four regions according to the top p_T, boosted vs. resolved, and the b-tagging score, CMS measures the single- and double-differential $t\bar{t}$ cross sections [99]. Here also the longitudinal momentum is measured well into the TeV range in one measurement starting in the resolved regime.

61.2.1.3 $t\bar{t}$ *plus heavy flavor production processes*

Further cross-section measurements are performed by ATLAS and CMS for $t\bar{t}$+heavy flavor. The measurement of the cross section for $t\bar{t}$+heavy flavour [148] and $t\bar{t}$+jets production as well as the differential measurement of the jet multiplicity in $t\bar{t}$ events is presented by ATLAS [149] and by CMS [120]. In addition, both experiments measure the production cross section of the $t\bar{t}b\bar{b}$ process as it is an interesting test of QCD due to the different mass scales involved. Furthermore, this process is of high relevance for top quark production as background to searches, for example for measurements of $t\bar{t}h$ production and measurements of 4-top quark production. At $\sqrt{s} = 8$ TeV, CMS measured the cross-section ratio $\sigma_{t\bar{t}b\bar{b}}/\sigma_{t\bar{t}jj}$ using 19.6 fb^{-1} [150]. ATLAS also measured the $t\bar{t}$ production cross section along with the branching ratios into channels with leptons and quarks

using 4.6 fb^{-1} of 7 TeV data [151]. They find agreement with the standard model at the level of a few percent.

Using 19.7 fb^{-1} of data recorded at 8 TeV, CMS measures the absolute and normalized differential cross section with respect to the jet multiplicity in $t\bar{t}$+jets events in the dilepton channel. The differential $t\bar{t}b$ and $t\bar{t}b\bar{b}$ cross sections are presented for the first time as a function of the kinematic properties of the leading additional b jets [152].

Using 139 fb^{-1} of $t\bar{t} \rightarrow$ dilepton events, ATLAS distinguishes in a dedicated analysis muons originating from $W \rightarrow \mu\nu$ decays and those from $W \rightarrow \tau\nu \rightarrow \mu\nu\nu\nu$ decays via their transverse momentum spectrum and the impact parameter of the muon track, that reflects the tau lifetime, yielding high sensitivity. The measured ratio of $R(\tau/\mu) = 0.992 \pm 0.013$ is in agreement with the hypothesis of universal lepton couplings [153].

Using 36 fb^{-1} of dilepton events at 13 TeV, ATLAS also measures differential cross sections with respect to high-resolution variables, constructed to characterize the longitudinal and transverse momentum distributions of the b-hadron within the b-jets [138]. They are used to test the heavy-quark-fragmentation modelling.

Using 137 fb^{-1} of dilepton events at 13 TeV, CMS measures differential cross sections with respect to the mass of the $t\bar{t}$ system and the rapidity difference of the top-quark and antiquark [154]. Exploiting their sensitivity to the top-quark Yukawa coupling yields a best fit value of $Y_t = 1.16^{+0.24}_{-0.35}$, bounding $Y_t < 1.54$ at a 95% confidence level.

At $\sqrt{s} = 13$ TeV, ATLAS measures the $t\bar{t}b\bar{b}$ cross section and cross section ratios in the dilepton and the $\ell + jets$ channels as inclusive and differential cross sections [155]. The measured inclusive fiducial cross-sections generally exceed the $t\bar{t}b\bar{b}$ predictions from various NLO matrix element calculations matched to a parton shower. CMS measures the $t\bar{t}b\bar{b}$ cross section and cross section ratios in the dilepton channel [156], in the dilepton and the lepton+jets channel [157], in the all-jet channel by selecting events containing at least eight jets, of which at least two are identified as b-jets [158]. In the latter, a combination of multivariate analysis techniques is used to reduce the large background from multijet events not containing a top quark pair, and to help discriminate between jets originating from top quark decays and other additional jets. In the all-hadronic channel, they later measured the $t\bar{t} + b\bar{b}$ cross section to $\approx 25\%$ precision employing a multivariate analysis technique and a 2-dimensional likelihood fit [159]. Using the full Run-2 dataset of 138 fb^{-1}, they measure the inclusive and normalized differential $t\bar{t}b\bar{b}$ cross sections in the lepton+jets decay channel of the top quark [160]. Measurements are made in four fiducial phase space regions, targeting different aspects of the process. Distributions are unfolded to the particle level through maximum likelihood fits, and compared with predictions from several event generators. In most cases, the measured inclusive cross sections exceed the predictions with the chosen generator settings. The differential cross sections show varying degrees of compatibility with the theoretical predictions.

CMS also measured the $t\bar{t} + c\bar{c}$ cross section using 41.5 fb^{-1} of events with dileptonic final states [161]. A multi-class neural network is employed to separate $t\bar{t} + b\bar{b}$, $t\bar{t} + c\bar{c}$ and $t\bar{t} + ll$. The results are compatible with the prediction within $1 - 2\,\sigma$.

The production of four top-quarks is an interesting test of QCD in a very rare process and at the same time sensitive to the top quark Yukawa coupling and to production mechanisms with new mediators with strong couplings to top quarks. The latest cross section calculation yields $\sigma_{t\bar{t}t\bar{t}} = 13.32^{+1.04}_{-1.78}$ fb [44]. Using the full Run-II data set of 139 fb^{-1}, ATLAS measures the four-tops cross section in the two-lepton same sign or three-lepton channel with 13% branching ratio and dominant $t\bar{t}V$ background as $\sigma_{t\bar{t}t\bar{t}} = 24^{+7}_{-6}$ fb [162]. Using the same data set in the one-lepton or two-lepton opposite-sign channel with 57% branching ratio and dominant $t\bar{t}$ + heavy flavor background, they measure $\sigma_{t\bar{t}t\bar{t}} = 26^{+17}_{-15}$ fb [163]. The combination yields $\sigma_{t\bar{t}t\bar{t}} = 24^{+7}_{-6}$ fb [163], corresponding to an observed (expected) significance of 4.7 (2.6) σ significance. Using the full Run-2 dataset

of 140 fb^{-1}, ATLAS presents the observation of the $t\bar{t}t\bar{t}$ production process in events containing two leptons with the same electric charge or at least three leptons (e or μ). Event kinematics are used to separate signal from background through a multivariate discriminant based on graph neural networks, and dedicated control regions are used to constrain the dominant backgrounds. The cross section is measured to be $\sigma(t\bar{t}t\bar{t}) = 22.5^{+6.6}_{-5.5}$ fb [164], almost twice the Standard Model prediction and compatible with it within 2 standard deviations. The observed (expected) significance of the measured signal with respect to the standard model (SM) background-only hypothesis is 6.1 (4.3) standard deviations. Data are also used to constrain the top-Higgs Yukawa coupling and effective field theory operator coefficients.

After a search for four-top production in 35.8 fb^{-1}, in the one-lepton or two-lepton opposite-sign channel [165], CMS uses the full Run-2 dataset of 137 fb^{-1} to measure the four-top cross section in the two-lepton same sign or three-lepton channel, yielding $\sigma_{t\bar{t}t\bar{t}} = 12.6^{+5.8}_{-5.2}$ fb [166], corresponding to an observed (expected) significance of 2.6 (2.7) σ significance. In the full Run-2 dataset, they manage to achieve evidence for the four-top production in events that have no leptons (all-hadronic), one lepton, or two opposite-sign leptons, yielding $\sigma(t\bar{t}t\bar{t}) = 36^{+12}_{-11}$ fb [167], corresponding to an observed significance of 3.9 standard deviations (1.5 expected). The combination with earlier CMS results in other final states yields $\sigma(t\bar{t}t\bar{t}) = 17 \pm 4(stat.) \pm 3(syst.)$ fb, corresponding to a significance of 4.0 standard deviations (3.2 expected).

Finally, CMS reports the observation of the four-tops production process based on events with two same-sign, three, or four charged leptons (e and μ) and additional jets. Updated identification techniques for charged leptons and jets originating from the hadronization of b quarks, as well as a revised multivariate analysis strategy via a multi-class boosted decision tree to distinguish the signal process from the main backgrounds, lead to an improved signal detection, yielding $\sigma(t\bar{t}t\bar{t}) = 17.7^{+3.7}_{-3.5}(stat.)^{+2.3}_{-1.9}(syst.)$ fb, corresponding to an observed significance of 5.6 standard deviations (4.9 expected) [168].

61.2.1.4 *Single-top production*

Top-quarks cannot only be produced in pairs via the strong interaction, but also individually via the electroweak interaction. This interaction is sensitive to the tWb coupling as well as to the CKM-Matrix Element V_{tb}. The single-top quark production process was first observed in 2009 by DØ [169] and CDF [170, 171] at the Tevatron. The production cross section at the Tevatron is roughly half that of the $t\bar{t}$ cross section, but the final state with a single W-boson and typically two jets, which tend to be emitted more in the forward direction, is less distinct than that for $t\bar{t}$ and much more difficult to distinguish from the background of W+jets and other sources. A comprehensive review of the first observation and the techniques used to extract the signal from the backgrounds can be found in [172]. A more recent one can be found in [173].

The dominant production at the Tevatron is through s-channel and t-channel W-boson exchange. Associated production with a W-boson (tW production) has a cross section that is too small to observe at the Tevatron. The t-channel process is $qb \to q't$, while the s-channel process is $q\bar{q}' \to t\bar{b}$. The s- and t-channel productions can be separated kinematically. This is of particular interest because potential physics beyond the Standard Model, such as fourth-generation quarks, heavy W and Z bosons, flavor-changing-neutral-currents [37], or a charged Higgs boson, would affect the s- and t-channels differently. However, the separation is difficult and initial observations and measurements at the Tevatron by both experiments were of combined $s + t$-channel production. The two experiments combined their measurements for maximum precision with a resulting $s + t$-channel production cross section of $2.76^{+0.58}_{-0.47}$ pb [174], which agrees well with the theoretical calculation at $m_t = 173$ GeV/c^2 of $\sigma_{s+t} = 3.12^{+0.00}_{-0.04}(scale) \pm 0.18(pdf)$ pb (including both top and anti-top production) [35, 175].

Using the full Run-II data set of up to 9.7 fb^{-1}, CDF and DØ have measured the t-channel single-top quark production to be $\sigma_{t+\bar{t}} = 2.25^{+0.29}_{-0.31}$ pb [176, 177]. In the same publication, they also present the simultaneously measured $s-$ and $t-$channel cross sections and the $s+t$ combined cross section measurement resulting in $\sigma_{s+t} = 3.30^{+0.52}_{-0.40}$ pb, without assuming the SM ratio of σ_s/σ_t. The modulus of the CKM matrix element obtained from the $s+t$-channel measurement is $|V_{tb}| = 1.02^{+0.06}_{-0.05}$ and its value is used to set a lower limit of $|V_{tb}| > 0.92$ at 95% C.L. Those results are in good agreement with the theoretical value at the mass 172.5 GeV/c^2 of $\sigma_t = 2.08 \pm 0.13$ pb [175]. It should be noted that the theory citations here list cross sections for t or $\bar{t}$ alone, whereas the experiments measure the sum. At the Tevatron, these cross sections are equal. The theory values quoted here already include this factor of two.

Using datasets of 9.7 fb^{-1} each, CDF and DØ combine their analyses and report the first observation of single-top-quark production in the s-channel, yielding $\sigma_s = 1.29^{+0.26}_{-0.24}$ pb [178]. The probability of observing a statistical fluctuation of the background of the given size is 1.8×10^{-10}, corresponding to a significance of 6.3 standard deviations.

t-channel at the LHC:
At the LHC, the t-channel cross section is expected to be more than three times as large as s-channel and tW production, combined.

At $\sqrt{s} = 5.02$ TeV, very recently, ATLAS measures the t-channel single-top quark production in a dedicated run using 255 pb^{-1}, yielding $\sigma(tq + \bar{t}q) = 27.1^{+4.4}_{-4.1}(stat.)^{+4.4}_{-3.7}(syst.)$ pb and a cross section ratio between top an antitop production $R_t = 2.73^{+1.43}_{-0.82}(stat.)^{+1.01}_{-0.29}(syst.)$ [179]. This result implies for the CKM-matrix element $f_{LV} \cdot |V_{tb}| = 0.94^{+0.11}_{-0.10}$ with f_{LV} being a left-handed form factor.

At $\sqrt{s} = 7$ TeV, using 4.59 fb^{-1} of data, ATLAS measures the t-channel single-top quark cross section in the lepton plus 2 or 3 jets channel with one b-tag by fitting the distribution of a multivariate discriminant constructed with a neural network, yielding $\sigma_t = 46 \pm 6$ pb, $\sigma_{\bar{t}} = 23 \pm 4$ pb with a ratio $R_t = \sigma_t/\sigma_{\bar{t}} = 2.04 \pm 0.18$ and $\sigma_{t+\bar{t}} = 68 \pm 8$ pb, consistent with SM expectations [180, 181]. CMS follows two approaches in 1.6 fb^{-1} of lepton plus jets events. The first approach exploits the distributions of the pseudorapidity of the recoil jet and reconstructed top-quark mass using background estimates determined from control samples in data. The second approach is based on multivariate analysis techniques that probe the compatibility of the candidate events with the signal. They find $\sigma^{t-chan.}_{t+\bar{t}} = 67.2 \pm 6.1$ pb, and $|V_{tb}| = 1.020 \pm 0.046(exp.) \pm 0.017(th.)$ [182]. All combined measurements are consistent with their corresponding SM predictions and yield 67.5 ± 5.7 pb [183].

At $\sqrt{s} = 8$ TeV, both experiments repeat and refine their measurements. ATLAS uses 20.2 fb^{-1} of data. Total, fiducial and differential cross-sections are measured for both top-quark and top-antiquark production [184]. An artificial neural network is employed to separate signal from background. The fiducial cross-section is measured with a precision of 5.8% (top quark) and 7.8% (top antiquark), respectively. The total cross-sections are measured to be $\sigma^{t-chan.}_t(tq) = 56.7^{+4.3}_{-3.8}$ pb for top-quark production and $\sigma^{t-chan.}_{\bar{t}}(\bar{t}q) = 32.9^{+3.0}_{-2.7}$ pb for top-antiquark production, in agreement with the SM prediction. In addition, the ratio of top-quark to top-antiquark production cross-sections is determined to be $R_t = 1.72 \pm 0.09$. The total cross-section is used to extract the Wtb coupling: $f_{LV} \cdot |V_{tb}| = 1.029 \pm 0.048$, which corresponds to $|V_{tb}| > 0.92$ at the 95% confidence level, when assuming $f_{LV} = 1$ and restricting the range of $|V_{tb}|$ to the interval $[0, 1]$. The differential cross-sections as a function of the transverse momentum and rapidity of both, top and antitop, are measured at both the parton and particle levels. The transverse momentum and rapidity differential cross-sections of the accompanying jet from the t-channel scattering are measured at particle level. All measurements are compared to various Monte Carlo predictions as well as to fixed-order QCD

calculations where available. The SM predictions provide good descriptions of the data. Using the same dataset, ATLAS probes the Wtb vertex structure from polarization observables in t-channel single-top quark events. The observables are extracted from asymmetries in angular distributions measured with respect to spin quantisation axes appropriately chosen for the top quark and the W-boson and found to be in agreement with the Standard Model predictions [185]. CMS uses 19.7 fb^{-1} in the e or μ plus jets channel, exploiting the pseudorapidity distribution of the recoil jet. They find $\sigma_t = 53.8 \pm 1.5(stat.) \pm 4.4(syst.)$ pb and $\sigma_{\bar{t}} = 27.6 \pm 1.3(stat.) \pm 3.7(syst.)$ pb, resulting in an inclusive t-channel cross section of $\sigma_{t+\bar{t}} = 83.6 \pm 2.3(stat.) \pm 7.4(syst.)$ [186]. They measure a cross section ratio of $R_t = \sigma_t/\sigma_{\bar{t}} = 1.95 \pm 0.10(stat.) \pm 0.19(syst.)$, in agreement with the SM. The CKM matrix element V_{tb} is extracted to be $|V_{tb}| = 0.998 \pm 0.038(exp.) \pm 0.016(th.)$. Later, CMS also provided a fiducial cross section measurement for t-channel single top in the same dataset in events with exactly one μ or e and two jets, one of which is associated with a b-hadron [187]. The total fiducial cross section is measured using different generators at NLO plus parton-shower accuracy. Using as reference the `aMC@NLO` MC predictions in the four-flavor scheme, $\sigma_t^{\mathrm{fid}} = 3.38 \pm 0.25(exp.) \pm 0.20(th.)$ pb is obtained, in good agreement with the theory predictions. All combined measurements are consistent with their corresponding SM predictions and yield 87.7 ± 5.8 pb [183].

At $\sqrt{s} = 13$ TeV, ATLAS uses 3.2 fb^{-1} to measure the t-channel cross section. Using a binned maximum-likelihood fit to the discriminant distribution of a neural network, the cross-sections are determined to be $\sigma_t(tq) = 156 \pm 5(stat.) \pm 27(syst.) \pm 3(lumi.)$ pb and $\sigma(\bar{t}q) = 91 \pm 4(stat.) \pm 18(syst.) \pm 2(lumi.)$ pb [188]. The cross-section ratio is measured to be $R_t = \sigma_t/\sigma_{\bar{t}} = 1.72 \pm 0.09(stat.) \pm 0.18(syst.)$. All results are in agreement with SM predictions. Using the full Run-2 dataset of 140 fb^{-1}, ATLAS measures the t-channel cross sections to be $\sigma(tq) = 137 \pm 8$ pb and $\sigma(\bar{t}q) = 84^{+6}_{-5}$ pb for top-quark and top-antiquark production, respectively [189]. The combined cross-section is found to be $\sigma(tq + \bar{t}q) = 221 \pm 13$ pb and the cross-section ratio is $R_t = \sigma(tq)/\sigma(\bar{t}q) = 1.636^{+0.036}_{-0.034}$, in good agreement with predictions made at NNLO in perturbation theory. The results are also used to demonstrate the potential to constrain parton distributions functions and interpreted in terms of effective field theory operators $-0.25 < C_{qQ}^{(1,3)} < 0.12$, and to derive the constraint $|V_{tb}| > 0.95$ at the 95% confidence level CMS uses 2.2 fb^{-1} for a first measurement. Fits to the transverse W-mass and the output of an artificial neural network allow the determination of the background and the signal contribution. The measured cross-section is $\sigma_t = 238 \pm 13(stat.) \pm 29(syst.)$ pb [190]. The CKM matrix element is determined to $|V_{tb}| = 1.05 \pm 0.07(exp.) \pm 0.02(th.)$. Using 35.9 fb^{-1} of data, CMS refines their measurement. Events with one μ or e are selected, and different categories of jet and b-jet multiplicity and multivariate discriminators are applied to separate the signal from the background, resulting in $\sigma_t(tq) = 130 \pm 1(stat) \pm 19(syst)$ pb and $\sigma_t(\bar{t}q) = 77 \pm 1(stat) \pm 12(syst)$ pb, respectively, and their ratio is $1.68 \pm 0.02(stat) \pm 0.05(syst)$ [191]. The results are in agreement with the predictions from the Standard Model. This dataset is also used to measure differential cross sections in this channel [192]. CMS used the same dataset to measure the CKM matrix elements from their t-channel single-top quark production cross section. In the standard model hypothesis of CKM unitarity, a lower limit of $|V_{tb}| > 0.970$ is measured at the 95% confidence level. Several theories beyond the standard model are considered, and by releasing all constraints among the involved parameters, the values $|V_{tb}| = 0.988 \pm 0.024$, and $|V_{td}|^2 + |V_{ts}|^2 = 0.06 \pm 0.06$ are measured [193].

tW-channel at the LHC:
The predicted cross section for the associated tW process at the LHC at $\sqrt{s} = 7$ TeV is 15.6 ± 1.2 pb [36]. This is of interest because it probes the Wtb vertex in a different kinematic region than s- and t-channel production, and because of its similarity to the associated production of a charged-Higgs boson and a top quark. The signal is difficult to extract because of its similarity

to the $t\bar{t}$ signature. Furthermore, it is difficult to uniquely define because at NLO a subset of diagrams has the same final state as $t\bar{t}$ and the two interfere [194]. The cross section is calculated using the *diagram removal* technique [195] to define the signal process. In the diagram removal technique the interfering diagrams are removed, at the amplitude level, from the signal definition (an alternative technique, *diagram subtraction* removes these diagrams at the cross-section level and yields similar results [195]). These techniques work provided the selection cuts are defined such that the interference effects are small, which is usually the case.

At $\sqrt{s} = 7$ TeV, both, ATLAS and CMS, provide evidence for the associated tW production [196, 197]. ATLAS uses 2.05 fb^{-1} in the dilepton plus missing E_T plus jets channel, where a template fit to the final classifier distributions resulting from boosted decision trees as signal to background separation is performed. The result is incompatible with the background-only hypothesis at the 3.3σ (3.4σ expected) level, yielding $\sigma_{tW} = 16.8 \pm 2.9(stat.) \pm 4.9(syst.)$ pb and $|V_{tb}| = 1.03^{+0.16}_{-0.19}$ [196]. CMS uses 4.9 fb^{-1} in the dilepton plus jets channel with at least one b-tag. A multivariate analysis based on kinematic properties is utilized to separate the $t\bar{t}$ background from the signal. The observed signal has a significance of 4.0σ and corresponds to a cross section of $\sigma_{tW} = 16^{+5}_{-4}$ pb [197]. All combined measurements are consistent with their corresponding SM predictions and yield 16.3 ± 4.1 pb [183].

At $\sqrt{s} = 8$ TeV, both experiments repeated their tW-analyses. ATLAS uses 20.3 fb^{-1} to select events with two leptons and one central b-jet. The tW signal is separated from the backgrounds using boosted decision trees, each of which combines a number of discriminating variables into one classifier. Production of tW events is observed with a significance of 7.7σ. The cross section is extracted in a profile likelihood fit to the classifier output distributions. The tW cross section, inclusive of decay modes, is measured to be $\sigma_{tW} = 23.0 \pm 1.3(stat.)^{+3.2}_{-3.5}(syst.) \pm 1.1(lumi.)$ pb, yielding a value for the CKM matrix element $|V_{tb}| = 1.01 \pm 0.10$ and a lower limit of 0.80 at the 95% C.L. [198]. A fiducial cross section is also measured. ATLAS and CMS also combine their early measurements and obtain $\sigma_{tW} = 16.3 \pm 4.1$ pb [199], in agreement with the NLO+NNLL expectation. Later, ATLAS used 20.2 fb^{-1} in the single-lepton channel with at least three jets to measure the Wt production cross section. A neural network is trained to separate the tW signal from the dominant $t\bar{t}$ background. The cross-section is extracted from a binned profile maximum-likelihood fit to a two-dimensional discriminant built from the neural-network output and the invariant mass of the hadronically decaying W boson. The measured cross section is $\sigma_{tW} = 26 \pm 7$ pb [200], in good agreement with the Standard Model expectation. CMS uses 12.2 fb^{-1} in events with two leptons and a jet originating from a b-quark. A multivariate analysis based on kinematic properties is utilized to separate the signal and background. The tW associate production signal is observed at the level of 6.1σ, yielding $\sigma_{tW} = 23.4 \pm 5.4$ pb and $|V_{tb}| = 1.03 \pm 0.12(exp.) \pm 0.04(th.)$ [201].

ATLAS and CMS also combine their early measurements and obtain $\sigma_{tW} = 23.1 \pm 3.6$ pb [183], in agreement with the NLO+NNLL expectation. The product of a form factor with the CKM matrix element V_{tb} is determined to be $|V_{tb}| = 1.02 \pm 0.04(meas.) \pm 0.02(theo.) > 0.79$.

At $\sqrt{s} = 13$ TeV, ATLAS uses 3.2 fb^{-1} of events with two opposite sign isolated leptons and at least one jet. They are separated into signal and control regions based on their jet multiplicity and the number of jets with b-tags. Signal is separated from background in two regions using boosted decision trees. The cross section is extracted by fitting templates to the data distributions, and is measured to be $\sigma_{tW} = 94 \pm 10(stat.)^{+28}_{-22}(syst.) \pm 2(lumi.)$ pb [202]. The measurement is in agreement with the SM prediction. CMS uses 36 fb^{-1} of events with two opposite sign isolated leptons, one tight and one loose jet and one b-tag. Signal and background is separated in categories depending on the number of jets and the subset of b-tagged jets using a boosted decision tree. A maximum likelihood fit yields $\sigma_{tW} = 63.1 \pm 1.8(stat.) \pm 6.4(syst.) \pm 2.1(lumi.)$ pb [203]. In this dataset, CMS

also analyses the single-lepton channel, where a boosted decision tree is used to separate the tW signal from the dominant $t\bar{t}$ background, whilst the subleading W+jets and multijet backgrounds are constrained using data-driven estimates. This result is the first observation of the tW process in final states containing a single μ or single e and several jets, with a significance exceeding 5 standard deviations. The cross section is determined to be $\sigma_{tW} = 89 \pm 4(stat) \pm 12(syst)$ pb [204], consistent with the Standard Model. Using the full Run-2 datset of 138 fb^{-1}, CMS measures the inclusive and normalised differential cross sections. Events containing one e and one μ in the final state are analysed. For the inclusive measurement, a multivariate discriminant, exploiting the kinematic properties of the events is used to separate the signal from the dominant $t\bar{t}$ background. A cross section of $79.2 \pm 0.9(stat)^{+7.7}_{-8.0}(syst) \pm 1.2(lumi)$ pb [205] is obtained, consistent with the predictions of the standard model. For the differential measurements, a fiducial region is defined according to the detector acceptance, and the requirement of exactly one jet coming from the fragmentation of a bottom quark. The resulting distributions are unfolded to particle level and agree with the predictions at NLO in perturbative QCD.

s-channel at the LHC:

At $\sqrt{s} = 7$ TeV, the s-channel production cross section is expected to be 4.6 ± 0.3 pb for $m_t = 173$ GeV/c^2 [35]. At ATLAS, a search for s-channel single top quark production is performed in 0.7 fb^{-1} using events containing one lepton, missing transverse energy and two b-jets. Using a cut-based analysis, an observed (expected) upper limit at 95% C.L. on the s-channel cross-section of $\sigma_s < 26.5$ (20.5) pb is obtained [206].

At $\sqrt{s} = 8$ TeV, ATLAS uses 20.3 fb^{-1} of data with one lepton, large missing transverse momentum and exactly two b-tagged jets. They perform a maximum-likelihood fit of a discriminant based on a Matrix Element Method and optimized in order to separate single top-quark s-channel events from the main background contributions which are $t\bar{t}$ and W+jets production. They find $\sigma_s = 4.8 \pm 0.8(stat.)^{+1.6}_{-1.3}(syst.)$ pb with a signal significance of 3.2 standard deviations [207], which provides first evidence for s-channel single-top production. The signal is extracted through a maximum-likelihood fit to the distribution of a multivariate discriminant defined using boosted decision trees to separate the expected signal contribution from background processes. At 7 TeV and 8 TeV, CMS uses 5.1 fb^{-1} and 19.3 fb^{-1}, respectively, and analyses leptonic decay modes by performing a maximum likelihood fit to a multivariate discriminant defined using a Boosted Decision Tree, yielding cross sections of $\sigma_s = 7.1 \pm 8.1$ pb and $\sigma_s = 13.4 \pm 7.3$ pb, respectively, and a best fit value of 2.0 ± 0.9 for the combined ratio of the measured σ_s values and the ones expected in the Standard Model [208]. The signal significance is 2.5 standard deviations.

ATLAS and CMS present the combinations of their single-top-quark production cross-section measurements, using Run-I data. For the s-channel cross-section, the combination yields 4.9 ± 1.4 pb at $\sqrt{s} = 8$ TeV. All combined measurements are consistent with their corresponding SM predictions [183].

At $\sqrt{s} = 13$ TeV, ATLAS uses 139 fb^{-1} to measure the s-channel cross section on events with an e or μ, missing transverse momentum and exactly two b-tagged jets in the final state. A discriminant based on matrix element calculations is used to separate single-top-quark s-channel events from the main background contributions, which are top-quark pair production and W-boson production in association with jets. The observed (expected) signal significance over the background-only hypothesis is 3.3 (3.9) standard deviations, and the measured cross-section is $\sigma = 8.2^{+3.5}_{-2.9}$ pb, consistent with the Standard Model prediction of $\sigma_{SM} = 10.32^{+0.40}_{-0.36}$ pb [209].

Both, ATLAS and CMS, also measured the electroweak production of single top-quarks in association with a Z-boson, see section 61.2.5.4 of this review.

Fig. 61.2 provides a summary of all single top cross-section measurements at the LHC as a function of the center-of-mass energy. All cross-section measurements are very well described by
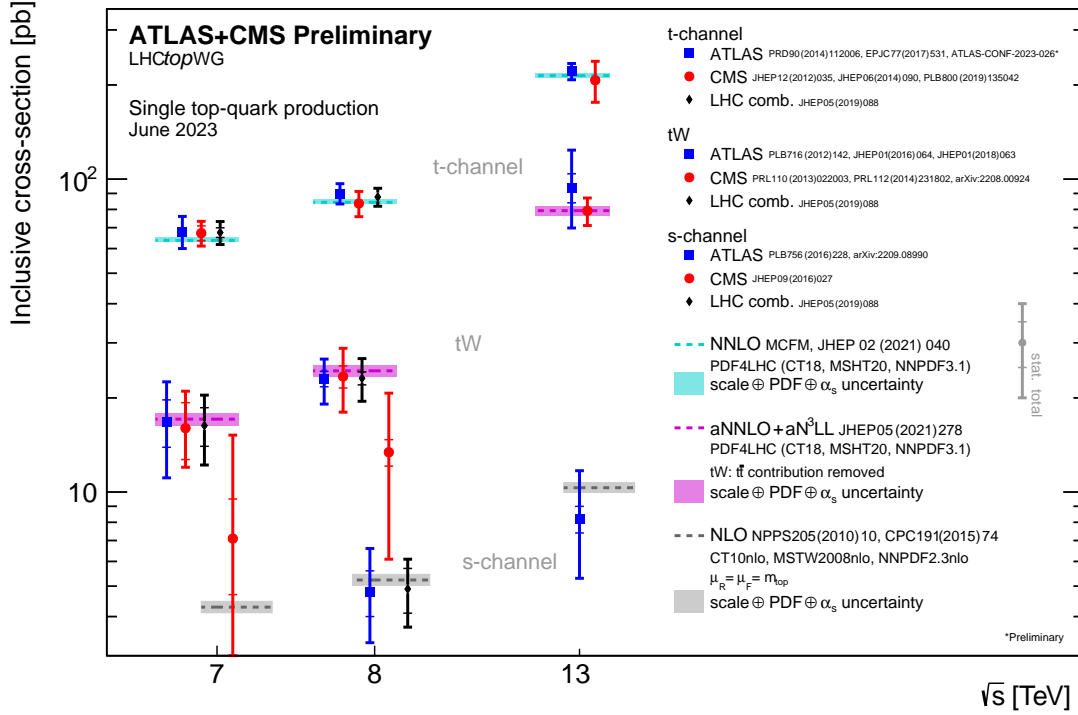
Figure 61.2: Measured and predicted single top production cross sections at LHC energies in *pp* collisions. The plot is kindly provided by the LHCtopWG working group, status as of June 2023, see https://twiki.cern.ch/twiki/bin/view/LHCPhysics/LHCTopWGSummaryPlots.

the theory calculation within their uncertainty.

Thanks to the large statistics now available at the LHC, both CMS and ATLAS experiments also performed differential cross-section measurements in single-top *t*-channel production [180], [210]. Such measurements are extremely useful as they test our understanding of both QCD and EW top-quark interactions. Using the full Run-2 dataset of 139 fb^{-1}, ATLAS measures the three components of the top-quark and top-antiquark polarisation vectors in t-channel single-top-quark production simultaneously from the distributions of the direction cosines of the charged-lepton momentum in the top-quark rest frame in single-lepton plus jets events. The three components of the polarisation vector for the selected top-quark event sample are $P_{x'} = 0.01 \pm 0.18$, $P_{y'} = -0.029 \pm 0.027$, $P_{z'} = 0.91 \pm 0.10$ and for the top-antiquark event sample they are $P_{x'} = -0.02 \pm 0.20$, $P_{y'} = -0.007 \pm 0.051$, $P_{z'} = -0.79 \pm 0.16$ [211]. They also present normalised differential cross-sections corrected to a fiducial region at the stable-particle level as a function of the charged-lepton angles for top-quark and top-antiquark events inclusively and separately, which are also used to derive bounds on the complex Wilson coefficient of the dimension-six O_{tW} operator.

The CMS collaboration has measured differential single top quark *t*-channel production cross sections as functions of the transverse momentum and the absolute value of the rapidity of the top quark. The analysis is performed in the leptonic decay channels of the top quark, with either a muon or an electron in the final state, using data collected with the CMS experiment at the LHC at $\sqrt{s} = 8$ TeV and corresponding to an integrated luminosity of 19.7 fb^{-1}. Neural networks are used to discriminate the signal process from the various background contributions. The results are found to agree with predictions from Monte Carlo generators [210]. Using the same data set and under the assumption that the spin analyzing power of a charged lepton is 100% as predicted in the SM, they are also able to measure the spin asymmetry, sensitive to the top quark polarization of

the top quark $A_\mu = 0.26 \pm 0.03(stat) \pm 0.10(syst)$ [212], which is compatible with a p-value of 4.6%, equivalent to 2.0 standard deviation. At 13 TeV, using 35.9 fb^{-1}, CMS measures the differential t-channel cross sections, for the first time in single-top production, and charge ratios for t-channel single top quark production [192]. The results are found to be in agreement with SM predictions using various NLO event generators and sets of parton distribution functions. Additionally, the spin asymmetry, sensitive to the top quark polarization, is determined from the differential distribution of the polarization angle at parton level to be 0.440 ± 0.070, in agreement with the SM prediction. This disfavours the results obtained at 8 TeV. ATLAS has measured the differential tW cross section in 36.1 fb^{-1} at 13 TeV with respect to the energy of the b-jet, the energy of the system of the two leptons and b-jet, and the transverse mass or mass of combinations of leptons, the b-jet and neutrinos [213]. Using 35.9 fb^{-1} of $e\mu$ events, CMS measures the differential tW cross section. A fiducial region is defined according to the detector acceptance, and the requirement of exactly one b-tagged jet. The resulting distributions are unfolded to particle-level and compared with predictions calculated at next-to-leading order in perturbative QCD. Within current uncertainties, all the predictions agree with the data [214].

Further measurements of electroweak single-top quark production in association with addition electroweak gauge bosons such as tZq or $t\gamma q$ production are covered in the section `Top-Quark Electroweak Charges and Couplings`, Sec 61.2.5.4.

61.2.2 *Top-Quark Asymmetries*

A forward-backward asymmetry in $t\bar{t}$ production at a $p\bar{p}$ collider arises starting at order α_S^3 in QCD from the interference between the Born amplitude $q\bar{q} \to t\bar{t}$ with 1-loop box production diagrams and between diagrams with initial- and final-state gluon radiation. The asymmetry, A_{FB}, is defined by

$$A_{FB} = \frac{N(\Delta y > 0) - N(\Delta y < 0)}{N(\Delta y > 0) + N(\Delta y < 0)}, \tag{61.5}$$

where $\Delta y = y_t - y_{\bar{t}}$ is the rapidity difference between the top- and the anti-top quark. Calculations at α_S^3 predict a measurable A_{FB} at the Tevatron. The most recent calculations up to order α_S^4, including electromagnetic and electroweak corrections, yield a predicted asymmetry of $\approx(9.5 \pm 0.7)\%$ [215]. This is about 10% higher than the previous calculation at NLO [216, 217], and improves the agreement with experiment.

Contrary to most measurements in the top sector, many measurements in this section are statistically limited. This is true - by construction - in the measurements in extreme corners of phase space (i.e. boosted measurements) and in rare production processes like ttW and $tt\gamma$. The progress in these measurements is expected to be achieved quite rapidly, as Run-3 athe the LHC and subsequent runs deliver more data.

Both CDF and DØ measured asymmetry values in excess of the SM prediction, fueling speculation about exotic production mechanisms (see, for example, [218] and references therein). The first measurement of this asymmetry by DØ in 0.9 fb^{-1} [219] found an asymmetry at the detector level of $(12 \pm 8)\%$. The first CDF measurement in 1.9 fb^{-1} [220] yielded $(24 \pm 14)\%$ at parton level. Both values were higher, though statistically consistent with the SM expectation. With the addition of more data, the uncertainties have been reduced, and the central values, if somewhat smaller, have remained consistent with the first measurements. At the same time, the improved calculations from theory have increased the predicted asymmetry values, improving the agreement between theory and experiment.

CDF and DØ have combined results using the full Tevatron dataset at $\sqrt{s} = 1.96$ TeV [221]. Three combined asymmetries are reported: $A_{FB}^{t\bar{t}}$ as defined in Eq. 61.5 for fully-reconstructed $t\bar{t}$ events, a single-lepton asymmetry, A_{FB}^{ℓ} defined as in Eq. 61.5 but with Δy replaced by the

product of the lepton charge and pseudo-rapidity, and a dilepton asymmetry, $A_{FB}^{\ell\ell}$, defined as in Eq. 61.5 but with Δy replaced by $\Delta\eta$ between the two leptons. The combined results are $A_{FB}^{t\bar{t}} = 0.128 \pm 0.021 \pm 0.014$, $A_{FB}^{\ell} = 0.073 \pm 0.016 \pm 0.012$, and $A_{FB}^{\ell\ell} = 0.108 \pm 0.043 \pm 0.016$, where the first uncertainty is statistical and the second systematic. These are to be compared to SM predictions at NNLO QCD and NLO electroweak of $A_{FB}^{t\bar{t}} = 0.095\pm0.007$ [215], $A_{FB}^{\ell} = 0.038\pm0.003$, and $A_{FB}^{\ell\ell} = 0.048 \pm 0.004$ [217], respectively. Both experiments have also measured differential asymmetries, in bins of $M_{t\bar{t}}$, Δy, $q_\ell \times \eta_\ell$, and $\Delta\eta_{\ell\ell}$, with consistent results, though the growth of $A_{FB}^{t\bar{t}}$ with increasing $M_{t\bar{t}}$ and Δy appears somewhat more rapid than the SM prediction [221].

At the LHC, where the dominant $t\bar{t}$ production mechanism is the charge-symmetric gluon-gluon fusion, the measurement is more difficult. For the sub-dominant $q\bar{q}$ production mechanism, the symmetric pp collision does not define a forward and backward direction. Instead, the charge asymmetry, A_C, is defined in terms of a positive versus a negative $t - \bar{t}$ rapidity difference, Δy

$$A_C^{t\bar{t}} = \frac{N(\Delta|y| > 0) - N(\Delta|y| < 0)}{N(\Delta|y| > 0) + N(\Delta|y| < 0)}. \tag{61.6}$$

Both CMS and ATLAS have measured A_C in the LHC dataset. Using lepton+jets events in 4.7 fb^{-1} of data at $\sqrt{s} = 7$ TeV, ATLAS measures $A_C^{t\bar{t}} = (0.6 \pm 1.0)\%$ [222]. ATLAS has reported on the same measurement performed at $\sqrt{s} = 8$ TeV with 20.3 fb^{-1} of data, with a result of $A_C^{t\bar{t}} = (0.9 \pm 0.5)\%$ [223]. In the dilepton channel at $\sqrt{s} = 8$ TeV, ATLAS measures [224] $A_C^{t\bar{t}} = (2.1 \pm 1.6)\%$, and $A_C^{\ell\ell} = (0.8 \pm 0.6)\%$ (defined in terms of the $\Delta\eta$ of the two leptons) in agreement with the SM predictions of $(1.11 \pm 0.04)\%$ and $(0.64 \pm 0.03)\%$, respectively [217]. Using lepton+jets events CMS has measured A_C at both $\sqrt{s} = 7$ and 8 TeV. They measure $A_C^{t\bar{t}} = (0.4 \pm 1.5)\%$ and $A_C^{t\bar{t}} = (0.33 \pm 0.26(stat.) \pm 0.33(syst.))\%$ in 5.0 fb^{-1} at $\sqrt{s} = 7$ TeV and in 19.7 fb^{-1} at $\sqrt{s} = 8$ TeV, respectively [225, 226]. Both measurements are consistent with the SM expectations of $A_C^{t\bar{t}} = (1.23 \pm 0.05)\%$ at $\sqrt{s} = 7$ TeV and $(1.11 \pm 0.04)\%$ at $\sqrt{s} = 8$ TeV [217], although the uncertainties are still too large for a precision test. In 19.5 fb^{-1} of dilepton events at $\sqrt{s} = 8$ TeV, CMS measures $A_C^{t\bar{t}} = (1.1 \pm 1.3)\%$ and $A_C^{\ell\ell} = (0.3 \pm 0.7)\%$ [227], consistent with SM expectations [228].

In their 7 and 8 TeV analyses, ATLAS and CMS also provide differential measurements as a function of $M_{t\bar{t}}$ and the transverse momentum p_T and rapidity y of the $t\bar{t}$ system. To reduce model-dependence, the CMS collaboration has performed a measurement in a reduced fiducial phase space [229], with a result of $A_C = (-0.35 \pm 0.72(stat.) \pm 0.31(syst.))\%$, in agreement with SM expectations.

To specifically address the dependence of the asymmetry on $M_{t\bar{t}}$, ATLAS has performed a measurement in boosted $t\bar{t}$ events [230]. In 20.3 fb^{-1} of data at $\sqrt{s} = 8$ TeV, in events with $M_{t\bar{t}} > 0.75$ TeV, and $|(\Delta|y|)| < 2$, ATLAS measures $A_C^{t\bar{t}} = (4.2 \pm 3.2)\%$ compared to a NLO SM prediction of $(1.60 \pm 0.04)\%$. The measurement is also presented in three bins of $M_{t\bar{t}}$, each in agreement, though with large uncertainties, with the SM expectations.

Both ATLAS and CMS have measured asymmetries in the distribution of leptons from $t\bar{t}$ decays. ATLAS, in 4.6 fb^{-1} of $\sqrt{s} = 7$ TeV data, has measured $A^{\ell\ell} = (2.4 \pm 1.5(stat.) \pm 0.9(sys.))\%$ in dilepton events [231]. Using a neutrino weighting technique in the same dataset to reconstruct the top quarks, ATLAS measures $A_C = (2.1\pm2.5 \text{ (stat.)}\pm1.7 \text{ (sys.)})\%$. CMS, in 5.0 fb^{-1} of $\sqrt{s} = 7$ TeV data, uses dilepton events to measure $A_C = (1.0\pm1.5 \text{ (stat.)}\pm0.6 \text{ (sys.)})\%$, where a matrix weighting technique is used to reconstruct the top quarks, and $A^{\ell\ell} = (0.9\pm1.0 \text{ (stat.)}\pm0.6 \text{ (sys.)})\%$ [232]. An earlier result using lepton+jets events from the same CMS dataset found $A_C = (0.4 \pm 1.0 \pm 1.1)\%$ [225]. Combined results from ATLAS and CMS have now been released [233]. At $\sqrt{s} = 7$ TeV the combined result is $A_C = (0.5 \pm 0.7 \text{ (stat.)} \pm 0.6 \text{ (sys.)})\%$, and at $\sqrt{s} = 8$ TeV it is $A_C =$

$(0.55 \pm 0.23 \pm 0.25)\%$. These results are all consistent, within their large uncertainties, with the SM expectations of $A^{\ell\ell} = (0.70 \pm 0.03)\%$ and $A_C = (1.23 \pm 0.05)\%$ [217].

ATLAS has released a charge asymmetry measurement at $\sqrt{s} = 13$ TeV using the full 139 fb^{-1} dataset, which combines data in the single-lepton and dilepton channels, and employs reconstruction techniques adapted to both the resolved and boosted topologies. A Bayesian unfolding procedure is performed to correct for detector resolution and acceptance effects. The combined inclusive $t\bar{t}$ charge asymmetry is measured to be $A^C_{t\bar{t}} = 0.0068 \pm 0.0015$, which differs from zero by 4.7 standard deviations. Differential measurements are performed as a function of the invariant mass, transverse momentum and longitudinal boost of the $t\bar{t}$ system. Both the inclusive and differential measurements are found to be compatible with the Standard Model predictions, at NLO in QCD with NLO electroweak corrections [234]. The measurements are interpreted in the framework of the Standard Model effective field theory, placing competitive bounds on several Wilson coefficients.

A model-independent comparison of the Tevatron and LHC results is made difficult by the differing $t\bar{t}$ production mechanisms at work at the two accelerators and by the symmetric nature of the pp collisions at the LHC. A recent result from the CMS Collaboration [235] in 35.9 fb^{-1} of lepton plus jets events at $\sqrt{s} = 13$ TeV, uses a likelihood analysis to separate the $q\bar{q}$ process from production via gluon-gluon and gluon-quark interactions and extract $A_{FB} = (4.8^{+8.8}_{-8.4}$ (stat.) ± 2.8 (sys.))%. In addition, given a particular model of BSM physics, a comparison can be obtained through the resulting asymmetry predicted by the model at the two machines, see for example [230].

Using 139 fb^{-1} of data at 13 TeV in the lepton plus jets channel, ATLAS presents a measurement of the charge asymmetry in $t\bar{t}$ production in association with a photon. While the $t\bar{t}$ asymmetry is diluted in inclusive measurements at the LHC owing to the large fraction of gluon–gluon-initiated $t\bar{t}$ events, it is enhanced in other topologies such as $t\bar{t}\gamma$ due to an increased fraction of the quark initiated production mode. The charge asymmetry is obtained from the distribution of the difference of the absolute rapidities of the top quark and antiquark using a profile likelihood unfolding approach. It is measured to be $A_C = -0.003 \pm 0.029$ in agreement with the Standard Model expectation [236], where the precision is limited by the presently available statistics.

In a similar fashion and using the same dataset, ATLAS also searches for the leptonic charge asymmetry (A_C^ℓ) of $t\bar{t}$ pair production in association with a W boson $(t\bar{t}W)$ in event final states with exactly three charged light leptons (electrons or muons). Here, the events are also enhanced in quark-initiated production processes. Additionally, the W boson in the initial state causes polarisation of the $t\bar{t}$ pair, which further leads to a sizeable asymmetry. A profile-likelihood fit to the event yields in multiple regions corresponding to positive and negative differences between the pseudorapidities of the charged leptons from top-quark and top-antiquark decays is used to extract the charge asymmetry. At reconstruction level, the asymmetry is found to be $-0.12 \pm 0.14(stat.) \pm 0.05(syst.)$. An unfolding procedure is applied to convert the result at reconstruction level into a charge-asymmetry value in a fiducial volume at particle level with the result of $-0.11 \pm 0.17(stat.) \pm 0.05(syst.)$. The Standard Model expectations for these two observables are calculated using Monte Carlo simulations with NLO plus parton shower precision in QCD and including NLO electroweak corrections. They are $0.084^{+0.005}_{-0.003}(scale) \pm 0.006(MCstat.)$ and $0.063^{+0.007}_{-0.004}(scale) \pm 0.004(MCstat.)$, respectively, and in agreement with the measurements [237].

ATLAS explores a so-called 'energy asymmetry' in $t\bar{t}$ production in association with a high-p_T jet ($t\bar{t}j$ production). The energy asymmetry is defined as a difference between the top and anti-top quarks' energies, and is measured in ATLAS in three bins of the associated high-p_T jet angle, θ_j. Both, the energies and jet angle, are measured in the $t\bar{t}j$ rest frame. A Bayesian unfolding method corrects for resolution and acceptance effects. The measurement is in agreement with the Standard Model at NLO accuracy [238].

In an early analysis of the Run-2 data, CMS analyzed 35.9 fb^{-1} of 13 TeV data, in par-

ticular using $t\bar{t}$ events decaying to muon or electron and jets in final states with low and high Lorentz boosts. Events are reconstructed using a fit of the kinematic distributions of the decay products to those expected for $t\bar{t}$ final states. The values found for the asymmetry parameters are $A_{FB} = 0.048^{+0.095}_{-0.087}(stat)^{+0.020}_{-0.029}(syst)$, for the anomalous chromomagnetic dipole moment $\mu^t = -0.024^{+0.013}_{-0.009}(stat)^{+0.016}_{-0.011}(syst)$, and a limit is placed on the magnitude of a possible anomalous chromoelectric dipole moment $|d^t| < 0.03$ at 95% confidence level [239].

The measurement of the charge asymmetry in $t\bar{t}$ events with highly Lorentz-boosted top quarks decaying to a single, nonisolated lepton and overlapping jets is presented by CMS using the complete Run-2 dataset of 138 fb^{-1} of 13 TeV data. The top quark charge asymmetry is measured for events with a $t\bar{t}$ invariant mass larger than 750 GeV, most relevant for BSM searches, and corrected for detector and acceptance effects using a binned maximum likelihood fit. The measured top quark charge asymmetry of $(0.69^{+0.65}_{-0.69})\%$ is in good agreement with the standard model prediction at NNLO in QCD with NLO electroweak corrections. The result is also presented for two invariant mass ranges, 750 – 900 and > 900 GeV [240].

61.2.3 *Top Quark Spin Correlations, Polarization, and Entanglement*

One of the unique features of the top quark is that it decays before its spin can be flipped by chromomagnetic interactions. Thus the top quark polarization is directly observable via the angular distribution of its decay products and it is possible to define and measure observables sensitive to the top quark spin and its production mechanism. Although the top- and antitop-quarks produced by strong interactions in hadron collisions are essentially unpolarized, the spins of t and $\bar{t}$ are correlated. For QCD production at threshold, the $t\bar{t}$ system is produced in a $^3S_1$ state with parallel spins for $q\bar{q}$ annihilation or in a $^1S_0$ state with antiparallel spins for gluon-gluon fusion. The situations at the Tevatron, where the production is primarily from $q\bar{q}$ annihilation, and at the LHC, where the production is primarily from gluon-gluon fusion, are therefore somewhat complementary. However, at the LHC production of $t\bar{t}$ pairs at large invariant mass occurs primarily via fusion of gluons with opposite helicities, and the $t\bar{t}$ pairs so produced have parallel spins as in production at the Tevatron via $q\bar{q}$ annihilation. The direction of the top quark spin is 100% correlated to the angular distributions of the down-type fermion (charged leptons or d-type quarks) in the decay. The joint angular distribution [241–243]

$$\frac{1}{\sigma}\frac{d^2\sigma}{d(\cos\theta_+)d(\cos\theta_-)} = \frac{1}{4}(1 + B_+\cos\theta_+ + B_-\cos\theta_- + \kappa\cdot\cos\theta_+\cdot\cos\theta_-), \qquad (61.7)$$

where θ_+ and θ_- are the angles of the daughters in the top-quark rest frame with respect to a particular spin quantization axis (assumed here to be the same for θ_+ and θ_-), is a very sensitive observable. The maximum value for κ, 0.782 at NLO at the Tevatron [244], is found in the off-diagonal basis [241], while at the LHC the value at NLO is 0.326 in the helicity basis [244]. The coefficients B_+ and B_- are near zero in the SM because the top quarks are unpolarized in $t\bar{t}$ production. In place of κ, $A\alpha_+\alpha_-$ is often used, where α_i is the spin analyzing power, and A is the spin correlation coefficient, defined as

$$A = \frac{N(\uparrow\uparrow) + N(\downarrow\downarrow) - N(\uparrow\downarrow) - N(\downarrow\uparrow)}{N(\uparrow\uparrow) + N(\downarrow\downarrow) + N(\uparrow\downarrow) + N(\downarrow\uparrow)}, \qquad (61.8)$$

where the first arrow represents the direction of the top quark spin along a chosen quantization axis, and the second arrow represents the same for the antitop-quark. The spin analyzing power α_i is +0.998 for positively charged leptons, -0.966 for down-type quarks from W decays, and -0.393 for bottom quarks [245]. The sign of α flips for the respective antiparticles. The spin correlation could be modified by a new $t\bar{t}$ production mechanism such as through a Z' boson, Kaluza-Klein gluons, a dark-matter mediator, or a Higgs boson.

The experiments typically use a Monte Carlo to provide templates for the measured distributions, or alternatively a matrix-element technique, and fit a parameter f, representing the fraction of events with the expected Standard Model correlation, with $(1 - f)$ the fraction with no correlation. The correlation coefficient is extracted via $A_{\text{meas}} = f \cdot A_{\text{SM}}$. A 'fraction' $f > 1$ means that the measured correlation coefficient is larger than the Standard Model expectation.

For a more complete introduction and discussion of the spin density matrix, see reference [246].

CDF and DØ have studied spin correlations in $t\bar{t}$ production in the dilepton and lepton+jets channel with limited sensitivity, showing first evidence (see the PDG listings for details).

Spin correlations have been conclusively measured at the LHC by both the ATLAS and CMS collaborations. In the dominant gluon fusion production mode for $t\bar{t}$ pairs at the LHC, the angular distribution between the two leptons in $t\bar{t}$ decays to dileptons is sensitive to the degree of spin correlation [247].

Measurements have been made at 7, 8, and now 13 TeV. While there is some interest in the $\sqrt{s}$ dependence of the correlations as a test of the production mechanism ($q\bar{q}$ vs gluon-gluon and possible sensitivity to new physics) the earlier measurements at 7 and 8 TeV [248–253] had relatively large uncertainties and have now been overtaken by the high-statistics 13 TeV measurements, which we review here.

In an ATLAS measurement at $\sqrt{s} = 8$ TeV [254], the spin-correlation coefficient κ is measured in the helicity basis to be $\kappa = 0.296 \pm 0.093$ in good agreement with the SM expectation of 0.318 (corresponding to a central value of f of 0.931). The polarization coefficients, B, in Eq. 61.7 are measured, also in the helicity basis, to be $B_+ = -0.044 \pm 0.038$ and $B_- = -0.064 \pm 0.040$, consistent with the SM predictions of 0.0030 ± 0.0010 and 0.0034 ± 0.00104, respectively.

The most recent result from ATLAS, in 36.1 fb^{-1} at $\sqrt{s} = 13$ TeV, uses $\Delta\phi$, the azimuthal angle between the two charged leptons in $e\mu$ events in an analysis that also measures the differential cross sections in $\Delta\phi$ and $\Delta\eta$ between the two leptons [255]. The result, measured by comparison with NLO Monte Carlo generators, is $f = 1.249 \pm 0.024 \pm 0.061^{+0.067}_{-0.090}$, where the uncertainties are statistical, systematic, and theoretical, is again greater than 1.0. Whereas the previous results were statistically consistent with the Standard Model expectation of 1.0, this result is slightly higher than the expectation and hence inconsistent at the level of 2.2σ. The NLO generators are NLO in QCD only (and only at the production level). Including electroweak couplings produces an expected Standard Model distribution consistent with the data, but results in a large scale uncertainty, giving $f = 1.03 \pm 0.13$.

In 35.9 fb^{-1} of data at $\sqrt{s} = 13$ TeV, CMS has studied spin correlations in dilepton events via the measurement of parton-level normalized differential cross sections, sensitive to each of the independent coefficients of the spin-dependent parts of the $t\bar{t}$ production density matrix. The measured distributions and extracted coefficients are compared with standard model predictions from simulations at NLO accuracy in QCD, and from NLO QCD calculations including electroweak corrections. The normalized differential cross sections are used in fits to constrain the anomalous chromomagnetic and chromoelectric dipole moments of the top $-0.24 < C_{tG}/\Lambda^2 < 0.07$ TeV^{-2} and $-0.33 < C_{tG}^I/\Lambda^2 < 0.20$ TeV^{-2}, respectively, at 95% confidence level [256]. These results are part of a complete study of the top quark spin density matrix at $\sqrt{s} = 13$ TeV, through the measurement of the coefficients of Eq. 61.7.

Entanglement is a striking feature of quantum mechanics [257–259]. If two particles are entangled, the state of one particle cannot be described independently from the other. More precisely, an entangled state is one that cannot be written as a convex combination of product states of density matrices [260, 261]. It has been observed in a wide variety of systems, ranging from the microscopic to the macroscopic scale. However, up to now entanglement has remained largely unexplored at high-energy colliders, except for flavor entanglement in $\Upsilon(4S) \to B_0\bar{B}_0$ decays [262] and a study of

Bell inequality violation in $B_0 \rightarrow J/\Psi K^*(892)^0$ decays [263]. Entanglement in top quark pairs has now been proposed to be studied for the first time via their spin correlation [264–271].

At the LHC, $t\bar{t}$ pairs are produced mainly via gluon-gluon fusion. When they are produced close to their production threshold, that is, when their invariant mass ($m_{t\bar{t}}$) is close to twice the mass of the top quark ($m_{t\bar{t}} \approx 2 \cdot m_t \approx 350$ GeV), they exist nearly in a spin singlet state, which is therefore expected to be maximally entangled. After averaging over all possible top-quark directions, entanglement only survives at threshold because there the $t\bar{t}$ pairs are produced in a spin singlet, which is rotationally invariant. The rotational invariance of a spin singlet implies that the trace of the spin correlation matrix C is a good entanglement witness. It is an observable that can signal the presence of entanglement without any assumption on the particular form of the quantum state, with $tr[C] + 1 < 0$ as a sufficient condition for entanglement. It is more convenient to define an entanglement witness using

$$D = tr[C]/3, \tag{61.9}$$

which can be experimentally measured as:

$$D = -3 \cdot \langle \cos \phi \rangle, \tag{61.10}$$

where $\langle \cos \phi \rangle$ is the average of the angle between the charged lepton directions in each one of the parent top quark and antitop quark rest frames which can be experimentally measured from an ensemble dataset. The existence of an entangled state is demonstrated if the measurement satisfies $D < -1/3$.

Using 139 fb^{-1} of Run-2 data, recorded at 13 TeV, ATLAS reports the highest-energy observation of entanglement so far in top–antitop quark events produced at the Large Hadron Collider. Spin entanglement is now detected from the measurement of a single observable D, inferred by the angle between the charged leptons in their parent top- and antitop-quark rest frames. The observable is measured on a narrow interval around the $t\bar{t}$ production threshold, where the entanglement detection is expected to be significant. The entanglement observable is measured in a fiducial phase-space with stable particles. The entanglement witness is measured to be $D = -0.547 \pm 0.002(stat.) \pm 0.021(syst.)$ for $340 < m_{t\bar{t}} < 380$ GeV [272]. The large spread in predictions from several mainstream event generators indicates that modelling this property is challenging. The predictions depend in particular on the parton-shower algorithm used. The observed result is more than five standard deviations from a scenario without entanglement and hence constitutes the first observation of entanglement in a pair of quarks, and the observation of entanglement at the highest energy to date.

61.2.4 *W-Boson Helicity in Top-Quark Decay*

The Standard Model dictates that the top quark has the same vector-minus-axial-vector $(V-A)$ charged-current weak interactions $\left(-i\frac{g}{\sqrt{2}}V_{tb}\gamma^\mu\frac{1}{2}(1-\gamma_5)\right)$ as all the other fermions. In the SM, the fraction of top-quark decays to longitudinally polarized W bosons is proportional to its Yukawa coupling and hence enhanced with respect to the weak coupling. It is expected to be [273] $\mathcal{F}_0^{\rm SM} \approx x/(1+x)$, $x = m_t^2/2M_W^2$ ($\mathcal{F}_0^{\rm SM} \sim 70\%$ for $m_t = 173$ GeV/c^2). Fractions of left-handed, right-handed, or longitudinal W bosons are denoted as $\mathcal{F}_-$, $\mathcal{F}_+$, and $\mathcal{F}_0$ respectively. In the SM, $\mathcal{F}_-$ is expected to be $\approx 30\%$ and $\mathcal{F}_+ \approx 0\%$. Predictions for the W polarization fractions at NNLO in QCD are available [274].

The Tevatron and the LHC experiments use various techniques to measure the helicity of the W boson in top-quark decays, in both the lepton+jets and in dilepton channels in $t\bar{t}$ production.

The first method uses a kinematic fit, similar to that used in the lepton+jets mass analyses, but with the top-quark mass constrained to a fixed value, to improve the reconstruction of final-state observables, and render the under-constrained dilepton channel solvable. Alternatively, in the dilepton channel the final-state momenta can also be obtained through an algebraic solution of the kinematics. The distribution of the helicity angle ($\cos\theta^*$) between the lepton and the b quark in the W rest frame provides the most direct measure of the W helicity. In a simplified version of this approach, the $\cos\theta^*$ distribution is reduced to a forward-backward asymmetry.

The second method (p_T^ℓ) uses the different lepton p_T spectra from longitudinally or transversely polarized W-decays to determine the relative contributions.

A third method uses the invariant mass of the lepton and the b-quark in top-quark decays ($M_{\ell b}^2$) as an observable, which is directly related to $\cos\theta^*$.

At the LHC, top-quark pairs in the dilepton channels are reconstructed using the neutrino weighting technique, see section 61.2.5.1.

Finally, the Matrix Element Method (MEM) has also been used [275], in which a likelihood is formed from a product of event probabilities calculated from the MEM for a given set of measured kinematic variables and assumed W-helicity fractions.

The results of recent CDF, DØ, ATLAS, and CMS analyses are summarized in Table 61.2. The datasets are now large enough to allow for a simultaneous fit of $\mathcal{F}_0$, $\mathcal{F}_-$ and $\mathcal{F}_+$, which we denote by '3-param' or $\mathcal{F}_0$ and $\mathcal{F}_+$, which we denote by '2-param' in the table. Results with either $\mathcal{F}_0$ or $\mathcal{F}_+$ fixed at its SM value are denoted '1-param'. For the simultaneous fits, the correlation coefficient between the two values is about -0.8. A complete set of published results can be found in the Listings. All results are in agreement with the SM expectation.

CDF and DØ combined their results based on $2.7 - 5.4$ fb^{-1} [276] for a top-quark mass of 172.5 GeV/c^2. ATLAS presents results from 1.04 fb^{-1} of $\sqrt{s} = 7$ TeV data using a template method for the $\cos\theta^*$ distribution and angular asymmetries from the unfolded $\cos\theta^*$ distribution in the lepton+jets and the dilepton channel [277]. CMS performs a similar measurement based on template fits to the $\cos\theta^*$ distribution with 5.0 fb^{-1} of 7 TeV data in the lepton+jets final state [278]. As the polarization of the W bosons in top-quark decays is sensitive to the Wtb vertex Lorentz structure and anomalous couplings, both experiments also derive limits on anomalous contributions to the Wtb couplings. CMS and ATLAS collaborations have also combined their results from 7 TeV data to obtain values on the helicity fractions as well as limits on anomalous couplings [279].

At 8 TeV, ATLAS came out with a measurement of the W-helicity fractions in 20.2 fb^{-1} in lepton+jets events with at least one b-tag [280]. Using 19.8 fb^{-1} of 8 TeV data, CMS measured the W-helicity in lepton $+$ 4 jet events with two b-tags [281] as well as in events with two opposite-sign leptons (electron or muon) in the final state, applying six kinematic constraints on the kinematics of the produced particles [282]. Also, using the same dataset, a first measurement of the W-boson helicity in top-quark decays was made in electroweak single top production [283], yielding similarly precise and consistent results. The 8 TeV results obtained in $t\bar{t}$ and single-top events by ATLAS and CMS have also been combined recently [284]. These results are in agreement with the standard model predictions at next-to-next-to-leading order in perturbative QCD and represent an improvement in precision of 25 (29)% for F_0 (F_L) with respect to the most precise single measurement. A limit on anomalous right-handed vector (V_R), and left- and right-handed tensor (g_L, g_R) tWb couplings and on corresponding Wilson coefficients is set.

Recently, ATLAS used 139 fb^{-1} of data recorded at 13 TeV in dilepton events with at least two b-tags to measure the normalised differential $t\bar{t}$ cross section with respect to $\cos\theta^*$ at parton level and from that, based on template fits, extract the helicity fractions. The results are complementary

to previous results and compatible with Standard Model expectations [285].

Table 61.2: Measurement and 95% C.L. upper limits of the W helicity in top-quark decays. The table includes both preliminary, as of September 2023, and published results. A full set of published results, including the results obtained at the Tevaton, is given in the Listings.

W Helicity	Source	$\int \mathcal{L}\mathrm{dt}$ (fb^{-1})	Ref.	Method
$\mathcal{F}_0 = 0.67 \pm 0.07$	ATLAS (7 TeV)	1.0	[277]	$\cos\theta^*$ 3-param
$\mathcal{F}_0 = 0.682 \pm 0.045$	CMS (7 TeV)	5.0	[278]	$\cos\theta^*$ 3-param
$\mathcal{F}_0 = 0.626 \pm 0.059$	ATLAS+CMS (7 TeV)	2.2	[279]	$\cos\theta^*$ 3-param
$\mathcal{F}_0 = 0.709 \pm 0.019$	ATLAS (8 TeV)	20.2	[280]	$\cos\theta^*$ 3-param
$\mathcal{F}_0 = 0.681 \pm 0.026$	CMS (8 TeV)	19.8	[281]	$\cos\theta^*$ 3-param
$\mathcal{F}_0 = 0.653 \pm 0.029$	CMS (8 TeV)	19.7	[282]	$\cos\theta^*$ 3-param
$\mathcal{F}_0 = 0.720 \pm 0.054$	CMS (8 TeV)	19.7	[283]	$\cos\theta^*$ 3-param
$\mathcal{F}_0 = 0.693 \pm 0.014$	ATLAS+CMS (8 TeV)	20	[284]	$\cos\theta^*$ 3-param
$\mathcal{F}_0 = 0.684 \pm 0.015$	ATLAS (13 TeV)	139	[285]	$\cos\theta^*$ 3-param
$\mathcal{F}_+ = 0.01 \pm 0.05$	ATLAS (7 TeV)	1.0	[277]	$\cos\theta^*$ 3-param
$\mathcal{F}_+ = 0.008 \pm 0.018$	CMS (7 TeV)	5.0	[278]	$\cos\theta^*$ 3-param
$\mathcal{F}_+ = 0.015 \pm 0.034$	ATLAS+CMS (7 TeV)	2.2	[279]	$\cos\theta^*$ 3-param
$\mathcal{F}_+ = -0.008 \pm 0.014$	ATLAS (8 TeV)	20.2	[280]	$\cos\theta^*$ 3-param
$\mathcal{F}_+ = -0.004 \pm 0.015$	CMS (8 TeV)	19.8	[281]	$\cos\theta^*$ 3-param
$\mathcal{F}_+ = 0.018 \pm 0.027$	CMS (8 TeV)	19.7	[282]	$\cos\theta^*$ 3-param
$\mathcal{F}_+ = -0.018 \pm 0.022$	CMS (8 TeV)	19.7	[283]	$\cos\theta^*$ 3-param
$\mathcal{F}_+ = -0.008 \pm 0.007$	ATLAS+CMS (8 TeV)	20	[284]	$\cos\theta^*$ 3-param
$\mathcal{F}_+ = -0.002 \pm 0.014$	ATLAS (13 TeV)	139	[285]	$\cos\theta^*$ 3-param

61.2.5 *Top-Quark Properties*

61.2.5.1 *Top-Quark Mass Measurements*

The most precisely studied property of the top quark is its mass. The top-quark mass has been measured in the lepton+jets, the dilepton, and the all-jets channel by all four Tevatron and LHC experiments, and now in single-top events at the LHC. The latest and/or most precise results are summarized in Table 61.3. The lepton+jets channel yields the most precise single measurements because of good signal to background ratio (in particular after b-tagging) and the presence of only a single neutrino in the final state. The momentum of a single neutrino can be reconstructed (up to a quadratic ambiguity) via the missing E_T measurement and the constraint that the lepton and neutrino momenta reconstruct to the known W boson mass. In the large data samples available at the LHC, measurements in the dilepton channel can be competitive and certainly complementary to those in the lepton+jets final state.

A large number of techniques have now been applied to measuring the top-quark mass. The original 'template method' [286], in which Monte Carlo templates of reconstructed mass distributions are fit to data, has evolved into a precision tool in the lepton+jets channel, where the systematic uncertainty due to the jet energy scale (JES) uncertainty is controlled by a simultaneous, *in situ* fit to the $W \to jj$ hypothesis [287]. All the latest measurements in the lepton+jets and the all-jets channels use this technique in one way or another. In 20.2 fb^{-1} of data at $\sqrt{s} = 8$ TeV in the lepton+jets channel, ATLAS achieves a total uncertainty of 0.53% with a statistical component of 0.23% [288]. The measurement is based on a 3-dimensional template fit, determining the top-quark

mass, the global jet energy scale and a b-to-light jet energy scale factor. The most precise CMS result in the lepton+jets channel uses an ideogram method and comes from a so-called 'hybrid' approach in which the prior knowledge about the jet energy scale is incorporated as a Gaussian constraint, with a width determined by the uncertainty on the jet energy corrections. In 19.7 fb^{-1} of $\sqrt{s} = 8$ TeV data, CMS achieves a total uncertainty of 0.30% with a statistical component of 0.09% with the hybrid approach [289]. Using this same method, CMS has released a top-mass measurement from $\sqrt{s} = 13$ TeV data. Using 35.9 fb^{-1} of lepton+jets events they measure the top mass with a precision of 0.36%, with a statistical component of 0.05% [290]. The measurements at $\sqrt{s} = 13$ TeV include, for the first time, an uncertainty due to 'color reconnection' [291,292]. In this same dataset, CMS has extracted a top mass from highly boosted top-quark decays by selecting events in which the hadronic-side top decay is reconstructed as a single jet with $P_T > 400$ GeV. The cross section as a function of jet mass is unfolded at the particle level to extract a top mass with a precision of 1.4% [293].

The template method is complemented by the 'matrix element' method. This method was first applied by the DØ Collaboration [294], and is similar to a technique originally suggested by Kondo *et al.* [275] and Dalitz and Goldstein [295]. In the matrix element method a probability for each event is calculated as a function of the top-quark mass, using a LO matrix element for the production and decay of $t\bar{t}$ pairs. The *in situ* calibration of dijet pairs to the $W \to jj$ hypothesis is now also used with the matrix element technique to constrain the jet energy scale uncertainty. In the lepton+jets channel, DØ uses the full Tevatron dataset of 9.7 fb^{-1} and yields an uncertainty of about 0.43% [296].

In the dilepton channel, the signal to background is typically very good, but reconstruction of the mass is non-trivial because there are two neutrinos in the final state, yielding a kinematically unconstrained system. A variety of techniques have been developed to handle this. An analytic solution to the problem has been proposed [297], but this has not yet been used in the mass measurement. One of the most precise measurements in the dilepton channel comes from using the invariant mass of the charged lepton and b-quark system ($M_{\ell b}$), which is sensitive to the top-quark mass and avoids the kinematic difficulties of the two-neutrino final state. In 4.6 fb^{-1} of $\sqrt{s} = 7$ TeV data, ATLAS has measured the top-quark mass in the dilepton channel to a precision of 0.53% using a template fit to the $M_{\ell b}$ distribution [298]. Using 19.7 fb^{-1} of data at $\sqrt{s} = 8$ TeV, CMS has released [299] a mass measurement in the dilepton channel based on a simultaneous fit to $M_{\ell b}$ and a transverse-mass-like variable M_{T2} [300]. The most precise result in this analysis, which comes from a linear combination of fits with the jet energy scale fixed at its nominal value and one that simultaneously determines the top mass and jet energy scale, has a total uncertainty of 0.54%. At the LHC, because of their precision, these techniques have largely displaced a number of earlier techniques in the dilepton channel, though these techniques are still included, and described, in the combined results from CMS, reported in Ref. [289].

In the neutrino weighting technique, used by CDF to analyze the full Run 2 dilepton dataset of 9.1 fb^{-1}, a weight is assigned by assuming a top-quark mass value and applying energy-momentum conservation to the top-quark decay, resulting in up to four possible pairs of solutions for the neutrino and anti-neutrino momenta. The missing E_T calculated in this way is then compared to the observed missing E_T to assign a weight [305]. The CDF result achieves a precision of 1.8% using a combination of neutrino weighting and an "alternative mass", which is insensitive to the jet energy scale [306]. The alternative mass depends on the angles between the leptons and the leading jets and the lepton four-momenta.

In the all-jets channel there is no ambiguity due to neutrino momenta, but the signal to background is significantly poorer due to the severe QCD multijets background. The emphasis therefore has been on background modeling, and reduction through event selection. The most recent mea-

Table 61.3: Measurements of top-quark mass from Tevatron and LHC. The results are a selection of both published and preliminary (not yet submitted for publication as of September 2023) measurements. For a complete set of published results see the Listings. Statistical uncertainties are listed first, followed by systematic uncertainties.

m_t (GeV/c^2)	Source	$\int \mathcal{L}\mathrm{dt}$ fb^{-1}	Ref.	Channel
$172.08 \pm 0.25 \pm 0.41$	ATLAS	20.2	[288]	ℓ+jets+$\ell\ell$+All jets
$172.44 \pm 0.13 \pm 0.47$	CMS	19.7	[289]	ℓ+jets+$\ell\ell$+All jets
$172.35 \pm 0.16 \pm 0.48$	CMS	19.7	[289]	ℓ+jets
$172.34 \pm 0.20 \pm 0.70$	CMS	35.9	[301]	$\ell\ell$
$173.72 \pm 0.55 \pm 1.01$	ATLAS	20.2	[302]	All jets
$172.25 \pm 0.08 \pm 0.62$	CMS	35.9	[290]	ℓ+jets
$172.6 \pm 0.4 \pm 2.4$	CMS	35.9	[293]	Boosted jets
$172.13 \pm 0.32^{+0.69}_{-0.70}$	CMS	35.9	[303]	Single top
$174.30 \pm 0.35 \pm 0.54$	CDF,DØ (I+II)	$\leq$9.7	[304]	publ. or prelim.
$173.34 \pm 0.27 \pm 0.71$	Tevatron+LHC	$\leq$8.7+$\leq$4.9	[29]	publ. or prelim.
$172.52 \pm 0.14 \pm 0.30$	ATLAS+CMS	$\leq$5+$\leq$20	[1]	prelim.

surement in the all-jets channel, by CMS in 35.9 fb^{-1} of $\sqrt{s} = 13$ TeV data [301], uses an ideogram method and a 2-dimensional simultaneous fit for m_t and the jet energy scale to extract the top-quark mass and achieves a precision of 0.36%. A measurement from ATLAS [302] uses a template fit to the ratio of three-jet (m_t) to two-jet (M_W) mass in the all-hadronic channel, the two-jet denominator provides an *in situ*, fit to the $W \to jj$ hypothesis. In 20.2 fb^{-1} of data at $\sqrt{s} = 8$ TeV, the result has a precision of 0.65%. A measurement from CDF in 9.3 fb^{-1} uses a two-dimensional template fit and achieves a precision of 1.1% [307].

The CMS Collaboration extracted a top-quark mass measurement from single-top events, something not previously done because of the poor signal to background ratio. The mass is extracted from the invariant mass of the muon, bottom quark, and missing transverse energy. The first measurement with 19.7 fb^{-1} of data at $\sqrt{s} = 8$ TeV, achieved a precision of 0.71% [308]. A more recent measurement in 35.9 fb^{-1} of data at $\sqrt{s} = 13$ TeV achieves 0.44% precision [303].

A dominant systematic uncertainty in these methods is the understanding of the jet energy scale, and so several techniques have been developed that have little sensitivity to the jet energy scale uncertainty. In addition to Reference [306] mentioned above, these include the measurement of the top-quark mass using the following techniques: Fitting of the lepton p_T spectrum of candidate events [309]; fitting of the transverse decay length of the b-jet (L_{xy}) [310]; fitting the invariant mass of a lepton from the W-decay and a muon from the semileptonic b decay [311,312], kinematic properties of secondary vertices from b-quark fragmentation [313], the invariant mass of the $J/\psi + \ell$ system in events in which a b-quark fragments to a J/ψ particle [314], fitting the b-jet energy peak [315], and dilepton kinematics in $e\mu$ events [316].

Several measurements have now been made in which the top-quark mass is extracted from the measured $t\bar{t}$ cross section using the theoretical relationship between the mass and the production cross section. These determinations make use of predictions calculated at higher orders, where the top mass enters as an input parameter defined in a given scheme. At variance with the usual methods, which involve the kinematic properties of the final states and therefore the pole mass, this approach can also directly determine a short-distance mass, such as the $\overline{\mathrm{MS}}$ mass [317]. With an alternative method ATLAS extracted the top-quark pole mass using $t\bar{t}$ events with at least one additional jet, basing the measurement on the relationship between the differential rate of gluon

radiation and the mass of the quark [318]. A similar analysis by CMS used the differential cross section as a function of the invariant mass of the $t\bar{t}$ system and the leading jet not associated with the top decays [319].

Each of the experiments has produced a measurement combining its various results. The combined measurement from CMS with up to 19.7 fb^{-1} of data achieves statistical and systematic uncertainties of 0.08% and 0.27%, respectively [289]. The combined measurement from ATLAS, with up to 20.3 fb^{-1} yields statistical and systematic uncertainties of 0.14% and 0.24%, respectively [288]. CDF has combined measurements with up to 9.3 fb^{-1} [320] and achieves a statistical precision of 0.33% and a systematic uncertainty of 0.43%. DØ achieves a 0.33% statistical+JES and a 0.28% systematic uncertainty by combining results in 9.7 fb^{-1} [321].

Combined measurements from the Tevatron experiments and from the LHC experiments take into account the correlations between different measurements from a single experiment and between measurements from different experiments. The Tevatron average [304], using up to 9.7 fb^{-1} of data, now has a precision of 0.37%. The LHC combination, using up to 4.9 fb^{-1} of data, has a precision of 0.56% [322], where more work on systematic uncertainties is required. A Tevatron-LHC combination has been released, combining the results of all four experiments, using the full Tevatron dataset and the $\sqrt{s} = 7$ TeV LHC data, with a resulting precision of 0.44% [29]. Recently, ATLAS and CMS have released a combinations of fifteen individual top quark mass measurements in semi-leptonic and hadronic decays of the top quark, and a measurement using events enriched in single top quark production via the electroweak t-channel. The data sets used correspond to an integrated luminosity of up to 5 and 20 fb^{-1}, recorded at 7 and 8 TeV, respectively, yielding a precision of 0.33 GeV (0.2%) [1].

The direct measurements of the top-quark mass, such as those shown in Table 61.3, correspond to the parameter used in the Monte Carlo generators, which is closely related to the pole mass [8]. The relation between the pole mass and short-distance masses, such as $\overline{\mathrm{MS}}$, is affected by non-perturbative effects. Recent calculations evaluate the size of this ambiguity to be below 250 MeV and therefore still smaller than the current measurement uncertainty [323,324]. ATLAS has recently performed a 'calibration' of the top mass parameter in POWHEG + PYTHIA 8 with respect to the so-called 'MSR' mass scheme [325]. Using simulated lepton+jets events and the mass distribution of large-radius jets containing the three quarks from the hadronically decaying top quark, they find a mass difference between the Monte Carlo mass and the MSR mass of 80 MeV with large uncertainties [326].

As a result of renormalization at higher-orders in perturbation theory, the top quark mass depends on the scale at which it is evaluated. The CMS collaboration has made the first measurement of the so-called running of the top-quark mass in the $\overline{\mathrm{MS}}$ scheme [327]. The running mass is extracted from a measurement of the differential cross section as a function of the $t\bar{t}$ invariant mass, unfolded back to the parton level, in $e\mu$ final states. The running mass varies by about 15% from $M_{t\bar{t}} = 400$ GeV to $M_{t\bar{t}} \approx 1$ TeV, in good agreement with the renormalization group calculation at one-loop level. Compared to the hypothesis of no running, the significance of the measured running is 2.6σ. However, caveats of such an interpretation have been raised as a result of the large theoretical uncertainties [328].

With the discovery of a Higgs boson at the LHC with a mass of about 125 GeV/c^2 [329, 330], the precision measurement of the top-quark mass takes a central role in the question of the stability of the electroweak vacuum because top-quark radiative corrections tend to drive the Higgs quartic coupling, λ, negative, potentially leading to an unstable vacuum. A calculation at NNLO [2] leads to the conclusion of vacuum stability for a Higgs mass satisfying $M_H \geq 129.4 \pm 5.6$ GeV/c^2 [331]. Given the uncertainty, a Higgs mass of 125 GeV/c^2 satisfies the limit, but the central values of the Higgs and top-quark masses put the electroweak vacuum squarely in the metastable region. The

uncertainty is dominated by the precision of the top-quark mass measurement and its interpretation as the pole mass. For more details, see the Higgs boson review in this volume.

As a test of the CPT-symmetry, the mass difference of top- and antitop-quarks $\Delta m_t = m_t - m_{\bar{t}}$, which is expected to be zero, can be measured. CDF measures the mass difference in 8.7 fb^{-1} of 1.96 TeV data in the lepton+jets channel using a template methode to find $\Delta m_t = -1.95 \pm 1.11(stat.) \pm 0.59(syst.)$ GeV/c^2 [332] while DØ uses 3.6 fb^{-1} of lepton+jets events and the matrix element method with at least one b-tag. They find $\Delta m_t = 0.8 \pm 1.8(stat.) \pm 0.5(syst.)$ GeV/c^2 [333]. In 4.7 fb^{-1} of 7 TeV data, ATLAS measures the mass difference in lepton+jets events with a double b-tag requirement and hence very low background to find $\Delta m_t = 0.67 \pm 0.61(stat.) \pm 0.41(syst.)$ GeV/c^2 [334]. CMS measures the top-quark mass difference in 5 fb^{-1} of 7 TeV data in the lepton+jets channel and finds $\Delta m_t = -0.44 \pm 0.46(stat.) \pm 0.27(syst.)$ GeV/c^2 [335]. They repeat this measurement with 19.6 fb^{-1} of 8 TeV data to find $\Delta m_t = -0.15 \pm 0.19(stat.) \pm 0.09(syst.)$ GeV/c^2 [336]. Now that the top mass has been measured in single-top events, the mass difference can be measured by tagging the top- or anti-top quark with the lepton charge. In 35.9 fb^{-1} of 13 TeV single-top candidate events CMS measures the mass ratio and difference to be $0.995^{+0.005}_{-0.006}$ and $0.83^{+0.77}_{-1.01}$ GeV, respectively [303]. All measurements are consistent with the SM expectation.

61.2.5.2 *Width*

Observation of top-quark spin correlations requires a top-quark lifetime less than the spin decorrelation timescale [337]. The top-quark width, inversely proportional to its lifetime, is expected to be of order 1 GeV/c^2 (Eq. 1). Early measurements made at CDF [338] and CMS [339] established confidence-level intervals for the width, but did not have the sensitivity to make a direct measurement.

The first direct measurement comes from an ATLAS analysis that directly fits reconstructed lepton+jets events in 20.2 fb^{-1} of data at $\sqrt{s} = 8$ TeV. They find $\Gamma_t = 1.76 \pm 0.33^{+0.79}_{-0.68}$ GeV/c^2 [340]. A more recent measurement from ATLAS with 139 fb^{-1} of data at $\sqrt{s} = 13$ TeV [341], uses a template fit to the lepton-b-quark invariant mass in dilepton final states. The result, $\Gamma_t = (1.9 \pm 0.5)$ GeV/c^2, is the most precise measurement to date.

The total width of the top-quark can also be determined from the partial decay width $\Gamma(t \to Wb)$ and the branching fraction $B(t \to Wb)$. DØ obtains $\Gamma(t \to Wb)$ from the measured t-channel cross section for single top-quark production in 5.4 fb^{-1}, and $B(t \to Wb)$ is extracted from a measurement of the ratio $R = B(t \to Wb)/B(t \to Wq)$ in $t\bar{t}$ events in lepton+jets channels with 0, 1 and 2 b-tags. Assuming $B(t \to Wq) = 1$, where q includes any kinematically accessible quark, the result is: $\Gamma_t = 2.00^{+0.47}_{-0.43}$ GeV/c^2 which translates to a top-quark lifetime of $\tau_t = (3.29^{+0.90}_{-0.63}) \times 10^{-25}$ s. Assuming a high mass fourth generation b' quark and unitarity of the four-generation quark-mixing matrix, they set the first upper limit on $|V_{tb'}| < 0.59$ at 95% C.L. [342]. A similar analysis has performed by CMS in 19.7 fb^{-1} of $\sqrt{s} = 8$ TeV data. It provides a better determination of the total width with respect to the measurement by DØ giving $\Gamma_t = 1.36 \pm 0.02(stat.)^{+0.14}_{-0.11}(syst.)$ GeV/c^2 [110].

61.2.5.3 *Yukawa coupling*

The top-Higgs Yukawa coupling is expected to be the largest among all Yukawa couplings. It can be accessed directly by measurements of the $t\bar{t}$ cross section in association with a Higgs boson, $t\bar{t}h$, or indirectly via loop processes in $h \to \gamma\gamma$ or $h \to WW$ decays or in the rare process of $t\bar{t}t\bar{t}$ production. A discussion of the former can be found in this review, See Sec. 11.3.3 of "Status of Higgs Boson Physics", in this Review. Searches for and recently the observation of $t\bar{t}t\bar{t}$ production is discussed in 61.2.1.3.

61.2.5.4 *Top-Quark Electroweak Charges and Couplings*

The top quark is the only quark whose electric charge has not been measured through production at threshold in e^+e^- collisions. Furthermore, it is the only quark whose electromagnetic coupling has not been observed and studied until recently. Since the CDF and DØ analyses on top-quark production did not associate the b, $\bar{b}$, and $W^\pm$ uniquely to the top or antitop, decays such as $t \to W^+\bar{b}, \bar{t} \to W^-b$ were not excluded. A charge 4/3 quark of this kind is consistent with current electroweak precision data. The $Z \to \ell^+\ell^-$ and $Z \to b\bar{b}$ data, in particular the discrepancy between A_{LR} from SLC at SLAC and $A_{FB}^{0,b}$ of b-quarks and $A_{FB}^{0,\ell}$ of leptons from LEP at CERN, can be fitted with a top quark of mass $m_t = 270$ GeV/c^2, provided that the right-handed b quark mixes with the isospin $+1/2$ component of an exotic doublet of charge $-1/3$ and $-4/3$ quarks, $(Q_1, Q_4)_R$ [343,344]. Also the third component of the top quark's weak isospin has not been measured so far.

DØ studied the top-quark charge in double-tagged lepton+jets events, CDF did it in single tagged lepton+jets and dilepton events. Assuming the top- and antitop-quarks have equal but opposite electric charge, then reconstructing the charge of the b-quark through jet charge discrimination techniques, the $|Q_{top}| = 4/3$ and $|Q_{top}| = 2/3$ scenarios can be differentiated. For the exotic model of Chang *et al.* [344] with a top-quark charge $|Q_{top}| = 4/3$, CDF excluded the model at 99% C.L. [345] in 5.6 fb^{-1}, while DØ excluded the model at a significance greater than 5 standard deviations using 5.3 fb^{-1} and set an upper limit of 0.46 on the fraction of such quarks in the selected sample [346]. These results indicate that the observed particle is indeed consistent with being a SM $|Q| = 2/3$ quark.

In 2.05 fb^{-1} at $\sqrt{s} = 7$ TeV, ATLAS performed a similar analysis, reconstructing the b-quark charge either via a jet-charge technique or via the lepton charge in soft muon decays in combination with a kinematic likelihood fit. They measure the top-quark charge to be $0.64 \pm 0.02(stat.) \pm 0.08(syst.)$ from the charges of the top-quark decay products in single lepton $t\bar{t}$ events, and hence exclude the exotic scenario with charge $-4/3$ at more than 8σ [347].

In 4.6 fb^{-1} at $\sqrt{s} = 7$ TeV, CMS discriminates between the SM and the exotic top-quark charge scenario in the muon+jets final states in $t\bar{t}$ events. They exploit the charge correlation between high-p_t muons from W-boson decays and soft muons from B-hadron decays in b-jets. Using an asymmetry technique, where $A = -1$ represents the exotic $Q = -4/3$ scenario and $A = +1$ the SM $Q = +2/3$ scenario, they find $A_{meas} = 0.97 \pm 0.12(stat.) \pm 0.31(sys.)$, which agrees with the Standard Model expectation and excludes the exotic scenario at 99.9% C.L. [348].

$t\bar{t}\gamma$ production:
The electromagnetic or the weak coupling of the top quark can be probed directly by investigating $t\bar{t}$ events with an additional gauge boson, such as $t\bar{t}\gamma$, $t\bar{t}W$, and $t\bar{t}Z$ events. The corresponding coupling can be extracted from the corresponding cross section, cross section ratios with respect to the $t\bar{t}$ cross section or extracted from effective field theory (EFT) fits to various measured distributions and differential cross sections.

CDF performed a first search for $t\bar{t}\gamma$ producton in events containing a lepton, a photon, significant missing transverse momentum, and a jet identified as containing a b-quark and at least three jets and large total transverse energy in 6.0 fb^{-1}. They reported evidence for the observation of $t\bar{t}\gamma$ production with a cross section $\sigma_{t\bar{t}\gamma} = 0.18 \pm 0.08$ pb and a ratio of $\sigma_{t\bar{t}\gamma}/\sigma_{t\bar{t}} = 0.024 \pm 0.009$ [349].

ATLAS performed a first measurement of the $t\bar{t}\gamma$ cross section in pp collisions at $\sqrt{s} = 7$ TeV using 4.6 fb^{-1} of data. Events are selected that contain a large transverse momentum electron or muon and a large transverse momentum photon. The production of $t\bar{t}\gamma$ events was observed with a significance of 5.3 standard deviations. The resulting cross section times branching ratio into the single lepton channel for $t\bar{t}\gamma$ production with a photon with transverse momentum above 20 GeV is $\sigma^{fid.}(t\bar{t}\gamma) \times BR = 63 \pm 8(stat.)^{+17}_{-13}(syst.) \pm 1(lumi.)$ pb per lepton flavor [350], which is consistent with leading-order theoretical calculations.

At 8 TeV, ATLAS has used 20.2 fb^{-1} of data to measure the $t\bar{t}\gamma$ cross section with a photon above 15 GeV and $|\eta| < 2.37$. The fiducial cross section is measured to be 139 ± 18 fb [351], in good agreement with the NLO prediction [352]. Using 19.7 fb^{-1} of data at 8 TeV, CMS performed a similar measurement of the $t\bar{t}\gamma$ production cross section in the lepton+jets decay mode with a photon transverse momentum above 25 GeV and $|\eta| < 1.44$. They obtain a normalized cross section $\mathcal{R} = \sigma_{t\bar{t}+\gamma}/\sigma_{t\bar{t}} = (5.7 \pm 1.8) \times 10^{-4}$ in e+jets and $(4.7 \pm 1.3) \times 10^{-4}$ in μ+jets. The fiducial $t\bar{t}\gamma$ cross section is obtained by multiplying by the measured $t\bar{t}$ fiducial cross section of $244.9 \pm 1.4(stat.)^{+6.3}_{-5.5}(sys.) \pm 6.4(lumi.)$ pb. Extrapolating to the full phase space, the result is $\sigma_{t\bar{t}\gamma} \times \text{BR} = (515 \pm 108)$ fb, per lepton+jets final state [353], in good agreement with the theoretical prediction.

At $\sqrt{s} = 13$ TeV, using 36.1 fb^{-1} of single-lepton and dilepton events with exactly one photon, ATLAS measures the $t\bar{t}\gamma$ cross section. They employ neural network algorithms to separate the signal from the backgrounds. The fiducial cross-sections are measured to be $521 \pm 9(stat.) \pm 41(sys.)$ fb and $69 \pm 3(stat.) \pm 4(sys.)$ fb for the single-lepton and dilepton channels, respectively. The differential cross-sections are measured as a function of photon transverse momentum, photon absolute pseudorapidity, and angular distance between the photon and its closest lepton in both channels, as well as azimuthal opening angle and absolute pseudorapidity difference between the two leptons in the dilepton channel. All measurements are in agreement with the theoretical predictions [354].

ATLAS uses 139 fb^{-1} of $\sqrt{s} = 13$ TeV $e\mu + \gamma$ events with at least two jets, out of which at least one is b-tagged, to measure the inclusive and differential cross-sections for the production of a top-quark pair in association with a photon. This analysis is sensitive to both processes, $t\bar{t}\gamma + tW\gamma$. The fiducial cross-section is measured to be $39.6^{+2.7}_{-2.3}$ fb in good agreement with the dedicated theoretical calculation provided by the authors of refs. [355, 356], which predicts a value of $\sigma_{fid} = 38.50^{+0.56}_{-2.18}$ (scale)$^{+1.04}_{-1.18}$ (PDF) fb for the chosen fiducial phase space. Differential cross-sections as functions of several observables are compared to state-of-the-art Monte Carlo simulations and NLO theoretical calculations. These include cross-sections as functions of the photon transverse momentum and absolute pseudorapidity and angular variables related to the photon and the leptons and between the two leptons in the event. All measurements are in agreement with the predictions [357].

Recently, CMS used 137 fb^{-1} of data to measure the $t\bar{t}\gamma$ cross section. In the lepton-plus-jets channel, they perform measurements in a fiducial volume defined at the particle level. Events with an isolated, highly energetic lepton, at least three jets from the hadronization of quarks, among which at least one is b-tagged, and one isolated photon are selected. The inclusive fiducial $t\bar{t}\gamma$ cross section, for a photon with transverse momentum greater than 20 GeV and pseudorapidity $|\eta| < 1.4442$, is measured to be $\sigma_{t\bar{t}\gamma} = 798 \pm 7(stat) \pm 48(syst)$ fb, in good agreement with the prediction from the standard model at NLO in QCD [358]. The differential cross sections are also measured as a function of several kinematic observables such as the transverse momentum of the photon, its rapidity, or the opening angle between the photon and the lepton. The measurements on detector-level are also interpreted in terms of limits on the Wilson coefficients in the context of the standard model effective field theory. The confidence intervals for the Wilson coefficients c_{tZ} and c_{tZ}^I are the most stringent to date. Using the same dataset, in the dilepton channel, an inclusive cross section of $174.4 \pm 2.5(stat) \pm 6.1(syst)$ fb is measured in a signal region with at least one b-tagged jet and exactly one photon with transverse momentum above 20 GeV [359]. In the same analysis, differential cross sections are measured as a function of several kinematic observables of the photon, leptons, and jet, and compared to standard model predictions. Combinations of the measurements in the l+jets and the dilepton channels are also interpreted in the standard model effective field theory framework, yielding the most stringent limits for the Wilson coefficients c_{tZ}

and c_{tZ}^{I} to date.

$tq\gamma$ production:

Using the full Run-2 data set of 139 fb^{-1} at 13 TeV, ATLAS observes the production of single top quark together with a photon. The analysis uses the presence of a forward jet, characteristic of t-channel production, and separates the signal from the background with neural networks. Requiring a photon with transverse momentum larger than 20 GeV and within the detector acceptance, the fiducial cross section is measured to be $688 \pm 23(stat.)_{-71}^{+75}(syst.)$ fb, to be compared with the Standard Model prediction of 515_{-42}^{+36} fb at NLO in QCD [360]. In 35.9 fb^{-1} of lepton-plus-photon-plus-jets events, CMS manages to establish the first evidence for the associated production of a single-top quark and a photon at $\sqrt{s} = 13$ TeV. They employ a multivariate discriminant based on topological and kinematic event properties to separate signal from background processes. An excess above the background-only hypothesis is observed, with a significance of 4.4 standard deviations. A fiducial cross section is measured for isolated photons with transverse momentum greater than 25 GeV in the central region of the detector. The measured product of the cross section and branching fraction is $\sigma(pp \to t\gamma j)B(t \to \mu\gamma b) = 115 \pm 17(stat) \pm 30(syst)$ fb, which is consistent with the SM prediction [361]. A precision test of the vector and axial vector couplings in $t\bar{t}\gamma$ events or searches for possible tensor couplings of top-quarks to photons will only be feasible with an integrated luminosity of several hundred fb^{-1} in the future [362].

$t\bar{t}Z$ and $t\bar{t}W$ production:

ATLAS and CMS have also studied the associate production of top-antitop quark pairs along with an electroweak gauge boson, $t\bar{t}W$ or $t\bar{t}Z$, where in the Standard Model the W-boson is expected to be produced via initial state radiation, while the Z-boson can also be radiated from a final-state top-quark and hence provides sensitivity to the top-quark neutral current weak gauge coupling, which implies a sensitivity to the third component of the top-quark's weak isospin, which has not been measured so far.

CMS performed measurements of the $t\bar{t}W$ and $t\bar{t}Z$ cross section at $\sqrt{s} = 7$ TeV with 5 fb^{-1}, yielding $\sigma_{t\bar{t}V} = 0.43_{-0.15}^{+0.17}(stat.)_{-0.07}^{+0.09}(syst.)$ pb $(V = Z, W)$ and $\sigma_{t\bar{t}Z} = 0.28_{-0.11}^{+0.14}(stat.)_{-0.03}^{+0.06}(syst.)$ fb, at about 3 standard deviations significance [363] and compatible with the SM expectations of $0.306_{-0.053}^{+0.031}$ pb and $0.137_{-0.016}^{+0.012}$ pb, respectively [364,365]. ATLAS performed a similar analysis with 4.7 fb^{-1} in the three-lepton channel and set an upper limit of 0.71 pb at 95% C.L. [366].

Using 20.3 fb^{-1} of 8 TeV data, ATLAS performs a simultaneous measurement of the $t\bar{t}W$ and $t\bar{t}Z$ cross section. They observe the $t\bar{t}W$ and $t\bar{t}Z$ production at the 5.0σ and 4.2σ level, respectively, yielding $\sigma_{t\bar{t}W} = 369_{-91}^{+100}$ fb and $\sigma_{t\bar{t}Z} = 176_{-52}^{+58}$ fb [367]. CMS performs an analysis where signal events are identified by matching reconstructed objects in the detector to specific final state particles from $t\bar{t}W$ and $t\bar{t}Z$ decays using 19.5 fb^{-1} of 8 TeV data. They obtain $\sigma_{t\bar{t}W} = 382_{-102}^{+117}$ fb and $\sigma_{t\bar{t}Z} = 242_{-55}^{+65}$ fb, yielding a significance of 4.8 and 6.4 standard deviation, respectively [368]. These measurements are used to set bounds on five anomalous dimension-six operators that would affect the $t\bar{t}W$ and $t\bar{t}Z$ cross sections.

The most recent measurements in these channels are made at 13 TeV from ATLAS and CMS in multilepton final states. ATLAS made a measurement using 36.1 fb^{-1} of events with two, three or four leptons. In multiple regions, the $t\bar{t}Z$ and $t\bar{t}W$ cross sections are simultaneously measured using a combined fit to all regions, yielding $\sigma_{t\bar{t}Z} = 0.95 \pm 0.08(stat) \pm 0.10(syst)$ pb and $\sigma_{t\bar{t}W} = 0.87 \pm 0.13(stat) \pm 0.14(syst)$ pb [369] to be compared with the NLO+NLL (QCD) and NLO (EW) SM predictions, $\sigma_{t\bar{t}W} = 579_{-9\%}^{+14\%}$ fb and $\sigma_{t\bar{t}Z} = 811_{-10\%}^{+11\%}$ fb [43]. Recently, ATLAS uses 139 fb^{-1} in three and four lepton events to measure the inclusive and differential $t\bar{t}Z$ cross section. The inclusive cross section is measured to be $\sigma_{t\bar{t}Z} = 0.99 \pm 0.05(stat.) \pm 0.08(syst.)$ pb [370], in agreement with the most precise theoretical predictions. The differential measurements are presented as a function of a number of kinematic variables which probe the kinematics of the $t\bar{t}Z$ system. Overall, good

agreement is observed between the unfolded data and the predictions. Using the same dataset of 140 fb^{-1}, ATLAS performs an improved measurement in both, the inclusive and differential $t\bar{t}Z$ production cross sections. Final states with two, three and four isolated leptons (electrons or muons) are targeted. The inclusive cross section is measured to be $\sigma_{t\bar{t}Z} = 0.86 \pm 0.04(stat.) \pm 0.04(syst.)$ pb and found to be in agreement with the most advanced Standard Model predictions [371]. The improvement with respect to the previous measurement using the same dataset is mainly in a better machine learning-based separation of signal and background, the addition of a 2-lepton signal region, and better modelling. The differential measurements are presented as a function of a number of observables that probe the kinematics of the $t\bar{t}Z$ system. Both absolute and normalised differential cross section measurements are performed at particle- and parton-level for specific fiducial volumes, and are compared with theoretical predictions at NLO+NNLL. The results are interpreted in the framework of the Standard Model Effective Field Theory and used to set limits on a large number of dimension-6 operators involving the top quark. CMS uses 35.9 fb^{-1} of $\sqrt{s} = 13$ TeV data to measure $\sigma_{t\bar{t}W} = 0.77^{+0.12}_{-0.11}(stat.)^{+0.13}_{-0.12}(syst.)$ pb and $\sigma_{t\bar{t}Z} = 0.99^{+0.09}_{-0.08}(stat.)^{+0.12}_{-0.10}(syst.)$ pb production cross sections, and significances over the background-only hypotheses of 5.5σ and 9.5σ, respectively [372], firmly establishing the observation of these processes. CMS measured the inclusive $t\bar{t}Z$ cross section in 77.5 fb^{-1} of events with three or four charged leptons, and the Z boson is detected through its decay to an oppositely charged lepton pair. The production cross section is measured to be $\sigma(t\bar{t}Z) = 0.95 \pm 0.05(stat) \pm 0.06(syst)$ pb. This measurement includes differential cross sections as functions of the transverse momentum of the Z boson and the angular distribution of the negatively charged lepton from the Z boson decay, which characterise the $t\bar{t}Z$ process in detail for the first time, as well as stringent direct limits on the anomalous tZ couplings [373]. Very recently, using the complete Run-2 dataset of 138 fb^{-1}, CMS searches for signs of new physics, interpreted in effective field theory, in $t\bar{t}$ events produced in association with a Lorentz-boosted Z or Higgs boson [374]. Selected events contain a single lepton and hadronic jets, including two identified with the decay of bottom quarks, plus an additional large-radius jet with high transverse momentum identified as a Z or Higgs boson decaying to a bottom quark pair. Machine learning techniques are employed to discriminate between $t\bar{t}Z$ or $t\bar{t}H$ events and events from background processes, which are dominated by $t\bar{t}$+jets production. No indications of new physics are observed. The signal strengths of boosted $t\bar{t}Z$ and $t\bar{t}H$ production are measured, and upper limits are placed on the $t\bar{t}Z$ and $t\bar{t}H$ differential cross sections as functions of the Z or Higgs boson transverse momentum, expressed as limits on eight possible dimension-six operators.

Recently, CMS measured the $t\bar{t}W$ cross section in 138 fb^{-1} at 13 TeV in events with two or three leptons (electrons and muons) and additional jets. In events with two leptons, a multiclass neural network is used to distinguish between the signal and background processes. Events with three leptons are categorized based on the number of jets and of jets originating from b quark hadronization, and the lepton charges. The inclusive $t\bar{t}W$ production cross section in the full phase space is measured to be $868 \pm 40(stat) \pm 51(syst)$ fb. The $t\bar{t}W^+$ and $t\bar{t}W^-$ cross sections are also measured as $553 \pm 30(stat) \pm 30(syst)$ fb and $343 \pm 26(stat) \pm 25(syst)$ fb, respectively, and the corresponding ratio of the two cross sections is found to be $1.61 \pm 0.15(stat)^{+0.07}_{-0.05}(syst)$ [375]. The measured cross sections are larger than but consistent with the standard model predictions within two standard deviations. Also ATLAS presents both, the inclusive and differential cross-sections of $t\bar{t}W$ production in 140 fb^{-1} of 13 TeV data using final states with two same-sign or three isolated leptons (electrons or muons). The inclusive production cross-section is measured to be 890 ± 80 fb, which turns out a bit high compared to the new reference theoretical prediction at NNLO in QCD of $745.3 \pm 49.9(scale) \pm 13.4(PDF)$ fb [46]. Differential cross-section measurements characterise this process in detail for the first time. Several particle-level observables are compared to a variety of theoretical predictions which are generally in good agreement with the normalised differential cross-

section results [376]. They also measure the $t\bar{t}W^+$ and $t\bar{t}W^-$ cross section individually, yielding a ratio of $R = 1.95^{+0.21}_{-0.18}(stat.)^{+0.16}_{-0.13}(syst.)$.

single-top + W/Z production:

The electroweak couplings can also be probed in single-top production in association with a Z boson. The $pp \to tZq$ process at the LHC probes both the WWZ coupling in the case where the Z emerges from the t-channel W in single-top production and, in the case where the Z is radiated from the top quark, the tZ coupling. A CMS search at 8 TeV using 19.7 fb^{-1} produced a hint of a tZq signal in tri-lepton events, with a significance compared to the background-only hypothesis of 2.4σ [377]. Very recently, CMS and ATLAS collaborations used 139 fb^{-1} at 13 TeV in three-lepton events to measure $tZ(\to \ell^+\ell^-)q$. CMS obtains $\sigma_{tZq} = 87.9^{+7.5}_{-7.3}(stat)^{+7.3}_{-6.0}(syst)$ fb for $m(\ell\ell) > 30$ GeV [378], following the evidence [361] of the observation of the process [379]. The ratio between the cross sections for the top quark and the top antiquark production in association with a Z boson is measured as $2.37^{+0.56}_{-0.42}(stat)^{+0.27}_{-0.13}(syst)$. Differential measurements at parton and particle levels are performed for the first time. Additionally, the spin asymmetry, which is sensitive to the top quark polarization, is determined from the differential distribution of the polarization angle at parton level to be $0.58^{+0.15}_{-0.16}$ (stat) ± 0.06 (syst), in agreement with SM predictions at next-to-leading order. Using neural networks, ATLAS improves the background rejection and extracts the signal. The measured cross-section for $m(\ell\ell) > 30$ GeV is $97 \pm 13(stat.) \pm 7(syst.)$ fb, consistent with the Standard Model prediction [380].

tWZ production:

Using 138 fb^{-1} at 13 TeV, CMS presents the first evidence for the standard model production of a top quark in association with a W and a Z boson in multilepton final states. The Z boson is reconstructed via its decays to electron or muon pairs. The measured cross section amounts to $0.37 \pm 0.05(stat) \pm 0.10(syst)$ pb, and corresponds to an observed (expected) significance of 3.5 (1.4) standard deviations [381].

Searches for and now also measurements of the associate production of a top-antitop quark pair along with a Higgs boson, $t\bar{t}h$, with various subsequent decays provide sensitivity to the top-Higgs Yukawa coupling. For further details, see the review on "Status of Higgs boson physics".

61.2.6 *New Physics*

The top quark plays a special role in the SM. Being the only quark with a coupling to the Higgs boson of order one, it provides the most important contributions to the quadratic radiative corrections to the Higgs mass exposing the issue of the naturalness of the SM. It is therefore very common for models where the naturalness problem is addressed to have new physics associated with the top quark. In SUSY, for instance, naturalness predicts the scalar top partners to be the lightest among the squarks and to be accessible at the LHC energies (see the review "Supersymmetry: Theory"). In models where the Higgs is a pseudo-Goldstone boson, such as Little Higgs models, naturalness predicts the existence of partners of the top quarks with the same spin and color, but with different electroweak couplings, the so-called vectorial t'. Stops and t''s are expected to have sizeable branching ratios to top quarks. Another intriguing prediction of SUSY models with universal couplings at the unification scale is that for a top-quark mass close to the measured value, the running of the Yukawa coupling down to 1 TeV naturally leads to the radiative breaking of the electroweak symmetry [382]. In fact, the top quark plays a role in the dynamics of electroweak symmetry breaking in many models [383]. One example is topcolor [384], where a large top-quark mass can be generated through the formation of a dynamic $t\bar{t}$ condensate, X, which is formed by a new strong gauge force coupling preferentially to the third generation. Another example is topcolor-assisted technicolor [385], predicting the existence of a heavy Z' boson that couples preferentially to the third generation of quarks. If light enough such a state might be directly accessible at the

present hadron collider energies, or if too heavy, lead to four-top interactions possibly visible in the $t\bar{t}t\bar{t}$ final state. This final state has been observed by CMS [168] and by ATLAS [164].

61.2.6.1 *Direct Searches for Physics Beyond the Standard Model*

In this section we review the latest direct searches for Physics Beyond the Standard Model (PBSM) in top-quark production and decay. These direct search come in two categories: $t\bar{t}$ resonance searches and searches for rare non-SM interactions involving top quarks, including Flavor-Changing-Neutral-Current (FCNC) searches. Top-sector resonance searches come in two categories, $t\bar{t}$ resonances in which a presumed heavy particle X decays into a $t\bar{t}$ pair, and searches in which a non-SM decay product of the top quark is observed via its resonant decay. The most recent results are of the latter category. We refer the reader to Refs. [386–388] for $X \to t\bar{t}$ searches. Searches for rare non-SM interactions and FCNC final states are interpreted using the EFT approach described in Section 61.1.1.2. In this section we focus on the branching-ratio limits from these searches, while the EFT interpretations are cited in Section 61.2.6.4.

61.2.6.2 *FCNC and Rare non-SM Interaction Searches*

The most recent FCNC searches target a $t \to qH$ decay in $t\bar{t}$ production, or an FCNC vertex in single-top production together with a Higgs boson. The ATLAS search in Ref. [389] looks for $H \to \tau\tau$ in both cases. A small, 2.3σ excess of events is observed and limits on $t \to qH$ branching ratios are set. The most recent CMS result uses Higgs decays to vector bosons in addition to $\tau\tau$. That result is combined with results from Refs. [390] and [391] that use the $b\bar{b}$ and $\gamma\gamma$ decay channels of the Higgs [392]. Table 61.4 shows the most recent independent limits for $q = u$ or $q = c$ and assume the other branching ratio is zero. Other results can be found in the Listings.

Table 61.4: 95% C.L. limits on branching ratios (BR) of the top quark for FCNC and other rare non-SM interactions.

bht! Process	BR limit	Reference
$t \to cH$	9.4×10^{-4}	[389]
	4.3×10^{-4}	[392]
$t \to cH$ Combined	3.7×10^{-4}	[392]
$t \to uH$	6.9×10^{-4}	[389]
	7.2×10^{-4}	[392]
$t \to uH$ Combined	1.9×10^{-4}	[392]
$t \to Zu$ LH	6.2×10^{-5}	[393]
$t \to Zc$ LH	1.3×10^{-4}	[393]
$t \to u\gamma$ LH	0.85×10^{-5}	[394]
$t \to c\gamma$ LH	4.2×10^{-5}	[394]
$t \to ug$	0.61×10^{-4}	[395]
$t \to cg$	3.7×10^{-4}	[395]
$t \to e\mu u$ (Scalar)	0.07×10^{-6}	[396]
$t \to e\mu u$ (Vector)	0.13×10^{-6}	[396]
$t \to e\mu u$ (Tensor)	0.25×10^{-6}	[396]
$t \to e\mu c$ (Scalar)	0.89×10^{-6}	[396]
$t \to e\mu c$ (Vector)	1.31×10^{-6}	[396]
$t \to e\mu c$ (Tensor)	2.59×10^{-6}	[396]
$t \to \mu\tau q$	11×10^{-7}	[397]

Searches targeting tZq couplings use leptonic decays of the Z-boson and a trilepton final state.

In $t\bar{t}$ events, the signal occurs through the FCNC decay $t \to Zq$, in single-top the signal occurs through the associated production of a top quark and a Z-boson. The branching-ratio limits shown in Table 61.4 are for tZu and tZc left-handed couplings and assume, for tZu, that the tZc coupling is zero and vice versa. Reference [393] also presents limits for right-handed couplings, which are close to the values quoted in Table 61.4 for left-handed couplings

Searches targeting $t\gamma q$ couplings focus on a high-P_T photon in the final state. As with tZq couplings, signal events occur through top-quark decay in $t\bar{t}$ and through associated production of a top quark and a photon in single-top events. In Ref. [394] limits are found for the EFT couplings shown in Table 61.7, and the limits shown in Table 61.4 are derived from the limits on the WCs. The table shows the limits assuming a left-handed coupling. Limits on right-handed couplings are also give in Ref. [394] and are only slightly weaker than those determined for left-handed couplings.

In Ref. [395] FCNC couplings tgq between a top quark, a gluon, and an up or charm quark are looked for in single-top production. The couplings increase the single-top production cross section and, in the case of the tgc coupling, also affect the rapidity distribution of the produced top quark because of the different PDFs for valence and sea quarks.

CMS searches for charged-lepton-flavor-violating interactions in both production, $q \to e\mu t$, and decay, $t \to e\mu q$, with $q = u$ or c [396]. The branching ratio limits set are included in Table 61.4 and the Wilson coefficients constrained are listed in Table 61.6.

ATLAS has searched for charged-lepton-flavor-violating $\mu\tau$ qt interactions which are sensitive to the two-quark-two-lepton operators of Table 61.1 [397]. The branching ratio limit set is included in Table 61.4 and the Wilson coefficients constrained are listed in Table 61.6.

61.2.6.3 *Resonance Searches*

While technically an FCNC search, a decay of the type $t \to qX$ where $q = u$ or c, could be missed when X is not the expected quark or boson. ATLAS has searched for $t \to qX$ where X is a light scalar with a mass below the top quark that decays to $b\bar{b}$ [398]. Such phenomena exist in composite Higgs models [403]. The ATLAS search used $t\bar{t}$ events and separated signal from

Table 61.5: Wilson coefficients (WC) corresponding to boson operators and related PBSM search references.

bht! WC	Process	Citations
C_{tW}	Single-top polarization	[211]
	$t\bar{t}Z, tZ$	[399]
	Boosted $t\bar{t}Z$, $t\bar{t}H$	[374]
	$t+$ additional leptons	[400]
	$t\bar{t}Z$	[371]
C_{tZ}	$t\bar{t}Z, tZ$	[399]
	$t\bar{t}Z$, $t\bar{t}H$	[374]
	$t+$ additional leptons	[400]
C_{bW}	Boosted $t\bar{t}Z$, $t\bar{t}H$	[374]
C_{tG}	Boosted $t\bar{t}$	[401]
	$t\bar{t}$ charge asymmetry	[234]
	$t\bar{t}Z$	[371]
C_{tB}	$t\bar{t}Z$	[371]
C_{Ht}	$t\bar{t}Z$	[371]
C_{HQ}^1	$t\bar{t}Z$	[371]
C_{HQ}^3	$t\bar{t}Z$	[371]

Table 61.6: Wilson coefficients (WC) corresponding to four-fermion operators and related PBSM search references.

WC	Process	Citations
C_{Qq}^{11}	$t\bar{t}$ charge asymmetry	[234]
	$t\bar{t}$ energy asymmetry in $t\bar{t}j$	[238]
	$t\bar{t}Z$	[371]
C_{Qq}^{18}	$t\bar{t}$ charge asymmetry	[234]
	$t\bar{t}$ energy asymmetry in $t\bar{t}j$	[238]
	Boosted all-hadronic $t\bar{t}$	[402]
	$t\bar{t}Z$	[371]
C_{tq}^{1}	$t\bar{t}$ charge asymmetry	[234]
	$t\bar{t}$ energy asymmetry in $t\bar{t}j$	[238]
	$t\bar{t}Z$	[371]
C_{tq}^{8}	$t\bar{t}$ charge asymmetry	[234]
	$t\bar{t}$ energy asymmetry in $t\bar{t}j$	[238]
	Boosted all-hadronic $t\bar{t}$	[402]
	Boosted $t\bar{t}$	[401]
	$t\bar{t}Z$	[371]
C_{tu}^{1}	$t\bar{t}$ charge asymmetry	[234]
	$t\bar{t}$ energy asymmetry in $t\bar{t}j$	[238]
	$t\bar{t}Z$	[371]
C_{td}^{1}	$t\bar{t}$ charge asymmetry	[234]
	$t\bar{t}Z$	[371]
C_{tu}^{8}	$t\bar{t}$ charge asymmetry	[234]
	$t\bar{t}$ energy asymmetry in $t\bar{t}j$	[238]
	Boosted all-hadronic $t\bar{t}$	[402]
	$t\bar{t}Z$	[371]
C_{td}^{8}	$t\bar{t}$ charge asymmetry	[234]
	Boosted all-hadronic $t\bar{t}$	[402]
	$t\bar{t}Z$	[371]
C_{Qd}^{8}	$t\bar{t}$ charge asymmetry	[234]
	Boosted all-hadronic $t\bar{t}$	[402]
	$t\bar{t}Z$	[371]
C_{Qu}^{8}	$t\bar{t}$ charge asymmetry	[234]
	Boosted all-hadronic $t\bar{t}$	[402]
	$t\bar{t}Z$	[371]
C_{Qu}^{1}	$t\bar{t}$ charge asymmetry	[234]
	$t\bar{t}Z$	[371]
C_{Qd}^{1}	$t\bar{t}$ charge asymmetry	[234]
	$t\bar{t}Z$	[371]
C_{Qq}^{31}	$t\bar{t}Z$	[371]
C_{Qq}^{38}	$t\bar{t}$ charge asymmetry	[234]
	Boosted all-hadronic $t\bar{t}$	[402]
	$t\bar{t}Z$	[371]
$C_{\ell equ}^{3(2313)}$	$t \to \mu\tau u$	[397]
$C_{\ell equ}^{1(2323)}$	$t \to \mu\tau c$	[397]
$C_{e\mu tu}$	top production & decay	[396]
$C_{e\mu tc}$	top production & decay	[396]

background by categorizing events according to the number of jets and the number of jets tagged as originating from b-quarks. The observed limits correspond to the product of the BR $t \to qX$

and $X \to b\bar{b}$. The limit in the $t \to uX(t \to cX)$ channel is $0.019\%(0.018\%)$ for $M_X = 20$ GeV and $0.062\%(0.078\%)$ for $M_X = 160$ GeV.

61.2.6.4 *Effective Field Theory Results*

As described in Section 61.1.1.2, EFTs have become a primary tool for evaluating the outcome of top PBSM searches. EFT provides both model-independent limits, a straightforward way to compare and contrast search results from different processes and different experiments, and a guide to the full space of possible top-quark-related PBSM. In a nice pedagogical paper [404], Zhang and Willenbrock elucidate the advantages of the EFT approach compared to the vertex-function approach for searching for PBSM in top-quark interactions, including the fact that the EFT approach incorporates the SM gauge symmetry and contact interactions that are neglected in the vertex-function approach. As a result of these advantages, EFTs have become the dominant technique for evaluating search limits, and we review the most recent results in this section.

As ATLAS and CMS do, we categorize the top-EFT operators as follows: four-fermion operators, vector-boson operators and scalar-boson operators. Operators can change the overall rate of top-quark production, modify the kinematics of production and/or decay, or produce new interactions, such as flavor-changing neutral currents (FCNC). To date, all results are consistent with the SM expectation of zero for each Wilson coefficient. The numerical values of the limits are not intuitively meaningful, especially given that they correspond to an arbitrarily chosen mass scale of $\Lambda = 1$ TeV. Therefore, rather than providing a table of confidence intervals, we refer the interested reader to the LHC Top Working Group page of summary plots where the limits on the Wilson coefficients are presented graphically [405], and to the references given below. Instead, the tables below provide the most recent relevant references (i.e. those using the full LHC dataset of 139 fb^{-1}) for limits on each coefficient wherein measurement, fitting, and limit derivation techniques can be found. Additional limits and references can be found in the listings and in references [359, 374, 396, 399, 400, 406–408].

Table 61.7: Wilson coefficients (WC) corresponding to flavor-changing-neutral-current (FCNC) operators and related PBSM search references.

WC	Process	Citations
$C_{uW}^{32} + C_{uB}^{32}$	$tq\gamma$	[394]
$C_{uW}^{(23)*} + C_{uB}^{(23)*}$	$tq\gamma$	[394]
$C_{uW}^{31} + C_{uB}^{31}$	$tq\gamma$	[394]
$C_{uW}^{(13)*} + C_{uB}^{(13)*}$	$tq\gamma$	[394]
C_{uW}^{32}, C_{uB}^{32}	tZc	[393]
$C_{uW}^{(23)*}, C_{uB}^{(23)*}$	tZc	[393]
C_{uW}^{31}, C_{uB}^{31}	tZu	[393]
$C_{uW}^{(13)*}, C_{uB}^{(13)*}$	tZu	[393]
C_{uG}	tgu	[395]
C_{cG}	tgc	[395]
$C_{u\phi}$	tHu	[389]
$C_{c\phi}$	tHc	[389]

61.3 Outlook

Top quark physics at hadron colliders has developed into precision physics. Various properties of the top quark have been measured with high precision, where the LHC has by now surpassed

the Tevatron precision and reach in the majority of relevant observables. Several $\sqrt{s}$-dependent physics quantities, such as the production cross-section, have been measured at several energies at the Tevatron and the LHC. Up to now, all measurements are consistent with the SM predictions and allow stringent tests of the underlying production mechanisms by strong and weak interactions. Given the very large event samples available at the LHC, top-quark properties will be further determined in $t\bar{t}$ as well as in electroweak single top-quark production. At the Tevatron, the $t-$ and $s-$channels for electroweak single top-quark production have been estblished separately. At the LHC, quick progress has been achieved in the last years yielding more than 3 sigma significance of the s-channel and more than 5 sigma significance for the t-chnnel and Wt-production. Furthermore, $t\bar{t}\gamma$, $t\bar{t}Z$, and $t\bar{t}W$ together with $t\bar{t}H$ associated production have started to provide key information on the top-quark electroweak couplings. Corresponding effective field theory (EFT) fits for the coupling extraction are being developed. At the same time various models of physics beyond the SM involving top-quark production are being constrained. While a majority of the Run-II data recorded at 13 TeV has been analysed or is in an advanced stage, the beginning of the Run-III at $\sqrt{s} = 13.6$ to 14 TeV and an expected integrated luminosity of $160 - 200$ fb^{-1}, doubling the Run-I plus Run-II data set, is immanent. With the first results being released, top-quark physics has the potential to shed light on open questions and new aspects of physics at the TeV scale.

CDF and DØ notes can be retrieved from

  https://inspirehep.net

with the search command "find CDF-NOTE-XXXXX" or "find D0 Note XXXX",

and ATLAS note references from

  https://twiki.cern.ch/twiki/bin/view/AtlasPublic/TopPublicResults,

and CMS note references from

  https://twiki.cern.ch/twiki/bin/view/CMSPublic/PhysicsResultsTOP,

and plots provided by the LHC Top Working Group from

  https://twiki.cern.ch/twiki/bin/view/LHCPhysics/LHCTopWGSummaryPlots.

References

[1] ATLAS Collab. and CMS Collab., ATLAS-CONF-2023-066, CMS-PAS-TOP-22-001.

[2] G. Degrassi *et al.*, JHEP **08**, 098 (2012), [arXiv:1205.6497].

[3] D. Buttazzo *et al.*, JHEP **12**, 089 (2013), [arXiv:1307.3536].

[4] A. Andreassen, W. Frost and M. D. Schwartz, Phys. Rev. D **97**, 5, 056006 (2018), [arXiv:1707.08124].

[5] A. H. Hoang *et al.*, JHEP **04**, 003 (2018), [arXiv:1704.01580].

[6] P. Marquard *et al.*, Phys. Rev. Lett. **114**, 14, 142002 (2015), [arXiv:1502.01030].

[7] P. Nason, *The Top Mass in Hadronic Collisions*, 123–151 (2019), [arXiv:1712.02796].

[8] A. H. Hoang, Ann. Rev. Nucl. Part. Sci. **70**, 225 (2020), [arXiv:2004.12915].

[9] S. Weinberg, Phys. Rev. Lett. **43**, 1566 (1979).

[10] W. Buchmuller and D. Wyler, Nucl. Phys. B **268**, 621 (1986).

[11] B. Grzadkowski *et al.*, JHEP **10**, 085 (2010), [arXiv:1008.4884].

[12] D. Barducci *et al.* (2018), [arXiv:1802.07237].

[13] J. A. Aguilar-Saavedra, Nucl. Phys. B **812**, 181 (2009), [arXiv:0811.3842].

[14] C. Zhang and S. Willenbrock, Phys. Rev. **D83**, 034006 (2011), [arXiv:1008.3869].

[15] R. S. Chivukula and H. Georgi, Phys. Lett. B **188**, 99 (1987).

[16] L. J. Hall and L. Randall, Phys. Rev. Lett. **65**, 2939 (1990).

[17] G. D'Ambrosio *et al.*, Nucl. Phys. B **645**, 155 (2002), [hep-ph/0207036].

[18] M. Jezabek and J. H. Kuhn, Nucl. Phys. **B314**, 1 (1989).

[19] A. Czarnecki and K. Melnikov, Nucl. Phys. **B544**, 520 (1999), [hep-ph/9806244]; K. G. Chetyrkin *et al.*, Phys. Rev. **D60**, 114015 (1999), [hep-ph/9906273].

[20] L.-B. Chen *et al.*, Phys. Rev. D **108**, 5, 054003 (2023), [arXiv:2212.06341].

[21] I. I. Y. Bigi *et al.*, Phys. Lett. **B181**, 157 (1986).

[22] A. H. Hoang *et al.*, Phys. Rev. **D65**, 014014 (2002), [hep-ph/0107144].

[23] K. Hagiwara, Y. Sumino and H. Yokoya, Phys. Lett. **B666**, 71 (2008), [arXiv:0804.1014].

[24] B. Fuks *et al.*, Phys. Rev. D **104**, 3, 034023 (2021), [arXiv:2102.11281].

[25] G. Eilam, J. L. Hewett and A. Soni, Phys. Rev. D **44**, 1473 (1991), [Erratum: Phys.Rev.D 59, 039901 (1999)].

[26] J. A. Aguilar-Saavedra, Acta Phys. Polon. B **35**, 2695 (2004), [hep-ph/0409342].

[27] M. Czakon, P. Fiedler and A. Mitov, Phys. Rev. Lett. **110**, 252004 (2013), [arXiv:1303.6254].

[28] S. Catani *et al.*, JHEP **07**, 100 (2019), [arXiv:1906.06535].

[29] ATLAS,CMS, CDF, & D0 Collab, [arXiv:1403.4427].

[30] S. Cortese and R. Petronzio, Phys. Lett. **B253**, 494 (1991).

[31] S. S. D. Willenbrock and D. A. Dicus, Phys. Rev. **D34**, 155 (1986).

[32] J. Campbell, T. Neumann and Z. Sullivan, JHEP **02**, 040 (2021), [arXiv:2012.01574].

[33] M. Brucherseifer, F. Caola and K. Melnikov, Phys. Lett. **B736**, 58 (2014), [arXiv:1404.7116].

[34] E. L. Berger, J. Gao and H. X. Zhu, JHEP **11**, 158 (2017), [arXiv:1708.09405].

[35] N. Kidonakis, Phys. Rev. **D81**, 054028 (2010), [arXiv:1001.5034].

[36] N. Kidonakis, Phys. Rev. **D82**, 054018 (2010), [arXiv:1005.4451].

[37] T. M. P. Tait and C. P. Yuan, Phys. Rev. **D63**, 014018 (2000), [hep-ph/0007298].

[38] S. Frixione, P. Nason and B. R. Webber, JHEP **08**, 007 (2003), [hep-ph/0305252]; W. Kim and H. Shin, JHEP **07**, 070 (2007), [arXiv:0706.3563]; S. Frixione, P. Nason and G. Ridolfi, JHEP **09**, 126 (2007), [arXiv:0707.3088]; J. M. Campbell *et al.*, JHEP **04**, 114 (2015), [arXiv:1412.1828]; T. Ježo *et al.*, Eur. Phys. J. **C76**, 12, 691 (2016), [arXiv:1607.04538].

[39] S. Frixione *et al.*, JHEP **03**, 092 (2006), [hep-ph/0512250]; V. Marotta and A. Naddeo, JHEP **08**, 029 (2008), [arXiv:0810.4759]; S. Alioli *et al.*, JHEP **09**, 111 (2009), [Erratum: JHEP02,011(2010)], [arXiv:0907.4076]; E. Re, Eur. Phys. J. **C71**, 1547 (2011), [arXiv:1009.2450]; R. Frederix, E. Re and P. Torrielli, JHEP **09**, 130 (2012), [arXiv:1207.5391]; R. Frederix *et al.*, JHEP **06**, 027 (2016), [arXiv:1603.01178].

[40] S. Frixione and B. R. Webber, JHEP **06**, 029 (2002), [hep-ph/0204244].

[41] P. Nason, JHEP **11**, 040 (2004), [hep-ph/0409146].

[42] J. Mazzitelli *et al.*, Phys. Rev. Lett. **127**, 6, 062001 (2021), [arXiv:2012.14267].

[43] A. Broggio *et al.*, JHEP **08**, 039 (2019), [arXiv:1907.04343].

[44] M. van Beekveld, A. Kulesza and L. M. Valero (2022), [arXiv:2212.03259].

[45] S. Catani *et al.*, Phys. Rev. Lett. **130**, 11, 111902 (2023), [arXiv:2210.07846].

[46] L. Buonocore *et al.* (2023), [arXiv:2306.16311].

[47] E. Todesco and J. Wenninger, Phys. Rev. Accel. Beams **20**, 8, 081003 (2017).

[48] V. M. Abazov *et al.* (D0), Phys. Rev. **D94**, 092004 (2016), [arXiv:1605.06168].

[49] T. Aaltonen *et al.* (CDF), Phys. Rev. **D88**, 091103 (2013), [arXiv:1304.7961].

[50] T. A. Aaltonen *et al.* (CDF, D0), Phys. Rev. **D89**, 7, 072001 (2014), [arXiv:1309.7570].

[51] T. A. Aaltonen *et al.* (CDF), Phys. Rev. **D89**, 9, 091101 (2014), [arXiv:1402.6728].

[52] T. Aaltonen *et al.* (CDF), Phys. Rev. Lett. **105**, 012001 (2010), [arXiv:1004.3224].

[53] V. M. Abazov *et al.* (D0), Phys. Rev. **D90**, 9, 092006 (2014), [arXiv:1401.5785].

[54] M. Czakon and A. Mitov, Comput. Phys. Commun. **185**, 2930 (2014), [arXiv:1112.5675].

[55] J. M. Campbell and R. K. Ellis, Nucl. Phys. Proc. Suppl. **205-206**, 10 (2010), [arXiv:1007.3492].

[56] R. Kleiss and W. J. Stirling, Z. Phys. C **40**, 419 (1988).

[57] M. Cacciari *et al.*, Phys. Lett. B **710**, 612 (2012), [arXiv:1111.5869].

[58] P. Bärnreuther, M. Czakon and A. Mitov, Phys. Rev. Lett. **109**, 132001 (2012), [arXiv:1204.5201].

[59] M. Czakon and A. Mitov, JHEP **12**, 054 (2012), [arXiv:1207.0236].

[60] M. Czakon and A. Mitov, JHEP **01**, 080 (2013), [arXiv:1210.6832].

[61] S. Catani *et al.*, Phys. Rev. D **99**, 5, 051501 (2019), [arXiv:1901.04005].

[62] G. Aad *et al.* (ATLAS), JHEP **06**, 138 (2023), [arXiv:2207.01354].

[63] A. M. Sirunyan *et al.* (CMS), JHEP **03**, 115 (2018), [arXiv:1711.03143].

[64] A. Tumasyan *et al.* (CMS), JHEP **04**, 144 (2022), [arXiv:2112.09114].

[65] G. Aad *et al.* (ATLAS), Eur. Phys. J. **C74**, 10, 3109 (2014), [Addendum: Eur. Phys. J.C76,no.11,642(2016)], [arXiv:1406.5375].

[66] ATLAS Collab., ATLAS-CONF-2011-121 (2011).

[67] G. Aad *et al.* (ATLAS), JHEP **05**, 059 (2012), [arXiv:1202.4892].

[68] ATLAS Collab., ATLAS-CONF-2011-140.

[69] ATLAS Collab., ATLAS-CONF-2012-024.

[70] G. Aad *et al.* (ATLAS), Eur. Phys. J. **C73**, 3, 2328 (2013), [arXiv:1211.7205].

[71] G. Aad *et al.* (ATLAS), Phys. Lett. **B717**, 89 (2012), [arXiv:1205.2067].

[72] ATLAS Collab., ATLAS-CONF-2012-031.

[73] M. Aaboud *et al.* (ATLAS), Phys. Rev. D **108**, 3, 032014 (2023), [arXiv:2212.00571].

[74] S. Chatrchyan *et al.* (CMS), JHEP **11**, 067 (2012), [arXiv:1208.2671].

[75] V. Khachatryan *et al.* (CMS), JHEP **08**, 029 (2016), [arXiv:1603.02303].

[76] S. Chatrchyan *et al.* (CMS), Phys. Lett. **B720**, 83 (2013), [arXiv:1212.6682].

[77] S. Chatrchyan *et al.* (CMS), JHEP **05**, 065 (2013), [arXiv:1302.0508].

[78] S. Chatrchyan *et al.* (CMS), Phys. Rev. **D85**, 112007 (2012), [arXiv:1203.6810].

[79] S. Chatrchyan *et al.* (CMS), Eur. Phys. J. **C73**, 4, 2386 (2013), [arXiv:1301.5755].

[80] G. Aad *et al.* (ATLAS, CMS), JHEP **07**, 213 (2023), [arXiv:2205.13830].

[81] G. Aad *et al.* (ATLAS), Eur. Phys. J. **C74**, 10, 3109 (2014), [Addendum: Eur. Phys. J.C76,no.11,642(2016)], [arXiv:1406.5375].

[82] G. Aad *et al.* (ATLAS), Phys. Rev. **D91**, 11, 112013 (2015), [arXiv:1504.04251].

[83] M. Aaboud *et al.* (ATLAS), Eur. Phys. J. **C78**, 487 (2018), [arXiv:1712.06857].

[84] M. Aaboud *et al.* (ATLAS), Phys. Rev. **D95**, 7, 072003 (2017), [arXiv:1702.08839].

[85] V. Khachatryan *et al.* (CMS), Eur. Phys. J. **C77**, 1, 15 (2017), [arXiv:1602.09024].

[86] S. Chatrchyan *et al.* (CMS), JHEP **02**, 024 (2014), [Erratum: JHEP02,102(2014)], [arXiv:1312.7582].

[87] V. Khachatryan *et al.* (CMS), Phys. Lett. **B739**, 23 (2014), [arXiv:1407.6643].

[88] V. Khachatryan *et al.* (CMS), Eur. Phys. J. **C76**, 3, 128 (2016), [arXiv:1509.06076].

[89] ATLAS Collab., ATLAS-CONF-2014-054, CMS Collab., CMS-PAS-TOP-14-016.

[90] R. Aaij *et al.* (LHCb), Phys. Rev. Lett. **115**, 11, 112001 (2015), [arXiv:1506.00903].

[91] G. Aad *et al.* (ATLAS), Eur. Phys. J. C **80**, 6, 528 (2020), [arXiv:1910.08819].

[92] ATLAS collab., ATLAS-CONF-2015-049.

[93] G. Aad *et al.* (ATLAS), Phys. Lett. B **810**, 135797 (2020), [arXiv:2006.13076].

[94] G. Aad *et al.* (ATLAS), JHEP **07**, 141 (2023), [arXiv:2303.15340].

[95] A. M. Sirunyan *et al.* (CMS), Eur. Phys. J. **C79**, 5, 368 (2019), [arXiv:1812.10505].

[96] A. M. Sirunyan *et al.* (CMS), JHEP **02**, 191 (2020), [arXiv:1911.13204].

[97] CMS Collab., CMS-PAS-TOP-15-005.

[98] A. M. Sirunyan *et al.* (CMS), JHEP **09**, 051 (2017), [arXiv:1701.06228].

[99] A. Tumasyan *et al.* (CMS) (2021), [arXiv:2108.02803].

[100] CMS Collab., CMS-PAS-TOP-16-013.

[101] A. Tumasyan *et al.* (CMS, TOTEM) (2023), [arXiv:2310.11231].

[102] R. Aaij *et al.* (LHCb), JHEP **08**, 174 (2018), [arXiv:1803.05188].

[103] G. Aad *et al.* (ATLAS) (2023), [arXiv:2308.09529].

[104] A. Tumasyan *et al.* (CMS), JHEP **08**, 204 (2023), [arXiv:2303.10680].

[105] A. M. Sirunyan *et al.* (CMS), Phys. Rev. Lett. **125**, 22, 222001 (2020), [arXiv:2006.11110].

[106] A. M. Sirunyan *et al.* (CMS), Phys. Rev. Lett. **119**, 24, 242001 (2017), [arXiv:1709.07411].

[107] ATLAS Collab., ATLAS-CONF-2023-063.

[108] V. M. Abazov *et al.* (D0), Phys. Rev. Lett. **107**, 121802 (2011), [arXiv:1106.5436].

[109] D. Acosta *et al.* (CDF), Phys. Rev. Lett. **95**, 102002 (2005), [hep-ex/0505091].

[110] V. Khachatryan *et al.* (CMS), Phys. Lett. **B736**, 33 (2014), [arXiv:1404.2292].

[111] M. Czakon, D. Heymes and A. Mitov, Phys. Rev. Lett. **116**, 8, 082003 (2016), [arXiv:1511.00549].

[112] G. D'Agostini, Nucl. Instrum. Meth. A **362**, 487 (1995).

[113] T. Adye, in "PHYSTAT 2011," 313–318, CERN, Geneva (2011), [arXiv:1105.1160].

[114] G. Aad *et al.* (ATLAS), Eur. Phys. J. C **80**, 10, 957 (2020), [Erratum: Eur.Phys.J.C 81, 29 (2021), Erratum: Eur.Phys.J.C 81, 398 (2021)], [arXiv:2004.03447].

[115] A. M. Sirunyan *et al.* (CMS), JHEP **01**, 183 (2019), [arXiv:1807.03825].

[116] A. Hocker and V. Kartvelishvili, Nucl. Instrum. Meth. A **372**, 469 (1996), [hep-ph/9509307].

[117] V. Blobel, in "Conference on Advanced Statistical Techniques in Particle Physics," 258–267 (2002), [hep-ex/0208022].

[118] S. Chatrchyan *et al.* (CMS), Eur. Phys. J. **C73**, 3, 2339 (2013), [arXiv:1211.2220].

[119] V. Khachatryan *et al.* (CMS), Phys. Rev. **D94**, 5, 052006 (2016), [arXiv:1607.00837].

[120] S. Chatrchyan *et al.* (CMS), Eur. Phys. J. **C74**, 3014 (2015), [Erratum: Eur. Phys. J.C75,no.5,216(2015)], [arXiv:1404.3171].

[121] G. Aad *et al.* (ATLAS), Eur. Phys. J. **C73**, 1, 2261 (2013), [arXiv:1207.5644].

[122] G. Aad *et al.* (ATLAS), Phys. Rev. **D90**, 7, 072004 (2014), [arXiv:1407.0371].

[123] G. Aad *et al.* (ATLAS), JHEP **06**, 100 (2015), [arXiv:1502.05923].

[124] M. Aaboud *et al.* (ATLAS), Phys. Rev. **D94**, 9, 092003 (2016), [arXiv:1607.07281].

[125] G. Aad *et al.* (ATLAS), Eur. Phys. J. **C76**, 10, 538 (2016), [arXiv:1511.04716].

[126] G. Aad *et al.* (ATLAS), Phys. Rev. **D93**, 3, 032009 (2016), [arXiv:1510.03818].

[127] V. Khachatryan *et al.* (CMS), Eur. Phys. J. **C75**, 11, 542 (2015), [arXiv:1505.04480].

[128] A. M. Sirunyan *et al.* (CMS), Eur. Phys. J. **C77**, 7, 459 (2017), [arXiv:1703.01630].

[129] V. Khachatryan *et al.* (CMS), Phys. Rev. **D94**, 7, 072002 (2016), [arXiv:1605.00116].

[130] M. Aaboud *et al.* (ATLAS), Eur. Phys. J. **C77**, 5, 292 (2017), [arXiv:1612.05220].

[131] M. Aaboud *et al.* (ATLAS), JHEP **11**, 191 (2017), [arXiv:1708.00727].

[132] G. Aad *et al.* (ATLAS), Eur. Phys. J. C **79**, 12, 1028 (2019), [Erratum: Eur.Phys.J.C 80, 1092 (2020)], [arXiv:1908.07305].

[133] M. Aaboud *et al.* (ATLAS), Phys. Rev. **D98**, 1, 012003 (2018), [arXiv:1801.02052].

[134] G. Aad *et al.* (ATLAS), JHEP **01**, 033 (2021), [arXiv:2006.09274].

[135] ATLAS Collab., ATLAS-CONF-2021-031.

[136] ATLAS Collab., ATLAS-CONF-2023-027.

[137] G. Aad *et al.* (ATLAS), Eur. Phys. J. C **83**, 6, 518 (2023), [arXiv:2209.07874].

[138] G. Aad *et al.* (ATLAS), Phys. Rev. D **106**, 3, 032008 (2022), [arXiv:2202.13901].

[139] CMS Collab., CMS-PAS-TOP-15-010.

[140] A. M. Sirunyan *et al.* (CMS), JHEP **04**, 060 (2018), [arXiv:1708.07638].

[141] V. Khachatryan *et al.* (CMS), Phys. Rev. **D95**, 9, 092001 (2017), [arXiv:1610.04191].

[142] A. M. Sirunyan *et al.* (CMS), JHEP **06**, 002 (2018), [arXiv:1803.03991].

[143] A. M. Sirunyan *et al.* (CMS), Phys. Rev. **D97**, 11, 112003 (2018), [arXiv:1803.08856].

[144] CMS Collab. CMS-PAS-TOP-2020-006.

[145] A. M. Sirunyan *et al.* (CMS), JHEP **02**, 149 (2019), [arXiv:1811.06625].

[146] A. M. Sirunyan *et al.* (CMS), Eur. Phys. J. C **80**, 7, 658 (2020), [arXiv:1904.05237].

[147] A. M. Sirunyan *et al.* (CMS), Phys. Rev. D **103**, 5, 052008 (2021), [arXiv:2008.07860].

[148] G. Aad *et al.* (ATLAS), Eur. Phys. J. **C76**, 1, 11 (2016), [arXiv:1508.06868].

[149] G. Aad *et al.* (ATLAS), JHEP **01**, 020 (2015), [arXiv:1407.0891].

[150] V. Khachatryan *et al.* (CMS), Phys. Lett. **B746**, 132 (2015), [arXiv:1411.5621].

[151] G. Aad *et al.* (ATLAS), Phys. Rev. **D92**, 7, 072005 (2015), [arXiv:1506.05074].

[152] V. Khachatryan *et al.* (CMS), Eur. Phys. J. C **76**, 7, 379 (2016), [arXiv:1510.03072].

[153] G. Aad *et al.* (ATLAS), Nature Phys. **17**, 7, 813 (2021).

[154] A. M. Sirunyan *et al.* (CMS), Phys. Rev. D **102**, 9, 092013 (2020), [arXiv:2009.07123].

[155] M. Aaboud *et al.* (ATLAS), JHEP **04**, 046 (2019), [arXiv:1811.12113].

[156] A. M. Sirunyan *et al.* (CMS), Phys. Lett. **B776**, 355 (2018), [arXiv:1705.10141].

[157] A. M. Sirunyan *et al.* (CMS), JHEP **07**, 125 (2020), [arXiv:2003.06467].

[158] A. M. Sirunyan *et al.* (CMS) (2019), [arXiv:1909.05306].

[159] A. M. Sirunyan *et al.* (CMS), Phys. Lett. B **803**, 135285 (2020), [arXiv:1909.05306].

[160] A. Hayrapetyan *et al.* (CMS) (2023), [arXiv:2309.14442].

[161] A. M. Sirunyan *et al.* (CMS), Phys. Lett. B **820**, 136565 (2021), [arXiv:2012.09225].

[162] G. Aad *et al.* (ATLAS), Eur. Phys. J. C **80**, 11, 1085 (2020), [arXiv:2007.14858].

[163] G. Aad *et al.* (ATLAS), JHEP **11**, 118 (2021), [arXiv:2106.11683].

[164] G. Aad *et al.* (ATLAS), Eur. Phys. J. C **83**, 6, 496 (2023), [arXiv:2303.15061].

[165] A. M. Sirunyan *et al.* (CMS), JHEP **11**, 082 (2019), [arXiv:1906.02805].

[166] A. M. Sirunyan *et al.* (CMS), Eur. Phys. J. C **80**, 2, 75 (2020), [arXiv:1908.06463].

[167] A. Tumasyan *et al.* (CMS), Phys. Lett. B **844**, 138076 (2023), [arXiv:2303.03864].

[168] A. Hayrapetyan *et al.* (CMS) (2023), [arXiv:2305.13439].

[169] V. M. Abazov *et al.* (D0), Phys. Rev. Lett. **103**, 092001 (2009), [arXiv:0903.0850]; V. M. Abazov *et al.* (D0), Phys. Rev. **D78**, 012005 (2008), [arXiv:0803.0739]; V. M. Abazov *et al.* (D0), Phys. Rev. Lett. **98**, 181802 (2007), [hep-ex/0612052].

[170] T. Aaltonen *et al.* (CDF), Phys. Rev. Lett. **103**, 092002 (2009), [arXiv:0903.0885]; T. Aaltonen *et al.* (CDF), Phys. Rev. **D81**, 072003 (2010), [arXiv:1001.4577].

[171] T. Aaltonen *et al.* (CDF), Phys. Rev. **D82**, 112005 (2010), [arXiv:1004.1181].

[172] A. Heinson and T. R. Junk, Ann. Rev. Nucl. Part. Sci. **61**, 171 (2011), [arXiv:1101.1275].

[173] A. Giammanco and R. Schwienhorst, Rev. Mod. Phys. **90**, 3, 035001 (2018), [arXiv:1710.10699].

[174] Tevatron Electroweak Working Group, (2009), [arXiv:0908.2171].

[175] N. Kidonakis, Phys. Rev. **D83**, 091503 (2011), [arXiv:1103.2792].

[176] CDF Collab., CDF conference note 11113 (2014), DØ Collab., DØ conference note 6448 (2014).

[177] T. A. Aaltonen *et al.* (CDF, D0), Phys. Rev. Lett. **115**, 15, 152003 (2015), [arXiv:1503.05027].

[178] T. A. Aaltonen *et al.* (CDF, D0), Phys. Rev. Lett. **112**, 231803 (2014), [arXiv:1402.5126].

[179] G. Aad *et al.* (ATLAS) (2023), [arXiv:2310.01518].

[180] G. Aad *et al.* (ATLAS), Phys. Rev. **D90**, 11, 112006 (2014), [arXiv:1406.7844].

[181] G. Aad *et al.* (ATLAS), Phys. Lett. **B717**, 330 (2012), [arXiv:1205.3130].

[182] S. Chatrchyan *et al.* (CMS), JHEP **12**, 035 (2012), [arXiv:1209.4533].

[183] M. Aaboud *et al.* (ATLAS, CMS), JHEP **05**, 088 (2019), [arXiv:1902.07158].

[184] M. Aaboud *et al.* (ATLAS), Eur. Phys. J. **C77**, 8, 531 (2017), [arXiv:1702.02859].

[185] M. Aaboud *et al.* (ATLAS), JHEP **04**, 124 (2017), [arXiv:1702.08309].

[186] V. Khachatryan *et al.* (CMS), JHEP **06**, 090 (2014), [arXiv:1403.7366].

[187] CMS Collab., CMS-PAS-TOP-15-007.

[188] M. Aaboud *et al.* (ATLAS), JHEP **04**, 086 (2017), [arXiv:1609.03920].

[189] ATLAS Collab., ATLAS-CONF-2023-026.

[190] A. M. Sirunyan *et al.* (CMS), Phys. Lett. **B772**, 752 (2017), [arXiv:1610.00678].

[191] A. M. Sirunyan *et al.* (CMS), Phys. Lett. B **800**, 135042 (2020), [arXiv:1812.10514].

[192] A. M. Sirunyan *et al.* (CMS), Eur. Phys. J. C **80**, 5, 370 (2020), [arXiv:1907.08330].

[193] A. M. Sirunyan *et al.* (CMS), Phys. Lett. B **808**, 135609 (2020), [arXiv:2004.12181].

[194] C. D. White *et al.*, JHEP **11**, 074 (2009), [arXiv:0908.0631].

[195] S. Frixione *et al.*, JHEP **07**, 029 (2008), [arXiv:0805.3067].

[196] G. Aad *et al.* (ATLAS), Phys. Lett. **B716**, 142 (2012), [arXiv:1205.5764].

[197] S. Chatrchyan *et al.* (CMS), Phys. Rev. Lett. **110**, 022003 (2013), [arXiv:1209.3489].

[198] G. Aad *et al.* (ATLAS), JHEP **01**, 064 (2016), [arXiv:1510.03752].

[199] M. Aaboud *et al.* (ATLAS, CMS), JHEP **05**, 088 (2019), [arXiv:1902.07158].

[200] G. Aad *et al.* (ATLAS), Eur. Phys. J. C **81**, 8, 720 (2021), [arXiv:2007.01554].

[201] S. Chatrchyan *et al.* (CMS), Phys. Rev. Lett. **112**, 23, 231802 (2014), [arXiv:1401.2942].

[202] M. Aaboud *et al.* (ATLAS), JHEP **01**, 063 (2018), [arXiv:1612.07231].

[203] A. M. Sirunyan *et al.* (CMS), JHEP **10**, 117 (2018), [arXiv:1805.07399].

[204] A. Tumasyan *et al.* (CMS) (2021), [arXiv:2109.01706].

[205] A. Tumasyan *et al.* (CMS), JHEP **07**, 046 (2023), [arXiv:2208.00924].

[206] ATLAS Collab., ATLAS-CONF-2011-118.

[207] G. Aad *et al.* (ATLAS), Phys. Lett. **B756**, 228 (2016), [arXiv:1511.05980].

[208] V. Khachatryan *et al.* (CMS), JHEP **09**, 027 (2016), [arXiv:1603.02555].

[209] G. Aad *et al.* (ATLAS), JHEP **06**, 191 (2023), [arXiv:2209.08990].

[210] CMS Collab., CMS-PAS-TOP-14-004.

[211] G. Aad *et al.* (ATLAS), JHEP **11**, 040 (2022), [arXiv:2202.11382].

[212] V. Khachatryan *et al.* (CMS), JHEP **04**, 073 (2016), [arXiv:1511.02138].

[213] M. Aaboud *et al.* (ATLAS), Eur. Phys. J. C **78**, 3, 186 (2018), [arXiv:1712.01602].

[214] CMS Collab., CMS-PAS-TOP-19-003.

[215] M. Czakon, P. Fiedler and A. Mitov, Phys. Rev. Lett. **115**, 5, 052001 (2015), [arXiv:1411.3007].

[216] W. Hollik and D. Pagani, Phys. Rev. **D84**, 093003 (2011), [arXiv:1107.2606].

[217] W. Bernreuther and Z.-G. Si, Phys. Rev. **D86**, 034026 (2012), [arXiv:1205.6580].

[218] S. Jung *et al.*, Phys. Rev. **D81**, 015004 (2010), [arXiv:0907.4112].

[219] V. M. Abazov *et al.* (D0), Phys. Rev. Lett. **100**, 142002 (2008), [arXiv:0712.0851].

[220] T. Aaltonen *et al.* (CDF), Phys. Rev. Lett. **101**, 202001 (2008), [arXiv:0806.2472].

[221] T. A. Aaltonen *et al.* (CDF, D0), Phys. Rev. Lett. **120**, 4, 042001 (2018), [arXiv:1709.04894].

[222] G. Aad *et al.* (ATLAS), JHEP **02**, 107 (2014), [arXiv:1311.6724].

[223] G. Aad *et al.* (ATLAS), Eur. Phys. J. **C76**, 2, 87 (2016), [Erratum: Eur. Phys. J.C77,564(2017)], [arXiv:1509.02358].

[224] G. Aad *et al.* (ATLAS), Phys. Rev. **D94**, 3, 032006 (2016), [arXiv:1604.05538].

[225] S. Chatrchyan *et al.* (CMS), Phys. Lett. **B717**, 129 (2012), [arXiv:1207.0065].

[226] V. Khachatryan *et al.* (CMS), Phys. Rev. **D93**, 3, 034014 (2016), [arXiv:1508.03862].

[227] V. Khachatryan *et al.* (CMS), Phys. Lett. **B760**, 365 (2016), [arXiv:1603.06221].

[228] M. Czakon *et al.*, Phys. Rev. **D98**, 1, 014003 (2018), [arXiv:1711.03945].

[229] V. Khachatryan *et al.* (CMS), Phys. Lett. **B757**, 154 (2016), [arXiv:1507.03119].

[230] G. Aad *et al.* (ATLAS), Phys. Lett. **B756**, 52 (2016), [arXiv:1512.06092].

[231] G. Aad *et al.* (ATLAS), JHEP **05**, 061 (2015), [arXiv:1501.07383].

[232] S. Chatrchyan *et al.* (CMS), JHEP **04**, 191 (2014), [arXiv:1402.3803].

[233] M. Aaboud *et al.* (ATLAS, CMS), JHEP **04**, 033 (2018), [arXiv:1709.05327].

[234] G. Aad *et al.* (ATLAS), JHEP **08**, 077 (2023), [arXiv:2208.12095].

[235] CMS Collab., CMS-PAS-TOP-15-018.

[236] G. Aad *et al.* (ATLAS), Phys. Lett. B **843**, 137848 (2023), [arXiv:2212.10552].

[237] G. Aad *et al.* (ATLAS), JHEP **07**, 033 (2023), [arXiv:2301.04245].

[238] G. Aad *et al.* (ATLAS), Eur. Phys. J. C **82**, 4, 374 (2022), [arXiv:2110.05453].

[239] A. M. Sirunyan *et al.* (CMS), JHEP **06**, 146 (2020), [arXiv:1912.09540].

[240] A. Tumasyan *et al.* (CMS), Phys. Lett. B **846**, 137703 (2023), [arXiv:2208.02751].

[241] G. Mahlon and S. J. Parke, Phys. Rev. **D53**, 4886 (1996), [hep-ph/9512264]; G. Mahlon and S. J. Parke, Phys. Lett. **B411**, 173 (1997), [hep-ph/9706304].

[242] G.R. Goldstein, in *Spin 96: Proceedings of the 12th International Symposium on High Energy Spin Physics,* Amsterdam, 1996, ed. C.W. Jager (World Scientific, Singapore, 1997), p. 328.

[243] T. Stelzer and S. Willenbrock, Phys. Lett. **B374**, 169 (1996), [hep-ph/9512292].

[244] W. Bernreuther *et al.*, Nucl. Phys. **B690**, 81 (2004), [hep-ph/0403035].

[245] A. Brandenburg, Z. G. Si and P. Uwer, Phys. Lett. **B539**, 235 (2002), [hep-ph/0205023].

[246] W. Bernreuther, D. Heisler and Z.-G. Si, JHEP **12**, 026 (2015), [arXiv:1508.05271].

[247] G. Mahlon and S. J. Parke, Phys. Rev. **D81**, 074024 (2010), [arXiv:1001.3422].

[248] G. Aad *et al.* (ATLAS), Phys. Rev. **D90**, 11, 112016 (2014), [arXiv:1407.4314].

[249] G. Aad *et al.* (ATLAS), Phys. Rev. Lett. **114**, 14, 142001 (2015), [arXiv:1412.4742].

[250] G. Aad *et al.* (ATLAS), Phys. Rev. **D93**, 1, 012002 (2016), [arXiv:1510.07478].

[251] S. Chatrchyan *et al.* (CMS), Phys. Rev. Lett. **112**, 18, 182001 (2014), [arXiv:1311.3924].

[252] V. Khachatryan *et al.* (CMS), Phys. Lett. **B758**, 321 (2016), [arXiv:1511.06170].

[253] V. Khachatryan *et al.* (CMS), Phys. Rev. **D93**, 5, 052007 (2016), [arXiv:1601.01107].

[254] M. Aaboud *et al.* (ATLAS), JHEP **03**, 113 (2017), [arXiv:1612.07004].

[255] M. Aaboud *et al.* (ATLAS), Eur. Phys. J. C **80**, 8, 754 (2020), [arXiv:1903.07570].

[256] A. M. Sirunyan *et al.* (CMS), Phys. Rev. **D100**, 7, 072002 (2019), [arXiv:1907.03729].

[257] A. Einstein, B. Podolsky and N. Rosen, Phys. Rev. **47**, 777 (1935).

[258] E. Schrödinger, Mathematical Proceedings of the Cambridge Philosophical Society **31**, 4, 555–563 (1935).

[259] J. S. Bell, Physics Physique Fizika **1**, 195 (1964).

[260] R. Horodecki *et al.*, Rev. Mod. Phys. **81**, 865 (2009), [arXiv:quant-ph/0702225].

[261] H. Casini and M. Huerta, PoS **TASI2021**, 002 (2023), [arXiv:2201.13310].

[262] A. Go *et al.* (Belle), Phys. Rev. Lett. **99**, 131802 (2007), [arXiv:quant-ph/0702267].

[263] M. Fabbrichesi *et al.* (2023), [arXiv:2305.04982].

[264] Y. Afik and J. R. M. n. de Nova, Eur. Phys. J. Plus **136**, 9, 907 (2021), [arXiv:2003.02280].

[265] M. Fabbrichesi, R. Floreanini and G. Panizzo, Phys. Rev. Lett. **127**, 16, 161801 (2021), [arXiv:2102.11883].

[266] C. Severi *et al.*, Eur. Phys. J. C **82**, 4, 285 (2022), [arXiv:2110.10112].

[267] Y. Afik and J. R. M. n. de Nova, Quantum **6**, 820 (2022), [arXiv:2203.05582].

[268] J. A. Aguilar-Saavedra and J. A. Casas, Eur. Phys. J. C **82**, 8, 666 (2022), [arXiv:2205.00542].

[269] Y. Afik and J. R. M. n. de Nova, Phys. Rev. Lett. **130**, 22, 221801 (2023), [arXiv:2209.03969].

[270] R. Ashby-Pickering, A. J. Barr and A. Wierzchucka, JHEP **05**, 020 (2023), [arXiv:2209.13990].

[271] J. A. Aguilar-Saavedra (2023), [arXiv:2307.06991].

[272] ATLAS Collab., ATLAS-CONF-2023-069.

[273] G. L. Kane, G. A. Ladinsky and C. P. Yuan, Phys. Rev. **D45**, 124 (1992).

[274] A. Czarnecki, J. G. Korner and J. H. Piclum, Phys. Rev. **D81**, 111503 (2010), [arXiv:1005.2625].

[275] K. Kondo, T. Chikamatsu and S. H. Kim, J. Phys. Soc. Jap. **62**, 1177 (1993).

[276] T. Aaltonen *et al.* (CDF, D0), Phys. Rev. **D85**, 071106 (2012), [arXiv:1202.5272].

[277] G. Aad *et al.* (ATLAS), JHEP **06**, 088 (2012), [arXiv:1205.2484].

[278] S. Chatrchyan *et al.* (CMS), JHEP **10**, 167 (2013), [arXiv:1308.3879].

[279] ATLAS and CMS Collab., ATLAS-CONF-2013-033, CMS-PAS-TOP-12-025.

[280] M. Aaboud *et al.* (ATLAS), Eur. Phys. J. **C77**, 4, 264 (2017), [Erratum: Eur. Phys. J.C79,no.1,19(2019)], [arXiv:1612.02577].

[281] V. Khachatryan *et al.* (CMS), Phys. Lett. **B762**, 512 (2016), [arXiv:1605.09047].

[282] CMS Collab., CMS-PAS-TOP-14-017.

[283] V. Khachatryan *et al.* (CMS), JHEP **01**, 053 (2015), [arXiv:1410.1154].

[284] G. Aad *et al.* (CMS, ATLAS), JHEP **08**, 08, 051 (2020), [arXiv:2005.03799].

[285] G. Aad *et al.* (ATLAS), Phys. Lett. B **843**, 137829 (2023), [arXiv:2209.14903].

[286] F. Abe *et al.* (CDF), Phys. Rev. **D50**, 2966 (1994).

[287] A. Abulencia *et al.* (CDF), Phys. Rev. **D73**, 032003 (2006), [hep-ex/0510048].

[288] M. Aaboud *et al.* (ATLAS), Eur. Phys. J. **C79**, 4, 290 (2019), [arXiv:1810.01772].

[289] V. Khachatryan *et al.* (CMS), Phys. Rev. **D93**, 7, 072004 (2016), [arXiv:1509.04044].

[290] A. M. Sirunyan *et al.* (CMS), Eur. Phys. J. **C78**, 11, 891 (2018), [arXiv:1805.01428].

[291] S. Argyropoulos and T. Sjöstrand, JHEP **11**, 043 (2014), [arXiv:1407.6653].

[292] J. R. Christiansen and P. Z. Skands, JHEP **08**, 003 (2015), [arXiv:1505.01681].

[293] A. M. Sirunyan *et al.* (CMS), Phys. Rev. Lett. **124**, 20, 202001 (2020), [arXiv:1911.03800].

[294] V. M. Abazov *et al.* (D0), Nature **429**, 638 (2004), [hep-ex/0406031].

[295] R. H. Dalitz and G. R. Goldstein, Phys. Rev. **D45**, 1531 (1992); R. H. Dalitz and G. R. Goldstein, Phys. Lett. **B287**, 225 (1992).

[296] V. M. Abazov *et al.* (D0), Phys. Rev. Lett. **113**, 032002 (2014), [arXiv:1405.1756].

[297] L. Sonnenschein, Phys. Rev. **D73**, 054015 (2006), [Erratum: Phys. Rev.D78,079902(2008)], [hep-ph/0603011].

[298] G. Aad *et al.* (ATLAS), Eur. Phys. J. **C75**, 7, 330 (2015), [arXiv:1503.05427].

[299] A. M. Sirunyan *et al.* (CMS), Phys. Rev. **D96**, 3, 032002 (2017), [arXiv:1704.06142].

[300] C. G. Lester and D. J. Summers, Phys. Lett. **B463**, 99 (1999), [hep-ph/9906349].

[301] A. M. Sirunyan *et al.* (CMS), Eur. Phys. J. **C79**, 4, 313 (2019), [arXiv:1812.10534].

[302] M. Aaboud *et al.* (ATLAS), JHEP **09**, 118 (2017), [arXiv:1702.07546].

[303] CMS Collab., CMS-PAS-TOP-19-009.

[304] The Tevatron Electroweak Working Group and Aaltonen, T., For the CDF and D0 Collab., arXiv:1608.01881, FERMILAB-CONF-16-298-E.

[305] B. Abbott *et al.* (D0), Phys. Rev. **D60**, 052001 (1999), [hep-ex/9808029]; F. Abe *et al.* (CDF), Phys. Rev. Lett. **82**, 271 (1999), [Erratum: Phys. Rev. Lett.82,2808(1999)], [hep-ex/9810029].

[306] T. Aaltonen *et al.* (CDF), Phys. Rev. **D92**, 3, 032003 (2015), [arXiv:1505.00500].

[307] T. A. Aaltonen *et al.* (CDF), Phys. Rev. **D90**, 9, 091101 (2014), [arXiv:1409.4906].

[308] A. M. Sirunyan *et al.* (CMS), Eur. Phys. J. **C77**, 5, 354 (2017), [arXiv:1703.02530].

[309] T. Aaltonen *et al.* (CDF), Phys. Lett. **B698**, 371 (2011), [arXiv:1101.4926].

[310] CMS Collab., CMS-PAS-TOP-12-030.

[311] T. Aaltonen *et al.* (CDF), Phys. Rev. **D80**, 051104 (2009), [arXiv:0906.5371].

[312] ATLAS Collab., ATLAS-CONF-2019-046.

[313] V. Khachatryan *et al.* (CMS), Phys. Rev. **D93**, 9, 092006 (2016), [arXiv:1603.06536].

[314] V. Khachatryan *et al.* (CMS), JHEP **12**, 123 (2016), [arXiv:1608.03560].

[315] CMS Collab., CMS-PAS-TOP-15-002.

[316] CMS Collab., CMS-PAS-TOP-16-002.

[317] V. M. Abazov *et al.* (D0), Phys. Rev. Lett. **100**, 192004 (2008), [arXiv:0803.2779]; S. Chatrchyan *et al.* (CMS), Phys. Lett. **B728**, 496 (2014), [Erratum: Phys. Lett.B738,526(2014)], [arXiv:1307.1907]; V. M. Abazov *et al.* (D0), Phys. Lett. **B703**, 422 (2011), [arXiv:1104.2887]; ATLAS Collab., ATLAS-CONF-2019-041; U. Langenfeld, S. Moch and P. Uwer, Phys. Rev. **D80**, 054009 (2009), [arXiv:0906.5273]; J. Fuster *et al.*, Eur. Phys. J. C **77**, 11, 794 (2017), [arXiv:1704.00540].

[318] G. Aad *et al.* (ATLAS), JHEP **11**, 150 (2019), [arXiv:1905.02302].

[319] CMS Collab., CMS-PAS-TOP-13-006 (2016).

[320] CDF Collab., CDF conference note 11080 (2014).

[321] V. M. Abazov *et al.* (D0), Phys. Rev. **D91**, 11, 112003 (2015), [arXiv:1501.07912].

[322] CMS Collab., CMS-PAS-TOP-13-005.

[323] M. Beneke *et al.*, Phys. Lett. **B775**, 63 (2017), [arXiv:1605.03609].

[324] A. H. Hoang, C. Lepenik and M. Preisser, JHEP **09**, 099 (2017), [arXiv:1706.08526].

[325] A. H. Hoang *et al.*, Phys. Rev. Lett. **101**, 151602 (2008), [arXiv:0803.4214].

[326] ATLAS Collab., ATL-PHYS-PUB-2021-034.

[327] A. M. Sirunyan *et al.*, Physics Letters B **803**, 135263 (2020), [arXiv:1909.09193].

[328] S. Catani *et al.*, JHEP **08**, 08, 027 (2020), [arXiv:2005.00557].

[329] G. Aad *et al.* (ATLAS), Phys. Lett. **B716**, 1 (2012), [arXiv:1207.7214].

[330] S. Chatrchyan *et al.* (CMS), Phys. Lett. **B716**, 30 (2012), [arXiv:1207.7235].

[331] S. Alekhin, A. Djouadi and S. Moch, Phys. Lett. **B716**, 214 (2012), [arXiv:1207.0980].

[332] T. Aaltonen *et al.* (CDF), Phys. Rev. **D87**, 5, 052013 (2013), [arXiv:1210.6131].

[333] V. M. Abazov *et al.* (D0), Phys. Rev. **D84**, 052005 (2011), [arXiv:1106.2063].

[334] G. Aad *et al.* (ATLAS), Phys. Lett. **B728**, 363 (2014), [arXiv:1310.6527].

[335] S. Chatrchyan *et al.* (CMS), JHEP **06**, 109 (2012), [arXiv:1204.2807].

[336] S. Chatrchyan *et al.* (CMS), Phys. Lett. **B770**, 50 (2017), [arXiv:1610.09551].

[337] A. F. Falk and M. E. Peskin, Phys. Rev. **D49**, 3320 (1994), [hep-ph/9308241].

[338] T. A. Aaltonen *et al.* (CDF), Phys. Rev. Lett. **111**, 20, 202001 (2013), [arXiv:1308.4050].

[339] CMS Collab., CMS-PAS-TOP-16-019.

[340] M. Aaboud *et al.* (ATLAS), Eur. Phys. J. **C78**, 2, 129 (2018), [arXiv:1709.04207].

[341] ATLAS Collab., ATLAS-CONF-2019-038.

[342] V. M. Abazov *et al.* (D0), Phys. Rev. **D85**, 091104 (2012), [arXiv:1201.4156].

[343] D. Choudhury, T. M. P. Tait and C. E. M. Wagner, Phys. Rev. **D65**, 053002 (2002), [hep-ph/0109097].

[344] D. Chang, W.-F. Chang and E. Ma, Phys. Rev. **D59**, 091503 (1999), [hep-ph/9810531]; D. Chang, W.-F. Chang and E. Ma, Phys. Rev. **D61**, 037301 (2000), [hep-ph/9909537].

[345] T. Aaltonen *et al.* (CDF), Phys. Rev. **D88**, 3, 032003 (2013), [arXiv:1304.4141].

[346] V. M. Abazov *et al.* (D0), Phys. Rev. **D90**, 5, 051101 (2014), [Erratum: Phys. Rev.D90,no.7,079904(2014)], [arXiv:1407.4837].

[347] G. Aad *et al.* (ATLAS), JHEP **11**, 031 (2013), [arXiv:1307.4568].

[348] CMS Collab., CMS-PAS-TOP-11-031.

[349] T. Aaltonen *et al.* (CDF), Phys. Rev. **D84**, 031104 (2011), [arXiv:1106.3970].

[350] G. Aad *et al.* (ATLAS), Phys. Rev. **D91**, 7, 072007 (2015), [arXiv:1502.00586].

[351] M. Aaboud *et al.* (ATLAS), JHEP **11**, 086 (2017), [arXiv:1706.03046].

[352] K. Melnikov, M. Schulze and A. Scharf, Phys. Rev. **D83**, 074013 (2011), [arXiv:1102.1967].

[353] A. M. Sirunyan *et al.* (CMS), JHEP **10**, 006 (2017), [arXiv:1706.08128].

[354] M. Aaboud *et al.* (ATLAS), Eur. Phys. J. **C79**, 5, 382 (2019), [arXiv:1812.01697].

[355] G. Bevilacqua *et al.*, JHEP **10**, 158 (2018), [arXiv:1803.09916].

[356] G. Bevilacqua *et al.*, JHEP **01**, 188 (2019), [arXiv:1809.08562].

[357] G. Aad *et al.* (ATLAS), JHEP **09**, 049 (2020), [arXiv:2007.06946].

[358] A. Tumasyan *et al.* (CMS), JHEP **12**, 180 (2021), [arXiv:2107.01508].

[359] A. Tumasyan *et al.* (CMS), JHEP **05**, 091 (2022), [arXiv:2201.07301].

[360] G. Aad *et al.* (ATLAS) (2023), [arXiv:2302.01283].

[361] A. M. Sirunyan *et al.* (CMS), Phys. Rev. Lett. **121**, 22, 221802 (2018), [arXiv:1808.02913].

[362] M. Cepeda *et al.* (HL/HE WG2 group) (2019), [arXiv:1902.00134].

[363] S. Chatrchyan *et al.* (CMS), Phys. Rev. Lett. **110**, 172002 (2013), [arXiv:1303.3239].

[364] J. M. Campbell and R. K. Ellis, JHEP **07**, 052 (2012), [arXiv:1204.5678].

[365] M. V. Garzelli *et al.*, JHEP **11**, 056 (2012), [arXiv:1208.2665].

[366] ATLAS Collab., ATLAS-CONF-2012-126.

[367] G. Aad *et al.* (ATLAS), JHEP **11**, 172 (2015), [arXiv:1509.05276].

[368] V. Khachatryan *et al.* (CMS), JHEP **01**, 096 (2016), [arXiv:1510.01131].

[369] M. Aaboud *et al.* (ATLAS), Phys. Rev. **D99**, 7, 072009 (2019), [arXiv:1901.03584].

[370] G. Aad *et al.* (ATLAS), Eur. Phys. J. C **81**, 737 (2021), [arXiv:2103.12603].

[371] ATLAS Collab., ATLAS-CONF-2023-065.

[372] A. M. Sirunyan *et al.* (CMS), JHEP **08**, 011 (2018), [arXiv:1711.02547].

[373] A. M. Sirunyan *et al.* (CMS), JHEP **03**, 056 (2020), [arXiv:1907.11270].

[374] A. Tumasyan *et al.* (CMS), Phys. Rev. D **108**, 032008 (2023), [arXiv:2208.12837].

[375] A. Tumasyan *et al.* (CMS), JHEP **07**, 219 (2023), [arXiv:2208.06485].

[376] ATLAS Collab., ATLAS-CONF-2023-019.

[377] A. M. Sirunyan *et al.* (CMS), JHEP **07**, 003 (2017), [arXiv:1702.01404].

[378] A. Tumasyan *et al.* (CMS), JHEP **02**, 107 (2022), [arXiv:2111.02860].

[379] A. M. Sirunyan *et al.* (CMS), Phys. Rev. Lett. **122**, 13, 132003 (2019), [arXiv:1812.05900].

[380] G. Aad *et al.* (ATLAS), JHEP **07**, 124 (2020), [arXiv:2002.07546].

[381] CMS Collab., CMS-PAS-TOP-22-008.

[382] S. P. Martin 1–98 (1997), [Adv. Ser. Direct. High Energy Phys.18,1(1998)], [hep-ph/9709356].

[383] C. T. Hill and E. H. Simmons, Phys. Rept. **381**, 235 (2003), [Erratum: Phys. Rept.390,553(2004)], [hep-ph/0203079].

[384] C. T. Hill, Phys. Lett. **B266**, 419 (1991).

[385] C. T. Hill, Phys. Lett. **B345**, 483 (1995), [hep-ph/9411426].

[386] S. Chatrchyan *et al.* (CMS), Phys. Rev. D **87**, 072002 (2013), URL `https://link.aps.org/doi/10.1103/PhysRevD.87.072002`.

[387] S. Chatrchyan *et al.* (CMS), JHEP **12**, 015 (2012), [arXiv:1209.4397].

[388] G. Aad *et al.* (ATLAS), JHEP **10**, 061 (2020), [arXiv:2005.05138].

[389] G. Aad *et al.* (ATLAS), JHEP **2306**, 155 (2023), [arXiv:2208.11415].

[390] A. Tumasyan *et al.* (CMS), JHEP **02**, 169 (2022), [arXiv:2112.09734].

[391] A. Tumasyan *et al.* (CMS), Phys. Rev. Lett. **129**, 032001 (2022), URL `https://link.aps.org/doi/10.1103/PhysRevLett.129.032001`.

[392] CMS Collab., CMS-PAS-TOP-22-002.

[393] ATLAS Collab., CERN-EP-2022-044, [arXiv:2301.11605].

[394] G. Aad *et al.* (ATLAS), Phys. Lett. B **842**, 137379 (2023), [arXiv:2205.02537].

[395] G. Aad *et al.* (ATLAS), Eur. Phys. J. C **82**, 4, 334 (2022), [arXiv:2112.01302].

[396] A. Tumasyan *et al.* (CMS), JHEP **06**, 082 (2022), [arXiv:2201.07859].

[397] ATLAS Collab., ATLAS-CONF-2023-001.

[398] G. Aad *et al.* (ATLAS), JHEP **07**, 199 (2023), [arXiv:2301.03902].

[399] A. Tumasyan *et al.* (CMS) (2021), [arXiv:2107.13896].

[400] CMS Collab., CMS-PAS-TOP-22-006.

[401] G. Aad *et al.* (ATLAS), JHEP **06**, 063 (2022), [arXiv:2202.12134].

[402] G. Aad *et al.* (ATLAS), JHEP **04**, 080 (2023), [arXiv:2205.02817].

[403] S. Banerjee, M. Chala and M. Spannowsky, Eur. Phys. J. C **78**, 8, 683 (2018), [arXiv:1806.02836].

[404] C. Zhang and S. Willenbrock, Nuovo Cim. C **033**, 4, 285 (2010), [arXiv:1008.3155].

[405] "LHC Top Working Group Summary Plots," `https://twiki.cern.ch/twiki/bin/view/LHCPhysics/LHCTopWGSummaryPlots`.

[406] A. M. Sirunyan *et al.* (CMS), JHEP **03**, 095 (2021), [arXiv:2012.04120].

[407] CMS Collab., CMS-PAS-TOP-21-013.

[408] CMS Collab., CMS-PAS-TOP-22-005.